Vaginal regulatory T cells in health and infection

Brianna R. Traxinger

A dissertation

submitted in partial fulfillment of the

requirements for the degree of

Doctor of Philosophy

University of Washington

2021

Reading Committee:

Jennifer M. Lund, Chair

Martin Prlic, Chair

Chetan Seshadri

Program Authorized to Offer Degree:

Pathobiology

University of Washington

Abstract

Vaginal regulatory T cells in health and infection

Brianna R. Traxinger

Chair of the Supervisory Committee:

Jennifer M. Lund
Department of Global Health

Martin Prlic
Departments of Global Health and Immunology

Regulatory T cells (Tregs) mediate immune homeostasis, yet also facilitate nuanced immune responses during infection, balancing pathogen control while limiting host inflammation. Recent studies have identified Treg populations in non-lymphoid tissues that are phenotypically distinct from Tregs in lymphoid tissues (LT), including performance of location-dependent roles. Mucosal tissues serve as critical barriers to microbes while performing unique physiologic functions, so we sought to identify distinct phenotypical and functional aspects of mucosal Tregs in the female reproductive tract. In healthy human and mouse vaginal mucosa, we found that Tregs are highly activated compared to blood or LT Tregs. To determine if this phenotype reflects acute activation or a general signature of vaginal tract (VT)-residency, we infected mice with HSV-2 to discover

that VT Tregs express granzyme-B (GzmB) and acquire a VT Treg signature distinct from baseline. To determine the mechanisms that drive GzmB expression, we performed *ex vivo* assays to reveal that a combination of type-I interferons and interleukin-2 is sufficient for GzmB expression. Together, we highlight that VT Tregs are activated at steady state and become further activated in response to infection; thus, they may exert robust control of local immune responses, which could have implications for mucosal vaccine design.

Additionally, little is known about the role of Tregs in recurrent HSV-2 outbreaks or secondary exposure to HSV-2. Tissue-resident memory T cells (Trm), which reside in tissue sites without recirculation, have been shown to be crucial for protection from HSV-2 in mouse models and HSV-2 control. However, HSV-2 symptoms and viral load are highly variable between infected individuals, despite the presence of vaginal Trm. Therefore, we predicted that Tregs prevent immune-mediated vaginal tissue damage during HSV-2 challenge by restraining CD4+ and CD8+ Trm responses, possibly at the expense of impaired viral clearance. Additionally, we hypothesized that Tregs may directly contribute to the repair of vaginal HSV-2 lesions through production of amphiregulin (Areg), a growth factor known to facilitate tissue repair in other tissue Tregs. We used immunohistochemistry to assess vaginal pathology in mice lacking Tregs at the time of HSV-2 challenge and found that Treg-depleted mice experienced delayed tissue healing by day 7 post-challenge, compared to Treg-replete controls. However, PCR revealed that vaginal HSV-2 viral titers were comparable in both groups, suggesting that tissue damage was immune-mediated. We also found that vaginal Tregs in mice express *Areg* transcript and Areg protein by day 7 post-HSV-2 primary infection, suggesting that Tregs may directly contribute to vaginal tissue repair of HSV-2 lesions, but further studies are necessary to functionally link Treg-produced Areg to vaginal

mucosa healing and confirm Treg production of Areg in human tissues. Experiments are ongoing to assess the role of Tregs on Trm abundance, activation, and cytotoxic activity after HSV-2 challenge, as well as to define the role of Treg-produced Areg in tissue pathology using conditional knockout mice. Together, these findings suggest that vaginal Tregs may have vagina-specific roles in tissue protection and immune control during viral infection, further evidencing the need to consider Tregs in mucosal vaccine design. Likewise, Treg-based therapeutics could be an important tool for reversing pathology in mucosal infection or autoimmunity.

TABLE OF CONTENTS

LIST OF FIGURES

LIST OF TABLES

ABBREVIATIONS

AF = antigen-free

APC = antigen-presenting cell

Areg = amphiregulin

AhR = aryl hydrocarbon receptor

BV = bacterial vaginosis

CRC = colorectal cancer

CTL = cytotoxic lymphocyte

CTLA-4 = cytotoxic T-lymphocyte-associated protein 4)

DC = dendritic cell

DEG = differentially expressed gene

dLN = (vaginal)-draining lymph node

DSS = dextran sodium sulfate

FACS = fluorescence-activated cell sorting

FoxP3 = forkhead box protein 3

FDR = false discovery rate

GC = germinal center

GI = gastrointestinal

GITR = glucocorticoid-induced TNFR-related receptor

GSEA = gene set enrichment analysis

GU = genitourinary

GzmB = granzyme B

HSV-2 = herpes simplex virus type 2

HSV-2 TK- = thymidine kinase-deficient HSV-2

IBD = inflammatory bowel diseases

ICOS = inducible costimulatory

IFNAR = interferon-alpha/beta receptor

IgA = immunoglobulin A

IEL = intraepithelial cells

IL = interleukin

IFN = interferon

IFN-I = Type-I interferons

i.p. = intraperitoneal

IPEX = immunodysregulation, polyendocrinopathy, and enteropathy, X-linked syndrome

i.v. = intravenous

ivag. = intravaginal

LT = lymphoid tissue

MAST = Model-based Analysis of Single Cell Transcriptomics

Mtb = Mycobacterium tuberculosis

NK = natural killer cell

NRP1 = neuropilin-1

PBMC = peripheral blood mononuclear cells

pDC = plasmacytoid DC

PFU = plaque-forming units

p.i. = post-infection

PPAR-g = peroxisome proliferator-activated receptor gamma

RA = retinoic acid

RNA-seq = RNA-sequencing

RORγT = RAR-related orphan receptor gamma

RSV = respiratory syncytial virus

s.c. = subcutaneous

SCFA = short-chain fatty acids

SPF = specific pathogen-free

spp. = species, plural

STI = sexually transmitted infection

Tconv = conventional T cell

TCR = T cell receptor

Tfr = T-follicular helper

Th = T-helper

TIGIT = T-cell immunoreceptor with immunoglobulin and ITIM domains

TLR = Toll-like receptor

Treg = regulatory T cell

Trm = Tissue-resident memory T cell

UMAP = uniform manifold approximation and projection

UMI = unique molecular identifier

VAT = visceral adipose tissue

VT = vaginal tract

WT = wildtype

ACKNOWLEDGEMENTS

This work was completed under the mentorship of two outstanding scientists, Jennifer Lund and Martin Prlic. I was fortunate to receive guidance from two T cell and mucosal immunology experts, each with their own complementary but distinct expertise. Jenny has the incredible ability to instantly situate data within the larger framework of the project and literature, creating excitement about even the smallest of findings and maintaining momentum for further research. Despite her incredible scientific and professional background and accomplishments, she is humble, kind, and always available for guidance. Perhaps most importantly, she facilitates a fun and positive work research environment, empowers women in science, and celebrates every small achievement within the lab. The Lund lab members are incredible and supportive friends and scientists who are always helpful and make science fun. I especially thank Jess Graham and Laura Richert-Spuhler for their mentorship and Jess Swarts for maintaining the lab. Martin has a remarkable technical acuity and eye for detail, and he and his lab have made me a better scientist through training in rigorous analysis and discussion. Martin will always spot a missing control or an experimental flaw, and can recall scientific papers, down to the figure, by memory. The Prlic lab has become a powerhouse in not only mucosal immunology but also in advanced techniques and have imparted their knowledge onto me. In particular, Amanda Woodward-Davis, Florian Mair, and Jami Erickson have been patient mentors.

In addition to the Lund and Prlic labs, many scientists at the University of Washington and the Fred Hutch have helped me over the past 5.5 years. My thesis committee members Nick Crispe, Chetan Seshadri, Marc Gavin, and Anthony Rongvaux have consistently given me critical but kind and helpful feedback to advance both my research project and my own abilities as a

scientist. Dr. LeeAnn Campbell has been an outstanding director of the Pathobiology program and a fierce advocate for students, with the administrative support of Ernie Lefler and Ashley Zigler. My classmates Andrew Gustin, Sara Ahmed, Tanvi Arkatkar, Veronica Davé, Rachael Parks, Nicole Potchen, and Irene Cruz Talavera, along with the rest of the Pathobiology students, are a consistent source of motivation, support, knowledge, and friendship. Julian Simon has been my Science Spotlight mentor for the last 3 years and has greatly improved my scientific writing and editing abilities. A fellow scientist and outdoor athlete, Bingjie Wang was the first friend I made in Seattle and continues to be a partner in both science and in the mountains. Likewise, Jessica Graham is my joint running and lab mentor, often in the same day. I also must thank the research cores and general staff at Fred Hutch, who provide a productive, clean, safe, and enjoyable work environment.

I would like to thank friends from outside of the lab. My childhood friends from Alaska have been my world for 25 years. I have too many friends to name in the trail running and mountaineering community, but our time together outdoors has been invaluable to my success in academia, as it has provided a fun and healthy outlet outside of work and kept me balanced both physically and mentally well during my academic training.

I received an excellent public education at Bettye Davis East Anchorage High School, which facilitated a concurrent passion for both the arts and science. Of note, Gary Snyder is responsible for initiating my excitement for biology by teaching one of the best courses I have ever taken, and I am lucky to still call him a friend and mentor today. Additionally, William Ennis instilled in me not only knowledge of physics, but a complete awe for science and the natural world. His

conviction that I belong in science—an encouragement that not all young female students receive—is a source of motivation to this day. He also shares my passion for books and writing and taught me that scientists don't have to forgo a love of language and literature.

My professors at Colorado College were excellent and helped shape my love of biology and research. In particular, Nancy Huang, Shane Heschel, Darrell Killian, and Phoebe Lostroh motivated me to pursue research and helped facilitate my career. Likewise, Rachel Friedman and Jordan Jacobelli at the University of Colorado Anschutz and National Jewish Health took a chance on me and taught me immunology and how to work in a lab, and I am forever grateful for their faith and training. Cara Mack, Roberta Pelanda, and Raul Torres were also instrumental in my path to immunology and grad school.

My parents Jim and Kim Traxinger did not attend college themselves and were adamant that I receive an education and therefore helped facilitate a wonderful education at Colorado College. However, I am no longer a first-generation college student, as my mom has since attended college to become a nurse. Likewise, my grandparents, Donna and Buddy Rodgers, did not have the opportunity to attend formal college but encouraged the pursuit of education in any form and were also interested in my studies, and my grandpa would be proud to know that I not only finished college, but a PhD as well.

I began grad school on my own, but I've ended school with a patient, kind, and supportive husband, Richard Lockwood. He has always put my school first and allowed me to focus, even when I've been too busy or stressed to contribute as a fun or helpful partner. As my primary

mountaineering partner, he's kept me healthy and balanced outside of school. I could have done grad school on my own, but it's been much better with him in my life. I'm also incredibly grateful for the Lockwood family for welcoming me into their lives and accommodating my school responsibilities. Lastly, my sweet greyhound Javier is my angel and has been my best friend for nearly 7 years.

DEDICATION

To Gary Snyder and William Ennis, who made me a scientist by fostering the need to understand the world around us.

The world looks so different after learning science. For example, trees are made of air, primarily. When they are burned, they go back to air, and in the flaming heat is released the flaming heat of the sun which was bound in to convert the air into tree, and in the ash is the small remnant of the part which did not come from air that came from the solid earth, instead. These are beautiful things, and the content of science is wonderfully full of them. They are very inspiring, and they can be used to inspire others.

- Richard Feynman

***

And to Priscilla Díaz Fernandez (1993-2018), my dear friend who lived with and died of complications from lupus, a devastating autoimmune disease. You taught me levity, kindness, perseverance, and give purpose to my pursuit of immunology.

...miren allá, donde el viento es ahora tan manso que se queda a dormir debajo de las camas, allá, donde el sol brilla tanto que no saben hacia dónde girar los girasoles, sí, allá, es el pueblo de Esteban.

-Gabriel García Márquez

Chapter 1. INTRODUCTION

1.1 REGULATORY T CELLS

Regulatory T cells (Tregs) are a subset of CD4+ T cells defined by expression of the transcription factor forkhead box P3 (Foxp3) and their ability to suppress conventional T cells and other immune cells[1-3]. Early on, Tregs were demonstrated to be an essential cell type, as patients with immunodysregulation polyendocrinopathy enteropathy X-linked (IPEX) syndrome and scurfy mice lacking a functional *Foxp3* gene suffered from various autoimmune-like conditions involving multiple tissues and organs, plus dysregulated effector T cell activity[4-6]. Additional studies demonstrated that *Foxp3* is the master regulator of Treg development and is indeed required for both their differentiation as well as function as suppressive cells[7-12]. Subsequently, a mouse model wherein Foxp3 is ablated in mature Tregs demonstrated that continuous Foxp3 expression is required to maintain the Treg developmental program and thus for Tregs to sustain suppressive function[13].

1.2 TREG-MEDIATED SUPPRESSION

Several decades of active research has since confirmed these findings and demonstrated Tregs to be critical mediators of the immune system. Immunosuppressive mechanisms utilized by Tregs are diverse and varied. Tregs express several immunosuppressive cytokines, including TGFb and IL-10[14, 15], and they have also been shown to express granzyme B, leading to death of immune cells including B cells, conventional T cells, and antigen-presenting cells (APC)[16-18]. More recently, this has been shown to occur under particular inflammatory conditions such as infection[19]. In addition, Tregs express high levels of CTLA-4 at steady state, which allows them

to limit availability of CD80 and CD86 on dendritic cells (DC) to conventional T cells[20]. Tregs also express the ectoenzymes CD39 and CD73, which facilitate the conversion of extracellular ATP to adenosine, which thus directly limits proliferation of effector T cells, as well as suppressing myeloid cells including DCs[21-24]. Finally, through their high expression of CD25, a subunit of the IL-2R, Tregs can serve as an IL-2 sink, effectively depriving effector T cells of IL-2 and thus limiting their proliferative capacity[25]. Not only do Tregs utilize these immunosuppressive mechanisms, and many others, to limit immune responses to self and other innocuous antigens to prevent autoimmunity at homeostasis[2, 26, 27], but they additionally mediate inflammatory responses to infection[28, 29].

1.3 NON-LYMPHOID TISSUE TREGS

Since their discovery, Tregs have been primarily studied in the thymus, where they develop, and in peripheral lymphoid organs. However, a growing body of research has shown that Tregs also reside in non-lymphoid organs, where they can have unique phenotypes and execute highly specialized roles outside of the canonical regulatory functions, suggesting that Treg phenotype and activity is highly context dependent. In particular, tissue Tregs have been described in visceral adipose tissue (VAT), skin, and muscle[30-32]. These non-lymphoid tissue Tregs are transcriptionally and phenotypically distinct from Tregs in spleen and lymph node (LN) and can perform highly specialized, location-dependent roles. Tregs in human skin, concentrated near hair follicles, regulate epithelial stem cell differentiation and display an activated memory phenotype, limiting inflammation and pro-fibrotic responses at steady state[32-34]. In the mouse VAT, Tregs express the IL-33 receptor (IL-33R), where IL-33 expressed by mesenchymal stromal cells promotes Treg accumulation and proliferation[35, 36]. These Tregs acquire robust

expression of the master regulator of adipose differentiation—peroxisome proliferator-activated receptor (PPAR)-γ—which maintains VAT insulin sensitivity[31, 35, 37]. Muscle Tregs respond to IL-33 produced by fibroblast-like fibro/adipogenic progenitor cells during muscle damage in mice and in turn produce amphiregulin (Areg), a growth factor that directly acts on satellite cells to facilitate muscle repair[30, 38].Thus, phenotypically distinct and highly specialized Treg populations reside in various non-lymphoid tissue sites, underscoring phenotypic and functional heterogeneity within Tregs based on tissue location. Furthermore, these studies suggest that dynamic populations likely exist throughout the body in other discrete tissue types.

1.4 MUCOSAL TISSUE TREGS

In addition to non-lymphoid organs such as the muscle, VAT, and skin, Tregs have also been characterized in several mucosal tissue sites. The mucosa has critical, location-dependent physiologic functions, including air exchange in the respiratory tract, nutrient absorption in the gastrointestinal tract, and reproduction in the genitourinary tract. The mucosal tissues also share a common barrier function in protecting the host from invading pathogenic stimuli, as the mucosa serves as a portal of entry for many pathogens of global health importance. The unique physiological and barrier roles of mucosal sites require a tightly coordinated immune response to allow for necessary tolerance to harmless antigens such as dietary antigens and sperm during reproduction, while also patrolling for and eliminating viral, bacterial, and fungal pathogens at infection entry sites. Given the canonical roles of Tregs as immune response regulators, as well as their more recently discovered location-specific functions, an increasing body of research demonstrates that Treg populations in mucosal tissues are crucial in both homeostasis and disease (Figure 1.1).

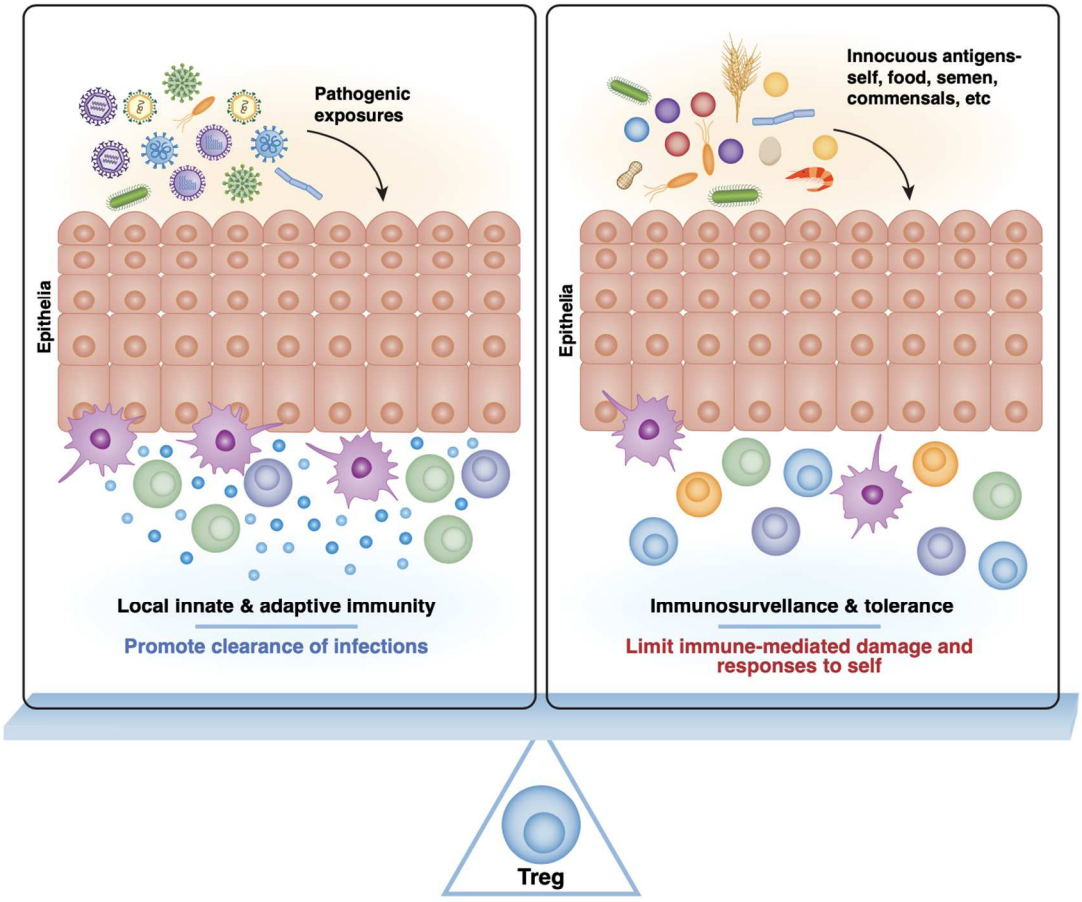

Figure 1.1. Tregs in mucosal tissue sites help to balance active immunity versus immunological tolerance in the face of diverse antigenic exposures.

Mucosal barrier tissues serve as portals of entry to a wide variety of antigens, both harmful and harmless to the host. Thus, the mucosal immune system has the complex job of balancing tolerance to innocuous antigens such as food, allergens, semen, and commensals while at the same time patrolling for pathogens so that an appropriate immune response can be generated to benefit but not harm the host. Tregs, depicted here at the fulcrum of this balance, participate in this process of maintaining a homeostatic state of active immunosurveillance and tolerance rather than persistent mucosal inflammation.

1.5 Respiratory Tract Mucosal Tregs

The respiratory tract experiences constant exposure to inhaled antigens and pathogens, yet this uniquely delicate mucosal tissue must generally maintain a state of relative quiescence for the

preservation of tissue architecture and oxygen exchange. In this regard, overt immune responses to perturbations such as infection must be tightly regulated—striking a balance between rapid pathogen clearance and tissue preservation (Figure 1.1). Tregs employ multiple mechanisms to dictate respiratory tract tissue homeostasis, including promoting effector immune responses mitigating inflammation, and facilitating tissue preservation and healing[15, 19, 29, 39-47]. Other reviews have more comprehensively detailed the multifaceted roles for Tregs during infection[28, 29, 42, 48]. Here, we mention only a handful of key examples of various functions of Tregs in the respiratory tract with the intention of setting the stage to consider the effects of respiratory tract tissue-specific cues on Treg phenotype and function.

In the context of influenza virus infection in mice, Tregs guide the formation of antigen-specific T follicular helper (Tfh) cell and germinal center (GC) B cell responses in the lymph node through their consumption of excess IL-2[41]. Thus, by controlling IL-2 availability, Tregs promote appropriate effector immune responses for viral clearance[41, 49]. Additionally, respiratory tract Tregs have been demonstrated to mount rapid and robust antigen-specific primary and memory recall responses to influenza virus infection, acting to appropriately limit antiviral T cell responses and ameliorate excess inflammation in mice[39, 45]. Importantly, after secondary influenza challenge, naïve Tregs are insufficient in recapitulating CD8+ T cell regulation[39]. Similarly, upon *Mycobacterium tuberculosis* (Mtb) challenge in mice, thymically derived Tregs specific to the immunodominant Mtb epitope expand robustly, exhibit an activated phenotype, and delay the priming and accumulation of effector T cells in the lung. These Mtb-specific Tregs are then specifically culled though Th1 inflammation-derived IL-12, which promotes high Tbet expression in Mtb-specific Tregs[50,51]. In other examples of respiratory tract infections such as

respiratory syncytial virus (RSV) in mice and SARS-CoV-2 in humans, disease severity and pulmonary pathology have been linked to functional differences among Tregs, where a loss in Tregs leads to accelerated viral clearance at the expense of immune-mediated tissue damage and worsened disease outcomes[19, 52-54]. Notably, one study identified a decrease in airway Tregs in patients with COVID-19 compared to healthy controls[54], thereby raising the possibility that a Treg deficit in the lung could be contributing to disease and the dysregulated immune response in COVID-19, though this requires further study of the mucosal immune responses to natural SARS-CoV-2 infection.

Recent studies employing a combination of epigenetic, single-cell chromatin accessibility, gene expression, and T cell receptor (TCR) fate mapping methods have identified a generalizable tissue-specific signature for Tregs that is conserved among mice and humans[55-61]. At homeostasis, roughly 10-20% of the total Tregs found in the lungs of specific pathogen-free (SPF) mice exhibit a tissue-specific profile[56]. Phenotypically, mouse tissue Tregs, including those found in the lungs, can be identified by their expression of KLRG1 and IL-33R and are regulated by BATF[56, 57]. Interestingly, lung tissue Tregs expressing IL-33R appear to be particularly sensitive to IL-33 signaling, undergoing a 60-fold expansion in response to treatment with rIL-33 *in vivo*, as compared to other nonlymphoid tissue IL-33R+ Tregs isolated from peripheral tissues such as fat (10-fold) and skin (5-fold)[56]. Other transcription factors contributing to the core tissue Treg signature in the lung include *Nfil3, GATA-3,* and *Maf*, as well as the Delta-Notch signaling pathway, among others[55-57]. Notably, although tissue Tregs isolated from various non-lymphoid tissues share an overlapping "core" signature with lung tissue Tregs,

tissue-specific cues also appear to influence their overall phenotype, revealing a possible relationship for site-specific functions.

Data elucidating a comprehensive ascription of the functional capacities for respiratory tract tissue Tregs is still being accumulated. However, it is clear that lung tissue Tregs play a major role in respiratory immunity and resolution. One prominent example is the ability of lung tissue Tregs (defined as $CD44^{hi}CD62L^{lo}$ with increased expression of CD103, PD-1, GITR, CTLA-4 and KLRG1) to promote tissue healing through their production of Areg after influenza infection in mice[44]. Importantly, the selective deficiency of Areg production by Tregs results in profound tissue damage and decreased oxygen exchange but does not impact other Treg suppressive functions, demonstrating a non-redundant requirement for tissue Tregs to produce Areg. Perhaps not surprisingly, IL-18 and IL-33 signaling are pivotal in initiating the tissue repair program, including among non-infectious scenarios[44, 62]. Conversely, when IL-18 signaling is antagonized by Notch4, Tregs lose their ability to produce Areg resulting in severe morbidity, as has been recently demonstrated for COVID-19 disease[63]. Themes of lung tissue-specific roles for Tregs are further recapitulated by a model of chronic inflammation and fibrosis established by repetitive *Aspergillus fumigatus* challenge wherein lung tissue Tregs ($CD69^{hi}CD103^{hi}$) ameliorate Th2-mediated pathology in mice, possibly through immunosuppressive functions and/or the production of amphirgulin[47] (Figure 1.2). Notably, other mechanisms of tissue healing may also be mediated by Treg expression of the soluble growth factor, keratinocyte growth factor (KGF), which can be induced in Tregs derived from lung tissue in mice and humans[64]. Characterization of additional functions for respiratory tract tissue Tregs are still forthcoming,

but will likely include quintessential Treg functions, possibly with extra guidance from tissue-specific cues during homeostasis and insult.

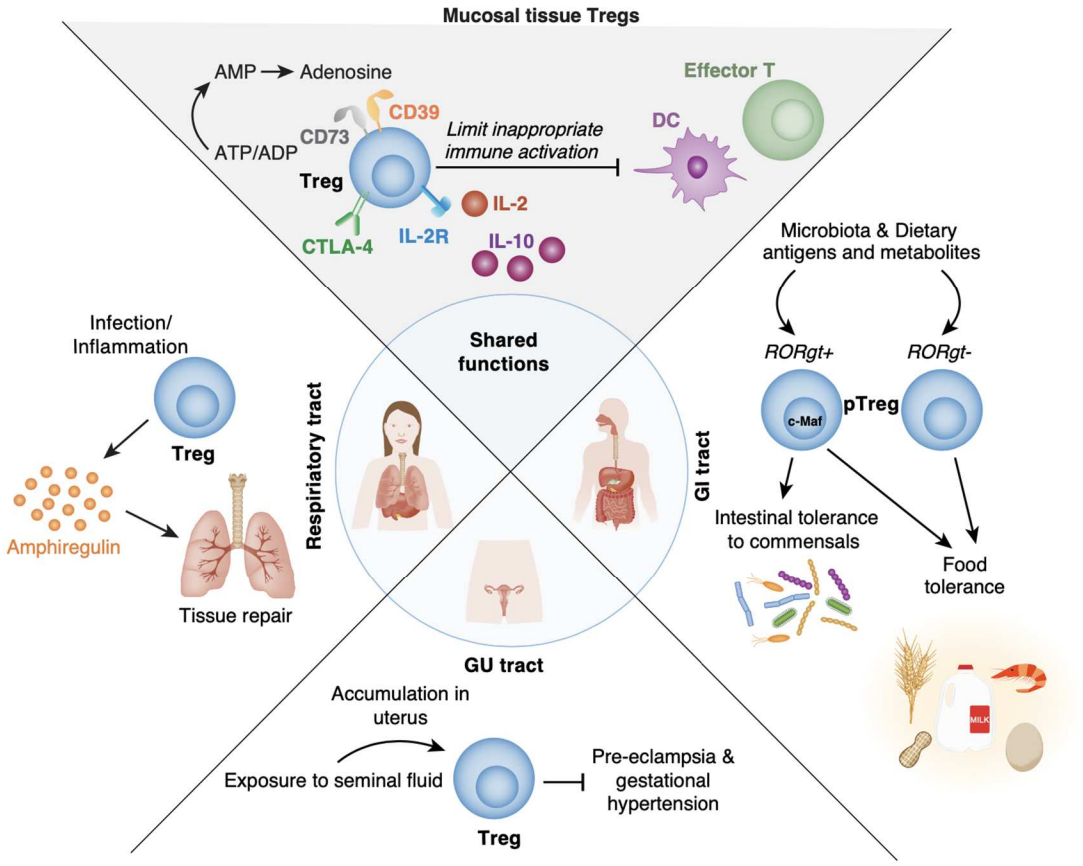

Figure 1.2. Mucosal tissue Tregs have both shared and specialized phenotypes and functions dependent on the tissue location.

Foxp3+ Tregs found throughout the body have immunosuppressive roles and can limit inappropriate inflammatory responses to self- and foreign antigens through a variety of mechanisms, including but not restricted to CTLA-4, ectoenzymes CD39 and CD73, IL-2 deprivation, and secretion of soluble regulatory mediators such as IL-10 and TGFβ. In addition, as has been demonstrated in non-mucosal and non-lymphoid tissues such as the visceral adipose tissue, skin, and muscle, Tregs can execute additional specialized functions that are induced by and meet the needs of their unique tissue environment. Here we highlight one example from each of the major mucosal tissue sites. In the respiratory tract, infection or inflammation can induce Tregs to produce amphiregulin, which promotes lung tissue repair. In the gastrointestinal tract, ingestion of dietary antigens early in life induces peripherally generated Tregs that are neuropilin-1 (NRP1) and Helios double-negative, as well as negative for the transcription factor RORγt. These cells have been shown to be critical for tolerance to dietary antigens, and so are major players in the prevention of food allergy. In addition, microbiota induces RORγt+ c-Maf+ pTregs that are crucial to maintain tolerance to both food and commensal bacteria. Finally, exposure to sperm and seminal fluid induces an increase in the number of Tregs present in uterine tissues, and Tregs have a demonstrated role in preventing pre-eclampsia and gestational hypertension.

In addition to immune responses to infection, respiratory tract Tregs have been implicated in restraining immune reactions to innocuous antigens to restrict allergic responses including asthma[65, 66]. In humans with loss-of-function mutations in *Foxp3* resulting in IPEX, clinical presentation includes not only autoimmune manifestations, but also severe allergic inflammatory conditions[67, 68], and mice with mutant *Foxp3* also spontaneously develop allergic airway inflammation[69]. Indeed, mouse model studies have demonstrated that Tregs can suppress Th2 responses to allergens through an IL-10-dependent mechanism and that Treg-mediated suppression of DC activation is also involved in restriction of the response[70, 71]. Furthermore, peripherally induced Tregs play a crucial role in restricting Th2-pathologies such as allergic inflammation and asthma in the lungs[72]. Consistent with this finding, patients with atopic asthma were documented to have decreased abundance of Tregs in bronchoalveolar lavage fluid[73].

Finally, whereas tissue-specific Tregs represent only a fraction of the total respiratory tract Treg population in SPF mice[56], it remains likely that this frequency would be impacted by antigen experience, such as in the context of "dirty/pet store" mice[74]. Interestingly, the frequency and distribution of tissue Tregs in humans appears to be related to age, wherein pediatric tissues demonstrate the highest frequencies of Tregs in mucosal and non-lymphoid tissues followed by a shift toward accumulation in lymphoid tissues during adulthood[75]. In this regard, whereas the total frequency of Tregs among total CD4+ T cells in the lung tissue of pediatric donors has been estimated to be roughly 15%, in adult lung tissue that number is reduced to roughly 5%. Phenotypically, among both children and adults, human lung tissue Tregs are mostly CD45RA- and CD69+, with a smaller fraction dually expressing CD103[75]. Importantly, each individual's past history of antigen experience is also likely to impact their current status[76-78]. Studies

examining the tissue-specific Treg TCR repertoire in the human respiratory tract will be influential[79]. Notably, among unmanipulated SPF mice, tissue context significantly impacts the Treg TCR repertoire wherein clonal diversity tends to be more restricted in peripheral tissues as compared to the spleen[57]. A final consideration, specific to the lung, is the elucidation of recent evidence demonstrating that respiratory tract tissue resident memory T cells (Trm) may, in fact, be more transient than has been reported for other peripheral tissues[80-82]. For example, the local draining lymph node may serve as a more permanent reservoir for respiratory Trm in lieu of long-term maintenance within the delicate pulmonary tissue[80], thereby raising the notion that respiratory tract Tregs may not persist long-term within the tissue parenchyma. In conclusion, studies further elucidating the functional capabilities, antigen-specificities, and longevity of respiratory tract-specific tissue Tregs among both mice and humans will be informative.

1.6 GASTROINTESTINAL TRACT MUCOSAL TREGS

The gastrointestinal (GI) tract, including the small intestine and colon, is the site of food ingestion and metabolite transport in addition to hosting a complex microbiome. Therefore, the mucosal GI immune system has the extraordinary task of tolerating orally ingested dietary antigens (a phenomenon known as oral tolerance)[83, 84] as well as beneficial commensal bacterial species (spp.), while concurrently providing barrier immunity against ingested and enteric pathogens (Figure 1.1). Tregs are crucial mediators of GI tract tolerance[84] and are maintained in high numbers in the GI tract, making up 20-30% of total CD4+ cells in the lamina propria of the small intestine and colon[85, 86]. Ablation of Tregs or mutations in *Foxp3* leads to systemic autoimmunity in mice and humans, including in the GI tract[5, 26, 87, 88]. Moreover, Tregs are necessary for prevention of GI tract inflammation and Inflammatory Bowel Diseases (IBD) such

as colitis[89, 90]. Due to the increased need for tolerance in the GI tract, Tregs have been widely studied in the small intestine and colon, and more than any other mucosal site, a large quantity of research has been published[91]. Here we provide a broad rather than exhaustive overview of the vast and nuanced field of GI tract Treg biology in both health and disease.

As we have briefly introduced, Tregs canonically arise in the thymus, where Foxp3 is expressed during thymic differentiation following relatively high avidity interactions of the TCR with self antigens[92-94]. These thymically derived Tregs have thus been termed tTreg[95] and are generally defined by the expression of the transcription factor Helios and cell surface receptor neuropilin1 (NRP1)[96, 97]. However, Tregs also arise in the periphery (pTreg) in response to particular signals generated under tolerogenic conditions, including TGFβ[98-101], and can sometimes express Helios despite having extra-thymic origins[102]. Given the major tolerogenic requirements of the GI tract, the colon and small intestine are a major site of pTreg induction[85, 95]. In the mouse and human colon, approximately 30-35% of Tregs are NRP1+ and Helios+[103, 104], suggesting that the majority of GI tract Tregs are induced locally[96, 97, 105]. However, some colonic Tregs share TCR repertoires with Tregs in the thymus, suggesting that the colon hosts a combination of both pTregs and tTregs[106]. Likewise, Helios+ Treg proportions are mouse strain-dependent and can vary greatly[107]. Numerous studies have identified pTreg to be critical for tolerance to dietary antigens and the microbiota; mice lacking pTregs present with increased type 2 immunity and pathologies as well as dysbiosis in the GI tract[72, 108], and pTreg have been shown to be important for preventing inappropriate responses to food antigens in the GI tract[109].

Given the demonstrated critical roles for pTreg in the GI tract, these cells have been intensely studied in recent years. pTregs in the GI tract can be further classified by expression of transcription factors associated with CD4+ effector T cell lineages. We will first discuss RORγt, the transcription factor associated with T-helper 17 (Th17) lineage differentiation[85]. In the mouse small intestine and colon, around 40% and 10%, respectively, of Tregs are negative for both RORγt and NRP1[85, 109]. In SPF mice weaned onto an antigen-free diet, small intestine NRP1^{lo} Treg numbers are reduced, mostly due to a loss of RORγt- Tregs[109]. Interestingly, SPF mice treated with antibiotics are depleted of RORγt+, but not RORγT- Tregs, demonstrating that dietary, but not microbial, antigens are crucial for induction of RORγt- Tregs[109]. Furthermore, SPF mice weaned onto an antigen-free diet followed by immunization and challenge with Ova develop intestinal allergy, implicating RORγt- pTregs in the prevention of food allergy[109] (Figure 1.2).

Thus, RORγt- Tregs in the small intestine, and, in smaller numbers, in the colon, are induced by dietary antigens and are also necessary for continued tolerance to food-derived antigens. Although preservation of dietary tolerance is mainly attributed to RORγt- Tregs, food allergy in human infants has been associated with a lack of microbiota-induced RORγt+ Tregs, and administration of oral antigen in mice increases RORγt+ Treg numbers, demonstrating a role for RORγt+ Tregs in maintaining tolerance to dietary antigens as well as to commensals[110-112]. Additionally, microbiota-induced pTregs arising around the age of weaning are later required to prevent spontaneous Th2-mediated allergic responses to dietary antigens and protect from dextran sodium sulfate (DSS)-mediated severe colitis in mice[113-115].

As briefly mentioned above, a large fraction of GI tract pTregs are RORγt positive. RORγt+ Tregs require expression of transcription factor c-Maf for development and function as highly suppressive Tregs that specifically regulate distinct T-helper subsets in different inflammatory contexts, such as limiting pathogenic Th17 inflammatory responses to *Helicobacter hepaticus*[103, 112, 116-118]. Many RORγt+ Tregs display a highly activated effector phenotype defined by expression of CD44, ICOS, and CTLA-4[111, 112, 116, 119]. IL-10, a critical anti-inflammatory cytokine, is constitutively expressed on a large percentage of RORγt+ Tregs in both the small intestine and colon, and a loss of IL-10 results in spontaneous colitis in mice and humans, demonstrating the importance of Treg-derived IL-10 in preventing GI tract inflammation and immunopathology[15, 120-122].

In the mouse colon, 40-60% of Tregs are RORγt+, while RORγτ+ Tregs make up a smaller fraction of small intestine Tregs[85, 103, 107, 112, 116]. In humans, IL-17-producing Tregs are found in the circulation and in the microenvironment of chronic ulcerative colitis[123], and circulating RORγT+ memory Tregs can be found in humans[124]. RORγt+ Treg abundance in small intestine and colon is dramatically reduced in germ-free mice or mice treated with antibiotics[103, 109, 112, 125], demonstrating that the commensal microbiota is required for the generation of RORγt+ Tregs. A loss of RORγt+ Tregs in mice results in increased Type-2 immune responses and more severe oxazolone-induced colitis, suggesting that commensals regulate intestinal immune responses through induction of RORγt+ Tregs[112]. Furthermore, local bacterial antigens mediate colonic pTreg selection, especially for RORγt+ Tregs[104, 109, 125, 126]. In support of Treg induction by commensal antigens, mouse colonic Tregs express TCR specific for *Clostridium* and commensal spp. that normally colonize the GI mucosal layer and expand in the presence of commensal

bacteria[126]. Other commensals such as lactobacilli and bifidobacteria also increase induction and maturation of GI tract Tregs[85]. In summary, the small intestine Treg compartment is predominantly RORγt- and responsible for dietary tolerance, while colonic RORγt+ Tregs facilitate tolerance to commensal microbiota, but this distinction is not finite and GI tract Treg phenotype and function overlap.

GI tract pTregs are also heavily influenced by dietary and commensal-derived metabolites. Compared to Tregs in other tissues or lymphoid organs, Tregs in the mouse small intestine and colon express more aryl hydrocarbon receptor (AhR)—a nuclear sensor of dietary, microbiota, and other derivatives[127]— suggesting an elevated AhR-mediated metabolite dependence in GI tract Tregs[91, 103, 128]. Tryptophan, which can be metabolized by commensal microbiota into various AhR ligands[127], promotes Treg development through various mechanisms[91, 129]. Retinoic acid (RA), the bioactive derivative of vitamin A, is abundantly found in the GI tract and induces pTregs in mice when in combination with TGFβ[91, 130-132]. Likewise, mice given Vitamin A-deficient diets or RA inhibitors display reduced RORγT+ but not Helios+ Treg numbers, suggesting a specific requirement for Vitamin A in the RORγT+ Treg population in the GI tract[91, 112]. Among others, vitamins D3 and B9 promote expression of Foxp3 and anti-apoptotic BCL-2 on colonic Tregs[85, 133, 134]. Although some Treg:metabolite processes function independently of the microbiota, others rely heavily on bacteria. Commensals facilitate metabolite production by fermenting dietary fiber to produce short chain fatty acids (SCFA) and other products that promote pTreg induction, expansion, and function, especially in the mouse colon[91, 112, 135-137]. Bacterial products can also function as Toll-like receptor (TLR) ligands, adjuvanting the induction and function of GI tract pTregs[85, 91, 138-141]. Recently, gut bacteria have

been shown transform bile acids into bioactive products that modulate local Treg function and promote pTreg induction in mouse and humans[142-144].

A third population of GI Tregs expressing GATA3, the master transcription factor for T-helper 2 (Th2) CD4+ T cell differentiation, make up around 20 and 15 percent, respectively, of mouse small intestine and colon Tregs[85, 112, 145, 146]. In humans, GATA3+ Tregs have thus far only been identified in blood[91]. GATA3 directly interacts with Foxp3 to regulate FoxP3 expression and transcriptional programs[111, 147, 148]. GATA3+ GI tract Tregs express Helios and are stable under germ-free conditions, suggesting thymic origins[103, 112]. GATA3+ Tregs express IL-33R, which recognizes IL-33, an alarmin produced by intestinal epithelial cells during inflammation[145, 146]. IL-33R ligation, along with TCR activation and IL-2, activates GATA3[145], which drives Treg-mediated suppression. A loss of GATA3 expression abrogates accumulation of Tregs in the small intestine, particularly in the context of inflammation, where GATA3+ Tregs are critical to protect mouse GI tissues from collateral immunopathology during enteric infection with pathogenic microbes[145]. Additionally, small intestinal Tregs maintain epithelial barrier integrity by preserving intraepithelial cells (IEC) though various IL-10-mediated mechanisms in mice[149], where the IEC physically separates lamina propria immune cells and the microbiota in the intestinal lumen[111]. Thus, GATA3+ Tregs are important for regulation of type-2 immunity and respond to cognate antigen and alarmins during inflammatory events to preserve GI tract tissues[111]. Further research is warranted to resolve whether GATA3+ Tregs also directly contribute to tissue repair, as is seen in other IL-33R+ Tregs[30, 38, 44, 111].

In addition to maintaining tolerance to commensal and dietary antigens, GI Tregs also contribute to humoral mucosal functions such as control of germinal center reactions to promote secretion of immunoglobulin A (IgA), which blocks invading pathogens from attaching to the mucosal epithelium[150]. Conversely, a loss of c-Maf+ RORγt+ Tregs leads to excessive, Th17 and IgA responses[118], suggesting that GI tract pTregs balance protective vs pathogenic mucosal humoral responses. Mouse Tregs expressing B cell lymphoma 6 (BCL-6) migrate via CXCR5 to Peyer's patches germinal centers where these Follicular Tregs (Tfr) control Tfh responses, thereby encouraging IgA production[151]. Small intestine Tregs specific for commensal flagellin antigens dampen mucosal uptake of commensal antigens through supporting production of IgA, in turn limiting local T cell activation and further maintaining tolerance to the microbiota in mice[152]. Finally, some GI Foxp3+ Tregs that receive environmental cues within Peyer's patches may convert into Tfh cells, in the process losing Foxp3 expression, to then interact with B cells in mice[153].

1.7 GASTROINTESTINAL TRACT MUCOSAL TREGS IN CANCER

While Tregs in the small intestine and colon are indispensable for maintaining appropriate immune tolerance during homeostasis, colonic Tregs within the aberrant context of a cancer environment can be counterproductive. Tregs, including those expressing cytotoxic molecule granzyme B, are enriched in colorectal cancer (CRC), colon-draining lymph nodes, and other tumor sites and are associated with poorer disease prognosis in mouse and humans, likely related to the suppression of anti-tumor effector T cells[154-159]. Tumor environment-mediated immune dysbiosis may abnormally increase Treg recruitment to the tumor through chemotactic receptors or by expanding Tregs through TGFβ or IL-10[160, 161], where they dampen anti-tumor immune

responses. To combat tumor-driven accumulation of Tregs in CRC tumors, therapeutic strategies to eliminate Tregs or block their suppressive functions may help to promote anti-tumor effector T cell immunity[155]. However, the role of Tregs in CRC is nuanced and context-dependent, as Tregs can also protect the mouse and human host from cancer-associated inflammation[162, 163] and BLIMP-1+ Tregs and Treg-derived IL-10 have been associated with decreased polyps and increased CRC survival in both mice and humans[164-166]. Together, these conflicting results suggest that distinct Treg subsets may perform distinct functions in intestinal cancers[167, 168]. For example, in mice, Treg-specific loss of transcription factor TCF-1 expression, a suppressor of genes co-bound by FoxP3, increases Treg-mediated T cell suppression and promotes tumor growth in polyposis, demonstrating a role for Treg TCF-1 expression in tumor clearance[169]. Additionally, tumor-infiltrating Tregs in human CRC express low TCF-1 expression, suggesting that TCF-1 expression levels may predict CRC outcomes[169]. Therefore, Treg involvement in mucosal tumor immunity warrants further study to understand which Treg subsets may predict improved CRC outcomes and which subsets could be targeted therapeutically to increase survival.

Treg dysfunction has major implications for chronic and debilitating GI tract disease; therefore, additional research is necessary to elucidate potential Treg-targeting therapies to ameliorate IBD and allergy. Furthermore, oral vaccine delivery is an attractive route as a non-invasive vaccine strategy that could induce protective immune responses at the mucosal barrier, as tissue-resident memory T cells (Trm) are known to be indispensable for protection from mucosal infections such as herpes simplex virus 2 (HSV-2)[170]. However, further studies are needed to understand

how to best leverage mucosal immune responses, including Tregs, at the site of infection while overcoming the tolerogenic tendencies of the oral mucosa and GI tract[84, 171-174].

1.8 GENITOURINARY TRACT MUCOSAL TREGS

The genitourinary (GU) tract, comprised of the urinary and reproductive organs, requires paradoxical immune responses. The mucosal GU tissues such as the vagina, cervix, and uterus serve as the entry point for both reproductive sperm and sexually transmitted infections (STIs). Therefore, the GU tract must be at once tolerant to select foreign antigens and commensal bacteria, while hostile to invading STI, poising the GU tract as a unique and complex immunological site. Mucosal Tregs are likely to be critical for facilitating the balance between tolerance and immunity.

A healthy mammalian pregnancy requires careful immune tolerance at every stage, from the introduction of male sperm to the end of successful gestation. During sexual reproduction, the GU tract immune system must allow sperm, a foreign antigen, and a fetus— essentially a semi-allogeneic graft—to be tolerated for an extended period. Tregs in the blood and at the maternal-fetal interface in the placenta increase during pregnancy and are known mediators of fetal tolerance, preventing spontaneous abortion, fetal resorption, and preeclampsia in mice and humans[175-178]. Given the critical need for Treg-mediated tolerance during pregnancy, it is unsurprising that Tregs resident in the mucosal GU tract also play a role in pregnancy. As early as first exposure to male seminal antigens and before embryonic implantation, Tregs accumulate in the uterus and uterine-draining lymph nodes in mice[179-181]. During pregnancy, CD25+ cells increase two-fold in the mouse iliac and inguinal lymph nodes and make up 30% of uterine

CD4+ T cells, and in both allogeneically and syngeneically mated mice, uterine *Foxp3* mRNA concentration is 1000-times higher than in age-matched non-pregnant mouse uterine tissue, suggesting a robust increase in uterine Tregs during pregnancy[175]. A reduction in Tregs in early pregnancy causes uterine artery dysfunction in mice, demonstrating a tissue-specific role for Treg-mediated prevention of gestational hypertension and preeclampsia[182] Given that immune responses in both mouse and human have been shown to be dampened during the luteal phase of the estrus cycle and in response to seminal extracellular vesicles, it is possible that GU mucosal Tregs in the uterus and vagina have additional immunosuppressive roles to promote pregnancy at the early stages of conception[183-187]. Treg-focused cellular therapies could be useful in preventing and treating preeclampsia and other pregnancy complications, but further research in humans is needed to design diagnostic tests for Treg function in early pregnancy and to identify the temporal window in which intervention is safe and effective[188].

Historically, Tregs are understudied in the cervical and vaginal mucosa. However, as a barrier tissue site with constitutive exposure to commensal microbiota, plus the potential for exposures to male seminal antigens and microbial pathogens, the dynamics of the vaginal immune system must be carefully orchestrated, likely in part by Tregs. In humans, the healthy vaginal mucosa hosts a microbiome dominated by *lacotobacillus,* and dysbiosis of the vaginal microbiome causes harmful overgrowth of fungal and bacterial pathogens, leading to bacterial vaginosis (BV), vaginal candidiasis, urinary tract infections, and dysregulated vaginal pH, all of which increase susceptibility to STIs and infertility[189, 190]. As in the GI tract, the vaginal immune system must remain tolerogenic to commensal bacteria while allowing for appropriate immune responses to deleterious microbes; therefore, we hypothesize that Tregs in the vagina may also

facilitate tolerance to commensal microbiota. In support of this, vaginal isolates of *Lactobacillus crispatus*, a predominant species of healthy vaginal bacteria, induces Tregs from conventional CD4+ T cells in a human mixed leukocyte reaction[191]. Vaginal dysbiosis such as BV or abnormal vaginal dominance by anerobic bacterial communities is associated with increased pro-inflammatory cytokines in the vagina and decreased peripheral Treg numbers, suggesting that a breach in normal vaginal commensals triggers a switch from tolerogenic to anti-microbial immune responses[190, 192, 193]. Thus, further studies are necessary to determine how Tregs may facilitate the tolerance:inflammation axis based on the presence of either commensals or harmful bacterial spp.

Vaginal and uterine Tregs help maintain a healthy mucosal environment during homeostasis and pregnancy, but they also facilitate appropriate immune responses to harmful pathogens. In vaginal herpes simplex virus 2 (HSV-2) infection in mice, Tregs in the vaginal-draining lymph nodes (dLN) are necessary to promote proper antigen-bearing dendritic cell (DC) migration from the vagina to the dLN, and a loss of these Tregs delays HSV-2-specific CD4+ T cell priming and results in worsened disease[194, 195]. This demonstrates that Tregs in the dLN tune the antiviral CD4 T cell responses in the nearby vaginal tissue. Moreover, Tregs accumulate in the mouse vaginal mucosa early after HSV-2 infection, suggesting an additional need for Treg-mediated immune regulation at the site of infection[194, 195]. Given the multitude of pathogens that may contact the vaginal mucosa, vaginal tissue Tregs likely have important roles in immune response coordination, such as limiting excessive inflammation during infection to prevent collateral immune-mediated tissue damage. In support of this, Treg-related cytokines exert anti-inflammatory effects during infection with *Trichomonas vaginalis*[196]. In the human endocervix,

Tregs are inversely correlated with inflammatory cytokine concentrations and abundance of CD4+ T cells, suggesting that Tregs in the GU tract prevent genital inflammation and could potentially lower HIV acquisition risk through limiting HIV target cell availability[197]. Importantly, the roles of vaginal and uterine Tregs must be considered when designing mucosal vaccines, as Tregs promote anti-pathogenic immunity in some contexts, but dampen mucosal Trm responses in others. For example, mice given intra-uterine immunization with non-adjuvanted UV-killed Chlamydia trachomatis induces uterine Tregs that abrogate the effects of local effector T cells elicited by the vaccine[198]. Additionally, vaginal Tregs may directly contribute to tissue repair through production of Areg after infection or injury, as has been shown in lung and muscle-resident Tregs in mice[30, 38, 44]. Further vaginal Treg studies in both mouse and especially in human are necessary to determine how vaginal Tregs modulate local anti-pathogen immune responses, prevent mucosal tissue damage, and potentially execute unique, location-specific functions.

1.9 Implications for mucosal Tregs

Peripheral Tregs are key mediators of systemic immune tolerance and immune orchestration, and mucosal tissue Tregs are no exception. In fact, Tregs at mucosal sites are charged with the paradoxical and highly nuanced role of facilitating protective immune responses to invading pathogens, while also allowing for immune quiescence in the context of sexual reproduction, inhaled or ingested harmless antigens, and commensal microbiota (Figure 1.1). This immune balance is especially critical within the very delicate and highly specialized mucosal tissues. Interestingly, although Tregs found in various mucosal tissues share the responsibility of balancing inflammatory immune responses, residency in distinct tissues is associated with

previously unappreciated location-specific functions that lie beyond canonical Treg roles (Figure 1.2). These specialized mucosal Tregs have implications for conditions such as allergy, autoimmunity, and cancer, where aberrant mucosal immune responses drive disease progression.

1.10 FUTURE DIRECTIONS AND THESIS GOALS

The role of mucosal Tregs in anti-microbial immunity—especially in STIs—should not be underestimated. Importantly, immunity elicited by mucosal vaccination, depending on the context, may be either hindered or helped by Tregs. Therefore, further studies are necessary to elucidate how to best leverage Tregs to overcome oral tolerance and elicit protective resident T cells responses at the sites of bacterial and viral infection. Based on this growing body of mucosal Treg data, there is precedent to continue to characterize Tregs in other mucosal and non-lymphoid tissue sites, which they may perform distinct, yet-unknown tissue-specific functions.

This thesis aims to investigate the previously uncharacterized Treg population in the vaginal mucosa of mice and humans, a barrier tissue that has important roles in both tolerance to pregnancy and immunity to STIs. This thesis will contribute to the existing body of mucosal Treg literature, summarized in Chapter 1, by defining a previously unknown location-specific phenotype and function of vaginal Tregs in both health viral infection, which is highly nuanced and context-dependent. Additionally, this thesis explores how vaginal Tregs may have non-canonical roles in the vaginal mucosa during infection or inflammation, which has implications for mucosal vaccine design and Treg-focused therapeutics for mucosal infection.

Using both human tissues and mouse models, Chapter 2 will describe the phenotype and function of vaginal Tregs during both homeostasis and after primary infection with HSV-2. Additionally, this chapter investigates the signals that drive the phenotype of vaginal Tregs. Chapter 3 will explore the role of Tregs in limiting immune-mediated vaginal pathology during HSV-2 challenge. Chapter 4 will discuss the implications of these findings as well as limitations and future directions raised by this body of work.

Chapter 2. MUCOSAL VIRAL INFECTION INDUCES A REGULATORY T CELL ACTIVATION PHENOTYPE DISTINCT FROM TISSUE RESIDENCY IN MOUSE AND HUMAN TISSUES

2.1 INTRODUCTION

Regulatory T cells (Tregs) are a subset of CD4+ T cells defined by the expression of transcription factor forkhead box P3 (FoxP3)[1, 7-9, 13]. Tregs are potent suppressors of other immune cells, and extensive research has shown Tregs to be critical in preventing aberrant immune responses to self as well as to dietary and commensal antigens. A loss of Tregs or FoxP3 leads to lethal autoimmunity, chronic inflammation, and allergy[3-6, 26, 85]. Early Treg studies focused on their development in the thymus and Tregs in lymphoid organs, where they promote peripheral tolerance, but more recently, Treg subsets have been identified in discrete tissue compartments such as hair follicles, skin, muscle, and visceral adipose tissue (VAT)[30-35, 37, 38, 199]. Although these tissue Treg populations share hallmarks of tissue residency, these populations have distinct transcriptional profiles, phenotypes, and clonally expanded T cell receptor (TCR) repertoires that do not overlap with lymphoid Treg counterparts or conventional T cells from the same tissue compartment[30, 32, 37, 51, 200]. Additionally, tissue Tregs carry out location-specific functions outside of their canonical suppressive roles. For example, in response to Interleukin-33 (IL-33) released by stromal cells during skeletal muscle injury, Tregs directly contribute to tissue healing by producing growth factor amphiregulin (Areg)[30, 38]. In the VAT, Tregs facilitate adipocyte metabolism and maintain insulin sensitivity through expression of peroxisome proliferator-activated receptor (PPAR)-g, the master regulator of adipocyte differentiation[31, 35, 37].

Thus, Treg functions extend beyond classical suppressor roles and are highly location-dependent, suggesting that other tissue sites may host their own specialized Treg populations.

More recently, distinct Treg phenotypes and functions have also been identified in mucosal tissues. The mucosa serves as a barrier against pathogens as well as the site of specialized functions such as nutrient and air exchange, necessitating that Tregs orchestrate carefully controlled, specialized immune responses. In the small intestine and colon, both thymically derived and peripherally induced Tregs contribute to gut homeostasis by facilitating oral tolerance to dietary antigens, commensal bacteria, and preventing Inflammatory Bowel Diseases (IBD)[85, 111]. Likewise, lung Treg populations are implicated in preventing allergy and airway inflammation[65-68, 70-73], and like muscle Tregs, have been shown to produce Areg in response to lung damage[44]. These discoveries suggest that specialized Tregs may be overseeing immune responses and performing yet-unknown functions in other mucosal tissues.

While Tregs have been extensively studied in homeostasis and the context of autoimmunity, the role of Tregs during infection is less defined and varies by infection[2, 29]. In the GI tract, GATA3+ Tregs prevent excessive inflammation during enteric infection, protecting the delicate mucosal tissues of the colon and small intestine[85, 145]. Likewise, lung Tregs promote influenza-specific T cell responses by regulating interleukin 2 (IL-2) availability, while concurrently preventing T cell-mediated lung pathology and producing Areg to resolve lung damage after infection[39, 41, 44, 49]. During vaginal infection with herpes simplex virus 2 (HSV-2), peripheral Tregs facilitate proper migration of antigen-bearing dendritic cells (DCs) to the vaginal-draining lymph node (dLN), and systemic Treg ablation causes a delay in antigen-specific T cell priming, associated

with worsened viral-mediated disease[194, 195]. Additionally, CD25+ Tregs limit T cell-mediated stromal keratitis in the cornea of mice infected with ocular herpes simplex virus type 1 (HSV-1)[201]. In other infection scenarios, the role of Tregs is highly nuanced. During lung infection with *mycobacterium tuberculosis* (Mtb) or respiratory syncytial virus (RSV) and during skin infection with *Leishmania major* (L. major), Tregs inhibit productive T cell responses, resulting in compromised pathogen clearance[50, 51, 202, 203]. However, removal of Tregs in these contexts leaves effector responses unchecked, resulting in T cell-mediated tissue damage and disease[50, 51, 202, 203]. In the case of RSV, Tregs have been reported to utilize granzyme B (GzmB) to kill effector CD8+ T cells[19], suggesting a possible additional mechanism for Tregs in preventing immunopathology. Together, these findings demonstrate that in infectious contexts, Tregs serve as a fulcrum between immunity and tolerance, tasked with allowing for productive effector immune responses while also limiting collateral tissue damage caused by aggressive inflammatory responses.

Tregs have now been described in various mucosal tissues and infections, but Tregs in the female genitourinary (GU) tract, including the uterus, cervix, and vaginal mucosa, are understudied in both health and infection. GU tissues are extraordinary in that they are the home of the tolerogenic processes of conception and pregnancy, but also the entry site of sexually transmitted infections (STIs). Therefore, the GU tract must facilitate tolerance to commensal bacteria, reproductive antigens, and the fetus, while also mounting early immune responses against invading infection. Although there is some evidence for uterine Treg-mediated tolerance during pregnancy[175, 179-181], GU tract Tregs, and more specifically vaginal tract (VT) Tregs, remain

poorly characterized. Considering the paradoxical immunological requirements of the vagina, it is likely that Tregs are crucial in maintaining the tolerance:immunity axis in this mucosal site.

Given the precedent for mucosa-localized Treg populations and the unique tolerogenic environment of the vagina, we hypothesized that VT Tregs are a unique, tissue-resident population that perform specialized functions in homeostasis and infection. To test this, we used flow cytometry and RNA-sequencing (RNA-seq) to interrogate the previously uncharacterized vaginal Treg compartment at homeostasis in mouse and human tissues. We then compared baseline Treg phenotypes to Tregs during active, local viral infection in mice. Finally, we investigated the inflammatory signals that drive differential phenotypes in vaginal Tregs. In summary, we demonstrate that vaginal mucosal Tregs in healthy mice and humans are more activated compared to circulating Tregs, suggesting that vaginal tissue localization alone confers a distinct phenotype on local Tregs. However, we also show that upon vaginal infection with HSV-2, vaginal Tregs become further activated, including the acquisition of robust, cytotoxic GzmB expression. We found that IL-2 in combination with type-I interferons (IFN-I) induce expression of GzmB on Tregs, uncovering the inflammatory cues that orchestrate Treg expression of GzmB. Overall, our findings demonstrate that the previously unstudied vaginal Treg population is constitutively activated in homeostasis but becomes further activated after infection, gaining expression of GzmB. These Tregs may be poised with cytotoxic potential to regulate local inflammation upon viral challenge.

2.2 RESULTS

2.2.1 *Vaginal mucosal Tregs in healthy women are activated compared to circulating Tregs*

To phenotype human VT Tregs, we analyzed collection time-matched vaginal mucosal biopsies and peripheral blood mononuclear cells (PBMC) from 14 healthy Seattle-area women without any known genital tract infections (Figure 2.1A, Table A). Using flow cytometry, Tregs were identified as CD3+CD4+CD25+CD127-FoxP3+, conventional CD4 T cells (CD4Tconv) as CD3+CD4+CD25-, and CD8 T cells as CD3+CD8+ (Figure 2.1B; Figure 2.2 and Table B). The average Treg frequency, quantified as the percentage of CD25+CD127-FoxP3+ cells of total CD4+ cells, was similar at approximately 3% in PBMC and VT, suggesting that a sizeable population of Tregs comparable to blood Treg frequency reside within healthy human vaginal tissue (Figure 2.1C). CD69 and integrin α_E (CD103) canonically define tissue-resident memory T cells (Trm)[204]. We quantified CD69 and CD103 expression on Tregs, CD4 Tconv, and CD8 T cells from PBMC and vaginal mucosa. As expected, T cells from blood were largely CD69-CD103-, while a majority (60%) of CD8 cells in the VT were double-positive for CD69 and CD103 (Figure 2.1D), consistent with our previous report[205]. A smaller fraction of CD4Tconv (30%) and only 3% of Tregs were CD69+CD103+, while the majority of vaginal Tregs were CD69+CD103- (67%), suggesting that CD103 expression may not be necessary for Treg mucosal tissue residency, as has been shown for other CD4+ Trm[206, 207] (Figure 2.1E).

We next sought to further phenotype these tissue Tregs. We performed surface and intracellular flow cytometry staining for markers of Treg activation and suppressive capacity, including glucocorticoid-induced tumor necrosis factor-related receptor (GITR), T-cell immunoglobulin and ITIM domain (TIGIT), Cytotoxic T-Lymphocyte Associated Protein 4 (CTLA-4), Inducible

T-cell costimulator (ICOS), and CD39[208]. We found that a significantly higher percentage of VT Tregs compared to blood Tregs expressed each of these markers (ICOS:5-fold increase, p =.0035; TIGIT: 1.5-fold, p <.0001; CD39: 1.7-fold, p <.0001; CTLA-4: 3.2-fold, p <.0001; GITR: 80-fold, p <.0001), demonstrating that human vaginal tissue Tregs, at baseline, appear more activated than their circulating counterparts (Figure 2.1F). Together, these findings suggest that a pool of highly activated tissue-localized Tregs are maintained in the vaginal mucosa of healthy women and are poised to rapidly modulate immune responses.

Table A. Human study participant demographics.

Human study participant demographics										
Age	Race	Ethnicity	HSV type 1	HSV type 2	Estradiol	unit	Progesterone	unit	Date of biopsy	Comments
32	White	Not hispanic or latino	Positive	Negative	62	pg/mL	0.3	ng/mL	8/5/19	
21	White	Not hispanic or latino	Positive	Negative	125	pg/mL	11.7	ng/mL	7/24/19	
23	Asian	Not hispanic or latino	Negative	Negative	<30	pg/mL	1.3	ng/mL	7/17/19	
37	American Indian, Asian, White	Hispanic or latino	Negative	Negative	<30	pg/mL	0.3	ng/mL	9/18/19	
23	Asian	Not hispanic or latino	Negative	Negative	<30	pg/mL	0.4	ng/mL	9/24/19	
45	White	Not hispanic or latino	Positive	Negative	34	pg/mL	1	ng/mL	10/1/19	
27	White	Not hispanic or latino	Positive	Negative	40	pg/mL	1.2	ng/mL	9/30/19	
29	American Indian, Black, White	Not hispanic or latino	Positive	Negative	245	pg/mL	0.6	ng/mL	11/5/19	
47	White	Not hispanic or latino	Positive	Negative	40	pg/mL	0.8	ng/mL	1/22/20	
27	White	Not hispanic or latino	Negative	Negative	72	pg/mL	0.5	ng/mL	1/29/20	Presence of candida on pap smear
26	Black, white	Not hispanic or latino	Negative	Negative	61	pg/mL	1.8	ng/mL	2/11/20	5/6 biopsies collected
26	White	Not hispanic or latino	Negative	Negative	<30	pg/mL	0.6	ng/mL	2/18/20	
26	White	Not hispanic or latino	Positive	Negative	<30	pg/mL	0.3	ng/mL	2/27/20	
29	White	Not hispanic or latino	Negative	Negative	51	pg/mL	0.8	ng/mL	2/27/20	

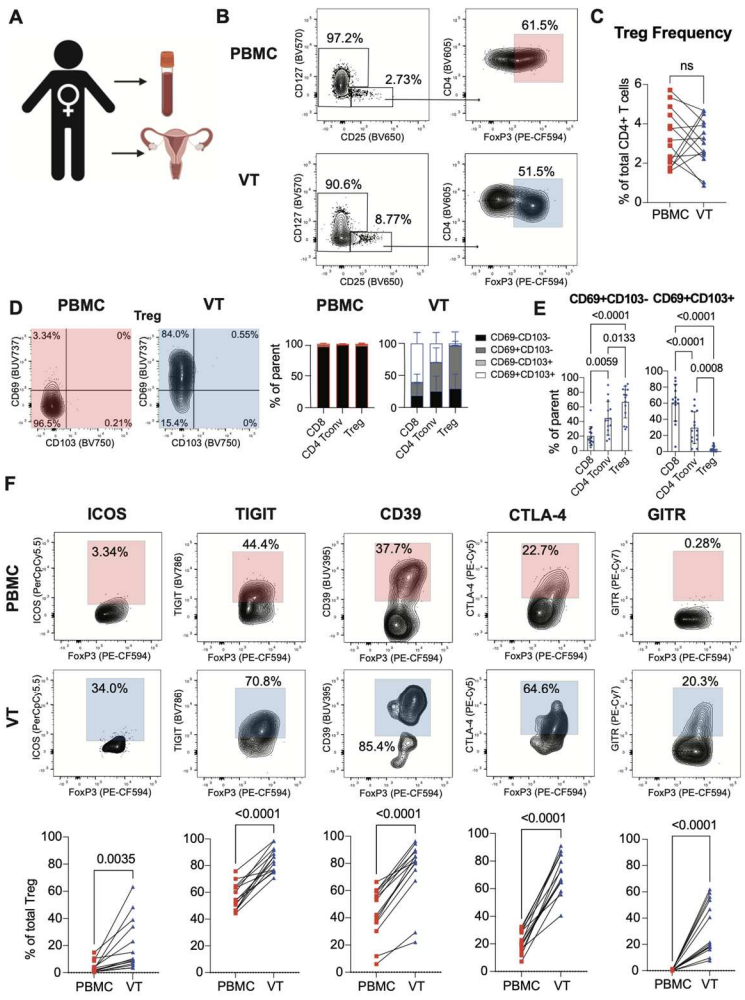

Figure 2.1. Human regulatory T cells in the vaginal mucosal display increased activation potential compared to circulating Tregs.

A) Peripheral blood mononuclear cell (PBMC) and paired mucosal biopsies from the vaginal tract (VT) were obtained from 14 healthy adult women with no genital tract infections. **B)** Tregs were identified by flow cytometry as CD4+CD127-CD25+FoxP3+ cells. **C)** Donor-matched frequency of Tregs out of total CD4+ T cells in PBMC and VT . **D)** Representative CD69 and CD103 staining, gated on Tregs (left), and CD69+ and CD103+ fractions of CD8, CD4 Tconv, and Treg populations from PBMC and VT, as a percentage of parent population (right). **E)** CD69+CD103- (left) and CD69+CD103+ (right) fractions of CD8, CD4 Tconv, and Tregs from VT. Significance determined by One-way ANOVA followed by Tukey's multiple comparisons test, $p < .05$. **F)** Representative Treg activation marker staining on PBMC (red) and VT (blue), gated on Tregs (top). Donor-matched frequencies of activation markers in PBMC and VT, gated on Tregs (bottom). n=14, Significance defined by paired t test; $p < .05$.

Table B. Human Treg flow cytometry panel.
Antibodies used for human blood and tissue flow cytometry analysis in Figures 2.1 and 2.2.

Human Treg flow cytometry panel				
Antigen	**Conjugate**	**Clone**	**Company**	**Dilution**
Viability stain (in 1X PBS)				
L/D	eFluor450	NA	Thermo Fisher Scientific	1:1000
Surface stain (in FACS buffer)				
CD39	BUV395	TU66	BD	1:40
CD8	UV500	RPA-T8	BD	1:500
CD3	UV661	UCHT1	BD	1:200
CD69	UV737	FN50	BD	1:50
CD45	BUV805	HI30	BD	1:200
LAG-3	BV421	11C3C65	Biolegend	1:80
CCR5	BV510	J418F1	Biolegend	1:80
CD127	BV570	A019D5	Biolegend	1:80
CD4*	BV605	RPA-T4	BD	1:40
CD25	BV650	BC96	Biolegend	1:80
Tim-3	BV711	7D3	BD	1:160
CD103	BV750	Ber-ACT8	BD	1:250
TIGIT	BV786	741182	BD	1:80
CCR7	AF488	G043H7	Biolegend	1:80
CXCR3	BB660	1C6-CXCR3	BD	1:40
ICOS	PerCp-Cy5.5	DX29	BD	1:80
CD101	BB790	V7.1	BD	1:160
GITR	PeCy7	108-17	Biolegend	1:80
IL33R**	APC	hIL33Rcap	Invitrogen	1:10
CD45RA	APC-H7	HI100	BD	1:40
Intracellular stain (in 1X eBioscience FoxP3/Transcription factor perm buffer)				
TCF-1	PE	C63D9	Cell Signaling	1:40
FoxP3	PE-CF594	236A/E7	BD	1:20
CTLA-4	PE-Cy5	BNI3	BD	1:160
Granzyme B	AF700	GB11	BD	1:80

*Some samples were stained with PD1, BV605, clone EH12.2H7, Biolegend, 1:20
**Some samples were stained with CD4, AF647, clone RPA-T4, Biolegend, 1:40

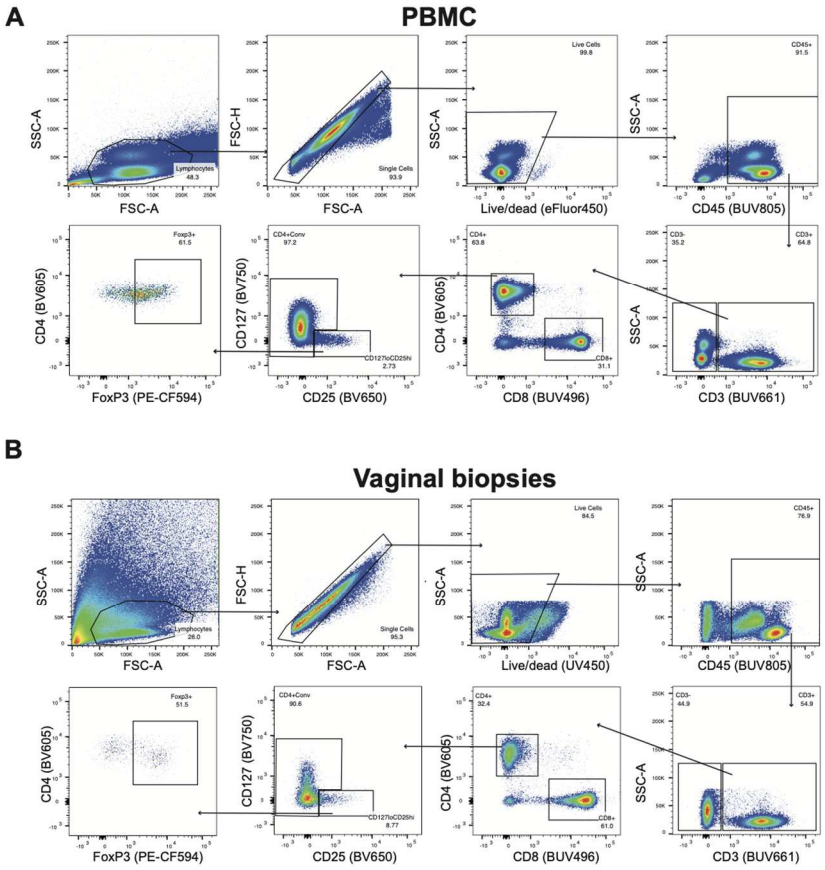

Figure 2.2. Human flow cytometry gating

Gating strategy for identifying Tregs, CD4Tconv, and CD8 T cells from **A)** blood and **B)** vaginal biopsies in flow cytometry from Figure 2.1.

2.2.2 *Vaginal tissue Tregs are activated compared to lymphoid Tregs in healthy mice*

However, although the biopsies were collected from women without any active infections, we could not rule out the possibility that local inflammation due to environmental antigens or sexual activity was driving activation in vaginal Tregs. To determine if the distinct VT Treg phenotype resulted from vaginal tissue residency alone, or alternatively, arose in response to active inflammatory signals, we employed a mouse model wherein inflammation and antigen exposure could be tightly controlled. To characterize VT Tregs, naïve C57BL/6J mice were synchronized

in the diestrus phase of the estrus cycle with a subcutaneous (s.c.) injection of medroxyprogesterone acetate (depo provera) 5-7 days before harvest[209]. VT and vaginal-draining lymph nodes (dLN) were harvested and stained with fluorescent antibodies for flow cytometry analysis (Table C). To exclude T cells derived from the circulation that could be contaminating VT tissues, mice were injected with intravascular (i.v.) CD45.2 antibody 3 minutes prior to sacrifice[210, 211] (Figure 2.3) and i.v. label+ cells were excluded from flow cytometry analysis in VT samples. Tregs, identified as CD4+FoxP3+, were assessed by flow cytometry and quantified as a percentage of total CD4+ T cells in each tissue (Figure 2.4, Figure 2.3). As previously reported[194, 195], Tregs in the dLN accounted for approximately 11% of total CD4+ cells; however, we found that they constituted an average of 21% of total vaginal CD4+ cells, demonstrating that Tregs make up a disproportionately large, albeit not statistically significantly different, fraction of vaginal CD4+ T cells (Figure 2.4A). Similar to our analysis of human Tregs, we then phenotyped VT and dLN Tregs and found that a significantly higher frequency of VT compared to dLN Tregs expressed activation markers CTLA-4 (1.5-fold increase; $p = .0012$) and GITR (1.6-fold increase, $p = .0004$) at steady state and although not significant, ICOS trended similarly (1.6-fold, $p > .05$ Figure 2.4B). However, CD69, which is also an indicator of recent activation[212] in addition to being a tissue residency marker, was comparably expressed in VT and dLN Tregs (Figure 2.4B). Thus, the VT Treg phenotype in naïve mice mirrored the heightened activation observed in healthy human VT Tregs, suggesting that VT tissue localization alone is at least partially responsible for the elevated activation potential.

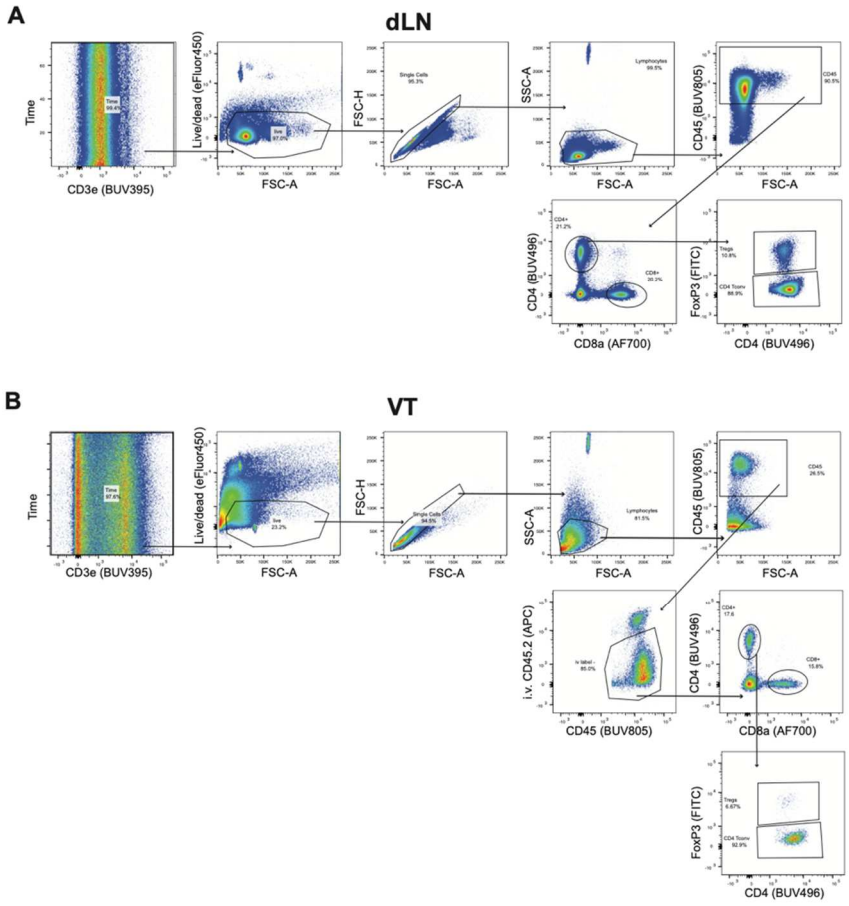

Figure 2.3. Mouse flow cytometry gating.

Flow cytometry gating strategy for identifying Tregs, CD4Tconv, and CD8 T cells from **A)** dLN and **B)** VT in flow cytometry from Figures 2.4, 2.5, 2.7, and 2.8.

Table C. Mouse Treg flow cytometry panel.

Antibodies used for mouse dLN and VT flow cytometry analysis in Figures 2.3, 2.4, 2.5, 2.7, 2.8.

Mouse Treg flow cytometry panel				
Antigen	**Conjugate**	**Clone**	**Company**	**Dilution**
Intravascular labeling (in 1X PBS)				
CD45.2	APC	104	Biolegend	3ug in 200ul
Viability stain (in 1X PBS)				
L/D	eFluor450	NA	Thermo Fisher Scientific	1:500
Surface stain (in FACS buffer)				
CD4	BUV496	GK1.5	BD	1:400
CD45	BUV805	30-F11	BD	1:400
ICOS	BV421	C398.4A	Biolegend	1:400
CCR2	BV605	SA203G11	Biolegend	1:50
GITR	BV750	DTA-1	BD	1:400
CD103	BV785	M290	BD	1:200
CD69	PE/Dazzle 594	H1.2F3	Biolegend	1:100
CD25	PECy5	PC61	Biolegend	1:800
CD8a	AF700	53-6.7	Biolegend	1:400
CD44	APC/Cy7	IM7	Biolegend	1:400
Intracellular stain (in 1X eBioscience FoxP3/Transcription factor perm buffer)				
CD3e	BUV395	145-2C11	BD	1:600
FoxP3	FITC	FJK-16s	Invitrogen	1:100
Granzyme B	PE	GB11	Thermo Fisher Scientific	1:100
CTLA-4	PE-Cy7	UC10-4B9	Biolegend	1:200

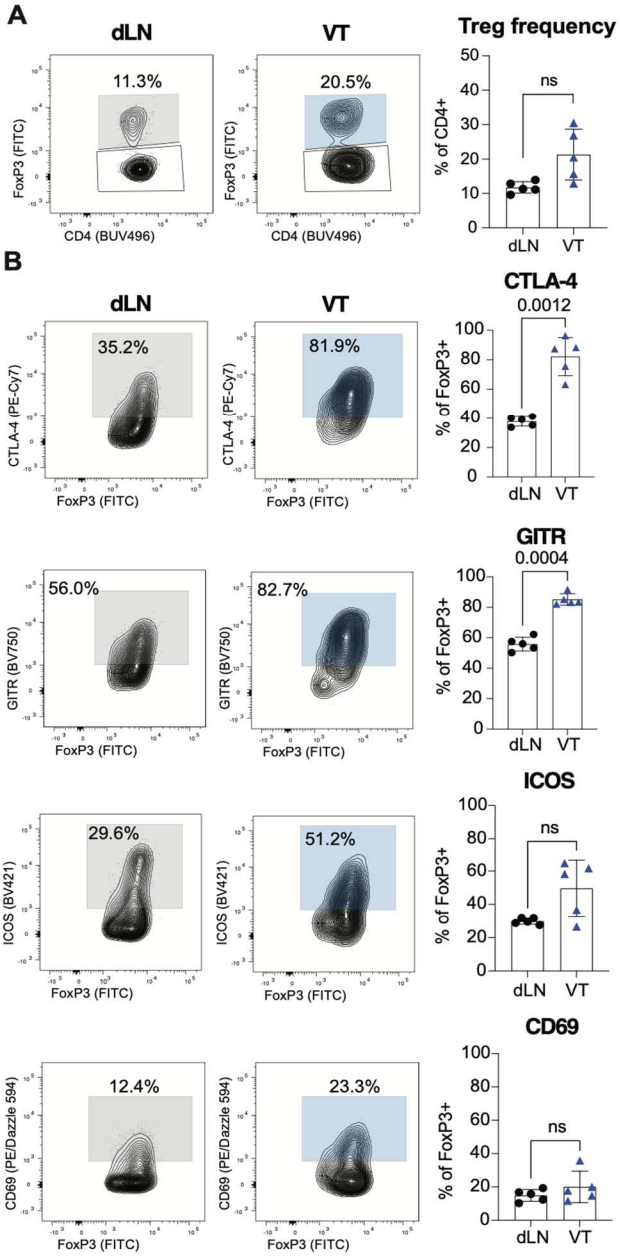

Figure 2.4. Vaginal tissue Tregs are highly activated compared to lymphoid tissue Tregs in healthy mice.

C57BL/6J mice were administered Depo provera s.c. in the neck ruff, and VT and vaginal-draining lymph nodes (dLN) were harvested 5-7 days later. **A)** Tregs were identified as CD4+FoxP3+ by flow cytometry. **B)** Representative staining for CTLA-4, GITR, ICOS, and CD69 on FoxP3+ Tregs (left; VT plot is the concatenated image of 5 individual VT tissues), quantified as a percentage of total FoxP3+ Tregs (right). n=5; data representative of 3 replicate experiments. Significance defined by paired t test; $p<.05$.

2.2.3 *Vaginal HSV-2 infection increases the accumulation of highly activated Tregs at the site of infection and drives increased expression of select activation markers consistent with a tissue signature.*

Our lab and others have previously used a mouse model of vaginal herpes simplex virus 2 (HSV-2) infection to study anti-viral T cell responses in primary infection[194, 195, 213]. To characterize murine VT Treg dynamics upon mucosal HSV-2 infection, mice were injected s.c. with depo provera 5-7 days before intravaginal infection to synchronize estrus cycle phases for consistent susceptibility to HSV-2 infection[209]. On days 3 and 7 post-infection (p.i.), frequency and phenotypes of dLN and VT Tregs were assessed by flow cytometry. VT Treg frequencies at day 3 p.i. were stable compared to Treg frequencies at day 0 , but absolute numbers of Tregs were dynamic, increasing 2-fold by day 3 and significantly increasing by 10-fold at day 7 ($p = .0089$, Figure 2.5A). Despite the increase in number of Tregs in the VT, by day 7, Treg frequency decreased by 2-fold due to the influx of CD4 effector cells[194, 195] (Figure 2.4A). Conversely, dLN Treg number increased insignificantly p.i. and their frequency as a percentage of total CD4+ T cells remained stable out to day 7 (Figure 2.5A). These results demonstrate the dynamic nature of Treg in the VT following HSV-2 infection.

We next assessed the Treg phenotype at day 3 and 7 p.i., and found that the frequency of Tregs expressing CTLA-4 and GITR increased only a small amount compared to uninfected mice, as over 80% of Tregs in the uninfected VT were already CTLA-4+ and GITR+ at day 0 (Figure 2.5B, Figure 2.4B). However, the absolute numbers of VT Tregs expressing CTLA-4 and GITR both increased 10-fold by day 7 compared to uninfected mice (Figure 2.5B). Conversely, dLN CTLA-4+ and GITR+ Treg numbers remained stable, and a significantly higher fraction of VT Tregs expressed CTLA-4 and GITR compared to dLN Tregs at both day 3 (CTLA-4: 2.5-fold, p

= .000498; GITR: 1.4-fold, p = .000128) and day 7 pi (CTLA-4: 2-fold, p = .000001; GITR: 1.5-fold, p = .000247Figure 2.5B). Thus, although CTLA-4 and GITR are constitutively expressed on nearly all VT but not dLN Tregs, infection with HSV-2 increases the numbers of these highly activated Tregs in the tissue, and a higher frequency in the VT compared to dLN Tregs consistently express CTLA-4 and GITR after infection.

Notably, the frequency of VT Tregs expressing ICOS was significantly increased over 1.5-fold at day 7 compared to uninfected (Figure 2.5B), and the number of VT Tregs expressing ICOS increased significantly by 16-fold (p = .0140) by day 7 compared to uninfected (Figure 2.5B). A higher frequency of VT Tregs expressed ICOS compared to dLN Tregs at both day 3 (1.7-fold, p = .005676) and day 7 (2.3-fold, p = .000285, Figure 2.5B), suggesting that HSV-2 infection drives potent ICOS expression in local Tregs. We also noted that the frequency of CD69+ VT Tregs is significantly (p=.001282) elevated 4-fold compared to LN Tregs at day 3 p.i. (Figure 2.5B). This result highlights the challenge of interpreting CD69 expression, which can be a marker of either tissue residency or activation, outside a well-defined infection model. Together, these findings demonstrate that viral infection exacerbates the activation phenotype of VT tissue but not dLN Tregs and significantly increases Treg numbers in the VT.

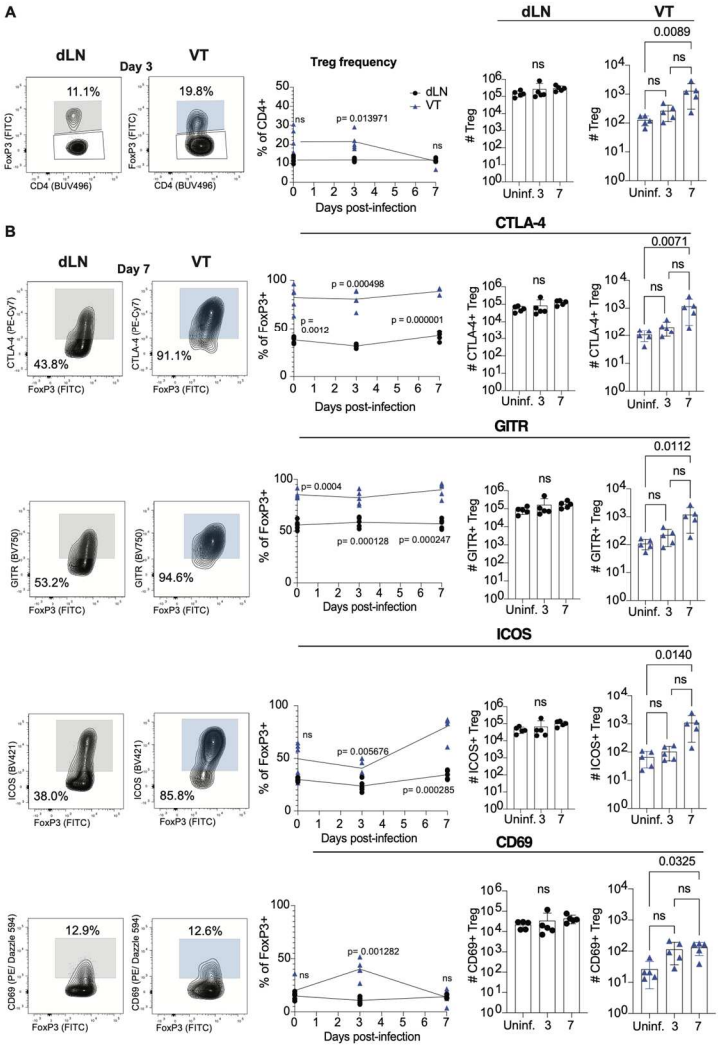

Figure 2.5. Vaginal HSV-2 infection increases the accumulation of highly activated Tregs at the site of infection and drives increased expression of select activation markers consistent with a tissue signature.

C57BL/6J mice were administered Depo provera s.c. in the neck ruff, and infected 5-7 days later with intravaginal (ivag.) HSV-2. On days 0 (uninfected [uninf.]), 3, and 7 post-infection, VT and dLN were harvested for flow cytometry analysis. **A)** Tregs were identified as CD4+FoxP3+ by flow cytometry. Representative Treg staining in dLN (grey) and VT (blue) on day 3 post-infection (left). Treg frequency was quantified as a percentage of total CD4+ T cells and absolute number of Tregs on days 0, 3, and 7 (right). **B)** Representative staining for CTLA-4, GITR, ICOS, and CD69 on FoxP3+ Tregs on day 7 post-infection (left), quantified as a percentage of total FoxP3+ Tregs and absolute number on days 0, 3, and 7 (right). n=5; data representative of 3 replicate experiments. Significance defined by paired t test or Kruskal-Walllis test followed by Dunn's multiple comparison test; $p<.05$.

2.2.4 *The vaginal Treg population is transcriptionally distinct from lymphoid Tregs*

To supplement our target flow cytometric analysis of canonical Treg markers of activation and suppression, we next sought to further interrogate VT and dLN Tregs at the population level through unbiased transcriptional analysis. We infected FoxP3^{GFP} mice[214] intravaginally with HSV-2 and harvested VT and dLN on day 7 p.i.. We then sorted Tregs (CD4+GFP+) from VT and dLN from infected (n=4) and uninfected (n = 3) mice and performed bulk RNA sequencing. Uninfected mice contained very few T cells in the VT; therefore, we did not recover sufficient Tregs from uninfected VT to obtain reliable sequencing results and this population was excluded from downstream analysis. When comparing Tregs from the VT and dLN of infected mice, we found differential expression of over 30 genes based on tissue location (Figure 2.6A). In VT Tregs, the transcripts for canonical Treg genes such as *IL-10* were elevated, as was transcription factor *Tbx21* (Tbet). Tbet+ Tregs represent a subset of Tregs that are known to be highly suppressive and selectively inhibit T helper type 1 (Th1) responses and CD8+ T cells[215]. Additionally, transcripts for *Ccr2,* a tissue-homing chemotactic receptor found on other non-lymphoid tissue Tregs that increases Treg CD25 expression in VAT Tregs, was significantly increased in VT Tregs. We also compared the transcriptional profile of Tregs from infected mice to the transcriptional program of Tregs resident in VAT and found that VT, but not dLN Treg signatures were significantly (FDR = 2.94E-14) enriched for genes in a previously published VAT Treg signature, suggesting overlap in the transcriptional profile and functions between non-lymphoid tissue Tregs[31] (Figure 2.6B, APPENDIX A). Altogether, our bulk RNA-seq results further confirmed the VT Treg compartment as a distinct population, with both phenotypic and transcriptional differences, compared to lymphoid Tregs.

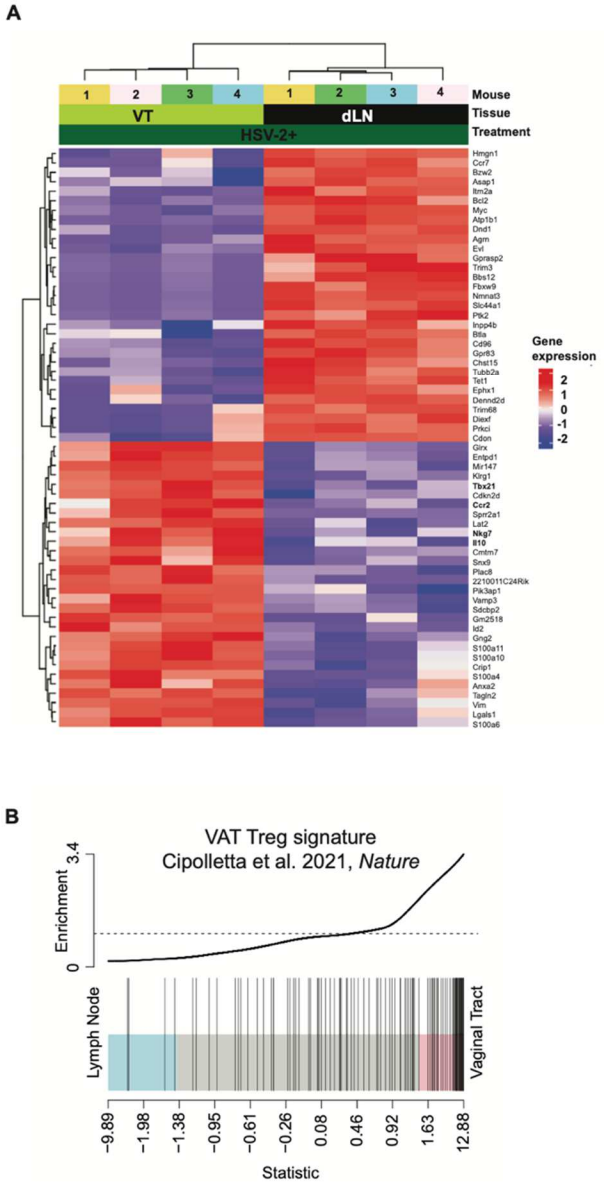

Figure 2.6. Vaginal Tregs are transcriptionally distinct from dLN Tregs and enriched for visceral adipose tissue Treg gene signature.

FoxP3^{GFP} mice were administered Depo provera s.c. in the neck ruff and infected ivag 5-7 days later with WT HSV-2. On day 7 post-infection, VT and dLN were harvested and prepared for fluorescence-activated cell sorting (FACS) to isolate CD4+ FoxP3+ Tregs. Bulk RNA-sequencing was performed on Tregs from dLN and VT. **A)** Differentially expressed genes (DEG) in dLN and VT Tregs were defined by a log2FC greater than 1 and a false discovery rate (FDR) < .05 and visualized in a heatmap. n= 4, DEG defined by FDR < .05. **B)** Gene set enrichment analysis (GSEA) of dLN and VT Tregs day 7 post-infection compared to a previously published gene signature for visceral adipose tissue Tregs[31]. n=4; FDR = 2.94E-14.

2.2.5 *Vaginal Tregs express Granzyme B after HSV-2 infection*

Thus far, our data demonstrated that VT tissue Tregs are transcriptionally and phenotypically distinct from dLN Tregs, and that phenotype is further exacerbated after HSV-2 infection, although it was generally difficult to distinguish changes in VT tissue Tregs after infection compared to steady state. We hypothesized that the vaginal Treg population might be heterogenous, with distinct subsets expressing distinct genes, which. Might ultimately suggest distinct functions between vaginal Treg subsets. To test this, further explored VT Tregs through unbiased transcriptional analysis on a single-cell level. We sorted CD4+GFP+ Tregs from the VT or dLN of FoxP3^{GFP} mice on day 7 post-HSV-2 infection, or from uninfected control mice for transcriptional analysis Figure 2.7). We used the Seurat pipeline[216] to perform graph-based clustering of Tregs in the VT and dLN, visualized with Uniform Manifold Approximation Projection (UMAP)[217]. As with our bulk RNA-seq, we were unable to recover sufficient VT Tregs from uninfected mice for sequencing. However, we found that VT Tregs from infected mice (shown in blue) grouped largely independently, with some overlap with dLN Tregs from infected mice (shown in grey) and little overlap with Tregs from uninfected dLN (green;Figure 2.7A). When we compared differentially expressed genes (DEG) using Model-based Analysis of Single-cell Transcriptomics (MAST)[218] in VT Tregs compared with dLN (Figure 2.7B), visualized in a heatmap with the top 20 DEG shown for each population, VT Tregs were enriched for genes related to Treg suppression and activation. For example, *Tnfrsf18* (GITR), *Tigit*, and *Ctla4* were differentially expressed in VT Tregs compared to dLN Tregs from infected or uninfected mice, as were tissue-homing chemokine receptors *Cxcr3* and *Ccr2,* as well as growth factor *Areg*, which other mucosal Tregs produce to mediate tissue repair[30, 38, 44]

(APPENDIX B). Notably, we previously observed by flow cytometry that GITR, TIGIT, and CTLA-4 were increased on vaginal Tregs compared to PBMC or dLN in both humans and mice (Figure 2.1, Figure 2.4, Figure 2.5) supporting our findings at the protein level.

In addition to these genes known to be important for tissue Treg function, we were surprised to find that *Gzmb* was the most highly upregulated gene in VT compared to dLN Tregs (2.4-fold, adjusted p value = 1.45E-46; Figure 2.7B, C). This trend was mirrored by *Nkg7* (1.2-fold, adjusted p value = 2.92E-13), a regulator of cytotoxic granule exocytosis which was also increased in VT Tregs by bulk RNA-seq (1.4-fold, FDR = .029)[219, 220] (Figure 2.7B-C, Figure 2.6A). After finding *Gzmb* transcript highly differentially expressed in VT Tregs after infection, we used flow cytometry to confirm GzmB protein expression on vaginal Tregs, compared to vaginal CD8+ or CD4+ Tconv from VT and dLN. In uninfected mice, neither VT (2.5%) nor dLN (.06%) Tregs highly expressed GzmB (Figure 2.7D). CD8+ T cells, which robustly express GzmB in response to viral infection or immunization[221-223], also expressed little to no GzmB in healthy mice (VT: 5.6%; dLN: .09%; Figure 2.7E). However, by day 7 p.i., 19% of VT Tregs expressed nearly 20-fold more GzmB than dLN Tregs (p= .000789, Figure 2.7D). Likewise, by day 7, absolute numbers of VT Tregs expressing GzmB increased 100-fold (p = .0011) compared to uninfected mice, and absolute numbers of dLN Tregs expressing GzmB increased 10-fold (p = .0071, Figure 2.7D). These results show that VT Tregs have the ability to produce GzmB in a similar pattern to CD8+ CTLs (Figure 2.7E). However, our data show that GzmB production is only induced after local infection and is not a general characteristic of vaginal tissue-resident Tregs.

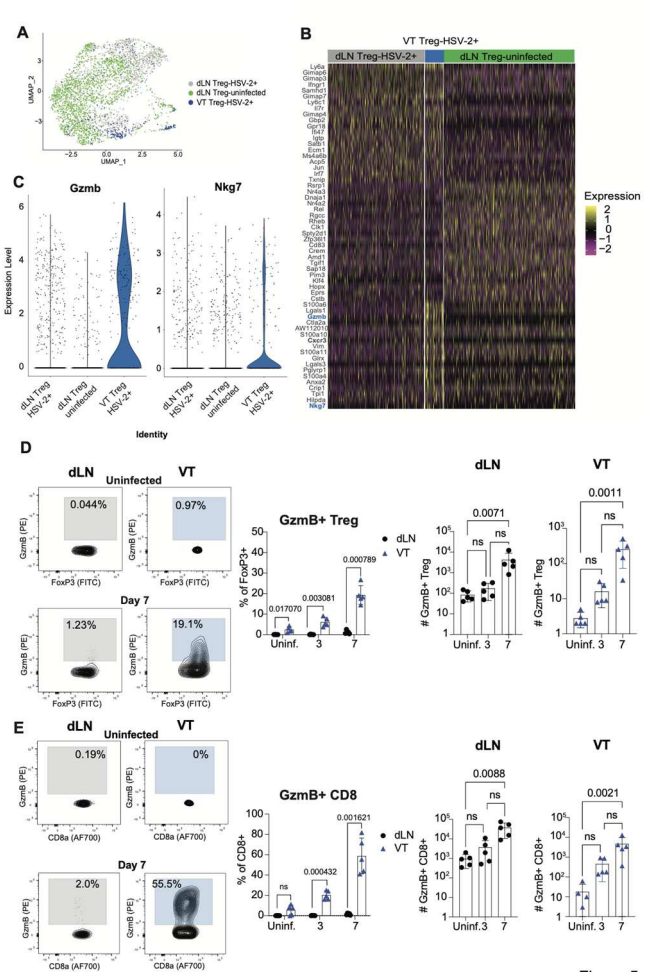

Figure 2.7. Vaginal tissue Tregs differentially express Granzyme B after HSV-2 infection.

FoxP3^{GFP} mice were administered Depo provera s.c. and infected 5-7 days later ivag with WT HSV-2; controls received Depo provera only. On day 7 post-infection, VT and dLN were harvested and prepared for FACS to isolate CD4+ FoxP3+ Tregs. Single-cell RNA-sequencing was performed on dLN and VT Tregs and analyzed with the Seurat pipeline in R. n = 5 HSV-2+ and n = 3 uninfected. **A**) UMAP visualization of graph-based clustering of VT and dLN Tregs from infected mice and dLN Tregs. **B**) Heatmap showing the top 20 DEG in VT and dLN Tregs. DEG were determined by log2FC > .5 and FDR <.01. A full DEG list can be found in Supplemental Table 3. **C**) Violin plots of *GzmB* and *Nkg7* expression in Treg populations. **D-E**) C57BL/6J mice were administered Depo provera s.c. in the neck ruff and infected ivag 5-7 days later with HSV-2. On days 0 (uninf.), 3, and 7 post-infection, dLN and VT were harvested for flow cytometry analysis. Tregs and CD8 T cells were identified as CD4+FoxP3+ and CD8+, respectively. Representative granzyme B (GzmB) *ex vivo* staining in dLN (grey) and VT (blue) in **D)** Tregs and **E)** CD8 on days 0 and 7 post infection (left), quantified as a percentage of total Treg or CD8+ and by absolute number (right). n=5 HSV-2+ and n = 5 uninfected. Data representative of 3 replicate experiments. Significance defined by multiple paired t test or Kruskal-Walllis test followed by Dunn's multiple comparison test; p <.05.

2.2.6 *Inflammatory cytokines induce GzmB expression in Tregs*

We next sought to identify the signals that regulate expression of GzmB in VT Tregs upon local mucosal infection. We hypothesized that local inflammatory signals induced by infection selectively act on Tregs to induce GzmB during the peak effector phase of the antiviral immune response to HSV-2. Given the high expression of CD25—the interleukin-2 (IL-2) receptor (IL-2Rα)—on Tregs and their dependency on IL-2 for development and function[7, 208], we hypothesized that IL-2 together with other inflammatory cytokines could induce GzmB. Along these lines, we hypothesized that Type-1 interferons (IFN-I), interferon-α (IFN-α) and interferon-β (IFN-β), which are critical antiviral cytokines produced early in HSV-2 infection by plamacytoid dendritic cells (pDCs)[224, 225], might act on Tregs through the IFN α/β receptor (IFNAR) to induce GzmB in infected tissue contexts. To test this, we cultured splenocytes from uninfected WT mice for 24 hours with IL-2 alone, IFN-α and IFN-β, or all three cytokines together (Figure 2.8). At 24 hours, Tregs, CD4+ Tconv, and CD8+ T cells were assessed for GzmB expression by flow cytometry. In media alone, Tregs expressed no GzmB. However, we found that IL-2 in combination with IFN-α and IFN-β significantly induced GzmB expression on Tregs compared to media alone (6%, $p < .00001$), comparable to 5.8% Treg expression of GzmB in response to TCR stimulation ($p > .05$; Figure 2.8A). In contrast, CD4+ Tconv cultured with IL-2 and IFN-I expressed a small but significant increase in GzmB compared to CD4 Tconv cultured in meida alone (1.4-fold, $p = .023$; Figure 2.8A). Notably, neither IL-2 nor IFN-α/β alone induced significant Treg GzmB expression compared to media controls, suggesting that dual cytokine signals are necessary for controlled Treg expression of GzmB Figure 2.8A).

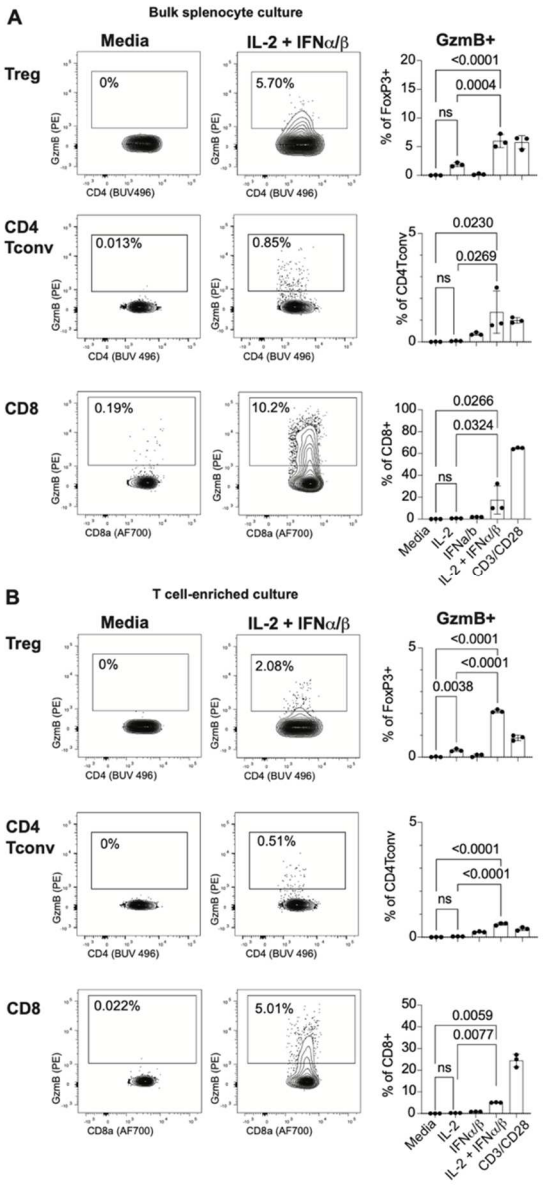

Figure 2.8. Inflammatory cytokines induce Granzyme B expression in Tregs.

Bulk splenocytes from a healthy C57BL/6J mouse were cultured in various cytokine conditions as indicated. **A)** After 24 hours, CD4+FoxP3+ Tregs (top), CD4+FoxP3- CD4Tconv (middle), and CD8+ T cells (bottom) were stained for GzmB expression by flow cytometry. Example staining (left) Tregs, CD4 Tconv, or CD8 expressing GzmB as a percentage of total FoxP3+, CD4+FoxP3-, or CD8+, respectively (right). **B)** Bulk splenocytes from a healthy mouse were enriched for T cells using magnetic separation and cultured in various cytokine conditions. After 24 hours, CD4+FoxP3+ Tregs (top), CD4+FoxP3- CD4Tconv (middle), and CD8+ T cells (bottom) were stained for GzmB expression by flow cytometry. Example staining (left) and Tregs, CD4 Tconv, or CD8 expressing GzmB as a percentage of total FoxP3+, CD4-FoxP3+, or CD8+, respectively (right). Data representative of two replicate experiments. Significance defined by one-way ANOVA followed by Tukey's test for multiple comparisons; $p < .05$.

2.2.7 *Inflammatory cytokines act directly on Tregs to induce GzmB expression*

We demonstrated that IL-2, in combination with IFN-I, could induce potent GzmB expression on lymphoid Tregs from naïve mice. However, these experiments were performed with bulk splenocytes where Tregs were cultured with other immune cells. To parse whether these cytokines can act directly on Tregs or instead were also activating other immune cells that could then produce additional inflammatory cytokines to secondarily activate GzmB expression in Tregs, we repeated these stimulations in cultures lacking antigen presenting cells (APCs) by purifying splenic T cells from naïve mice using pan-T cell negative selection. Although to a lesser degree than our bulk splenocyte cultures, a significant percentage (2%) of Tregs in the pure T cell cultures exposed to IL-2 and IFN-I produced GzmB compared to Tregs cultured in media, which produced no GzmB ($p < .001$; Figure 2.8B). IL-2 alone induced a very small but significant increase in the frequency of Tregs expressing of GzmB (0.88%, $p = .0038$) on Tregs compared to media control. This suggests that IL-2 and IFN-I work synergistically on Tregs to induce GzmB, but when other immune cells are present, this effect is indirectly augmented, likely through the activation of APCs or other immune cells which in turn act on Tregs to increase GzmB expression.

2.3 DISCUSSION

We found that vaginal mucosal Tregs in healthy humans express increased CTLA-4, GITR, and ICOS compared to circulating (blood) Tregs. We similarly observed increased expression of CTLA-4, GITR, and ICOS in VT Tregs compared to dLN Tregs in uninfected mice, suggesting that this activated phenotype is driven by vaginal tissue localization. The differences that we

observed between vaginal and dLN Tregs are consistent with existing tissue Treg literature showing discrete tissue sites such as skin, lung, muscle, and VAT host Treg populations with unique, activated phenotypes[30-35, 37, 38, 199]. The increased expression of CTLA-4, GITR, and ICOS has been previously reported for steady-state VAT, lung, and skin Tregs, and like VAT Tregs, VT Tregs had a predominantly CD69+CD103- phenotype[37].

To assess whether this VT Treg phenotype is further altered in the context of a local viral infection, we infected mice intravaginally with HSV-2. We found that the vaginal Treg population further increased expression of CTLA-4, GITR, and ICOS indicating a highly activated phenotype consistent with increased suppressor potential. The VT Treg population significantly expanded by day 7 post-infection, while Treg numbers in the dLN remained stable. Although absolute numbers of VT Tregs increased after infection, the frequency of VT Treg expressing GITR and CTLA-4 at steady state was largely unchanged after infection, while the frequency of VT Tregs expressing CD69 was only transiently increased at day 3 p.i.. Together, these findings highlight that distinguishing acutely activated VT Tregs from those that are simply localized in the vaginal mucosa is challenging. This is particularly the case if etiological stimuli are not well defined such as in human mucosal barrier tissues.

We next wanted to determine if there are biomarkers in the mouse model system that are able to identify markers of acute VT Treg activation using an RNAseq approach. Notably, we found that after infection with HSV-2, vaginal Tregs differentially express cytotoxic GzmB at both the transcriptional and protein level, demonstrating an inflammation-dependent Treg phenotype that is not induced by vaginal residency alone. Tregs in mouse have been previously shown to

express GzmB in response to TCR stimulation and in specific contexts, including roles in colorectal and other cancers[16, 18, 19, 154, 226-228]. Related to our findings, Loebbermann et al. have previously shown that in the lung, but not in lung-draining lymph nodes, Tregs express GzmB after RSV infection, and that Tregs help to attenuate lung immunopathology by killing CD8+ T cells through a GzmB-mediated mechanism[19]. Thus, similar to their role in the lung, vaginal Tregs may degranulate GzmB to cull aggressive tissue T cell responses during the height of the anti-HSV-2 immune response, preventing collateral tissue damage. This putative GzmB+ Treg function warrants further study, as does the relationship between GzmB+ Treg and HSV-2 viral clearance, as Treg restraint of vaginal T cells may prevent mucosal damage at the expense of efficient viral control. Additionally, our detection of *Areg* in VT Tregs after infection potentially indicates an ability to directly contribute to tissue repair through IL-33-mediated Areg production[30, 38, 44]. However, elucidation of whether or not VT Tregs can exert repair functions akin to lung and muscle Tregs, either at steady state or following local infection, will require further investigation.

Previous studies have indicated a critical role for TCR signaling to acquire GzmB expression[227, 229, 230]. Given the large fraction of GzmB+ VT Tregs, we hypothesized that inflammatory cues could be sufficient to drive GzmB expression[231]. We found that in combination with IFNα and IFNβ, IL-2 induced GzmB expression in Tregs isolated from naïve mice. However, neither IL-2 nor IFN-I alone induced comparable GzmB expression. This suggests that Tregs require at least two separate signals to acquire GzmB expression, which may prevent aberrant cytotoxicity in inappropriate contexts. Although our study used *in vitro* stimulations to test the effects of IL-2 and IFN-I on Treg GzmB expression, these cytokines are present in the VT during HSV-2

infection. CD4+ T cells are early responders to local infection, where they produce interferon γ (IFN-γ) and IL-2[194, 195, 232, 233]. Likewise, pDCs produce IFN-I early after infection with HSV-2[225]. Thus, our findings demonstrate a mechanism by which vaginal Tregs acquire GzmB in HSV-2.

We acknowledge that our study is constrained by low T cell numbers in vaginal tissue, precluding certain analyses. In an effort to compensate for this constraint, we confirmed results in multiple experiments containing large groups of mice and validated our findings at both the transcriptional and protein levels.

We were not able to test the direct function of GzmB+ Tregs, as follow up experiments to address if and how GzmB+ Tregs can kill target cells were not feasible due to the low absolute number of Tregs recovered from murine VT. Given that GzmB acquisition occurs in the absence of agonist TCR signals, potential target cells may be recognized in a TCR-independent manner[231, 234]. Likewise, we recovered insufficient cell numbers to perform informative TCR repertoire analysis from any VT Tregs. Finally, due to the ongoing SARS-CoV-2 pandemic we were unable to obtain additional vaginal biopsies from HSV-2+ women, which could confirm, in parallel with our mouse data, the exacerbated activation phenotype we observed in infected animals compared to uninfected. We hope to interrogate the vaginal immune compartment of HSV-2+ women once recruitment of study participants is again feasible.

In summary, we show that vaginal Tregs are transcriptionally and phenotypically distinct from vaginal-draining lymph node Tregs at steady state. We propose a model wherein a small population of Tregs reside within the vaginal mucosa at homeostasis and are moderately

activated compared to lymphoid Tregs. However, vaginal mucosal infection greatly augments vaginal Treg numbers and leads to acquisition of a cytotoxic phenotype, including expression of GzmB in vaginal Tregs, suggesting that viral infection drives a differential phenotype in vaginal Tregs. Additionally, we show that IL-2, in combination with antiviral IFN-I, induce *in vitro* GzmB expression in Tregs from naïve mice, highlighting a two-signal mechanism by which the acquisition of GzmB is tightly controlled in Tregs, allowing for precise expression during highly inflammatory environments. Our findings demonstrate that the previously uncharacterized vaginal Treg population is dynamic and poised to respond to locally acquired infections with highly suppressive and cytotoxic potential, possibly to restrain aggressive effector T cell responses that may cause collateral tissue damage.

Together, these findings also have implications for mucosal vaccines design. Extensive research has shown that a successful mucosal vaccine must elicit Trm at the site of infection[204, 223, 235-238], but so far, these studies have not considered how Tregs may help or hinder local anti-viral T cell responses. Therefore, it is critical to understand how Treg function could be therapeutically leveraged to increase vaccine-elicited antigen-specific Trm responses. Going forward, further work is needed to interrogate the origins, TCR requirement, and functions of vaginal Tregs during HSV-2 and determine how Tregs could be harnessed to support effective viral clearance, Trm responses, and tissue healing.

2.4 MATERIALS AND METHODS

2.4.1 *Study population*

Healthy, assigned female sex at birth, HIV-1 negative adults (n=14) were recruited at the Vaccine Trial Unit (Fred Hutchinson Cancer Research Center) in Seattle, WA. Informed consent was obtained from all participants for the collection of blood and vaginal biopsies and was approved by Fred Hutchinson Cancer Research Center internal review board (IR5640). Eligibility criteria included aged $\geq$ 18 and < 45, non-menopausal, not pregnant, currently using reliable contraceptives, negative for Hepatitis C, HSV-2, and vaginal *N. gonorrheae* and *C. trachomatis* and normal PAP smear. A normal vaginal exam at time of biopsy was required. The ages of study participants were 21-47, with a median age of 27. Vaginal biopsies were obtained from the fornices using a Baby Tischler Biopsy Forceps (Wallach Surgical, Trumbull, CT, USA) and lidocaine was not used. All biopsies were transported to the laboratory on wet ice and processed on the day of collection.

2.4.2 *Human sample processing*

PBMCs were isolated from whole blood by Lymphoprep (Stemcell) gradient and centrifuged for 20 minutes at 800xg. Biopsies were prepared for flow cytometry as follows: after mincing, biopsies were digested in collagenase II (700U/ml; Sigma) and DNAse (400U/ml; Sigma) at 37 degrees C for 30 minutes. The digested tissues were passed through a 70um strainer to create a single-cell suspension and prepared for flow cytometry analysis.

2.4.3 *Mice*

6-8 week-old female wildtype C57BL/6J (Jackson Laboratories, Bar Harbor, ME) or FoxP3^{GFP} [214] (bred at Fred Hutch) mice were used for experimental groups. All animal experiments were approved by Fred Hutch IACUC and the study was conducted in strict compliance with the PHS Policy on Humane Care and Use of Laboratory Animals.

2.4.4 *Infections*

Mice were injected subcutaneously in the neck ruff with 2 mg of medroxyprogesterone acetate (Depo-Provera) 5-7 days prior to intravaginal (ivag.) infection with 10^4 PFU of HSV-2 derived from a human clinical isolate[239].

2.4.5 *Intravascular labeling*

3 minutes prior to sacrifice with CO2, mice were administered an intravascular (i.v.) tail vein injection of CD45.2 antibody (3ug in 200ul PBS) in PBS to label circulating lymphocytes for exclusion from VT samples.

2.4.6 *Mouse tissue processing*

Vaginal tract (VT), including the vagina and cervix, was harvested and minced with scissors followed by a 30-minute incubation in RPMI containing collagenase D (2mg/ml; Sigma) and DNAse (15ug/ml; Sigma) at 37 degrees C. Following incubation, collagenase reaction was quenched with 5mM EDTA in HBSS without calcium and magnesium and passed through 70um

strainer to prepare a single-cell suspension. After harvesting, vaginal-draining lymph nodes (dLN), including the inguinal and iliac lymph nodes, were harvested and passed through 70um filter to prepare a single-cell suspension.

2.4.7 *Cell sorting and flow cytometry*

Cells were incubated in fixable viability dye (Invitrogen) and blocked for non-specific Fc binding in PBS for 30 minutes. Cells were then stained for surface proteins in FACS buffer (PBS containing .02% sodium azide and 2% fetal calf serum) for 20 minutes, fixed for 30 minutes with Foxp3 Transcription Factor Staining Buffer Set (eBioscience) fixative, followed by 2 washes with Foxp3 Transcription Factor Staining Buffer perm buffer and stained for 30 minutes with intracellular antibodies in perm buffer. Cells were acquired with the FACSymphony (BD Biosciences, San Jose, CA) and data analyzed with FlowJo software version 10.6.1 (Treestar, Ashland, OR). For this list of all antibodies used, reference Table B and Table C.

Cell sorting for RNA-sequencing experiments was performed on the FACSAria (BD Biosciences, San Jose, CA). Tregs and CD4+ T_{conv} isolated from vaginal tissue and vaginal-draining lymph nodes were sorted from $FoxP3^{GFP}$ mice on CD4+ GFP+ and CD4+ GFP-, respectively. Tregs and CD4+T_{conv} from vaginal tissues were additionally sorted on intravascular label- population to exclude blood T cell contamination. To estimate total cell counts, $2x10^4$ AccuCheck Counting Beads (Thermo Fisher Scientific) were added to each sample prior to acquisition on the cytometer.

2.4.8 *In vitro T cell stimulation assays*

For T cell stimulation assays, spleens were harvested from uninfected C57BL/6J mice. Pan-T cells were enriched with magnetic T cell negative selection kit (Stem Cell Technologies, Vancouver, Canada) from healthy mouse splenocytes. Single cell suspensions from spleen were either lysed for red blood cells and plated whole or enriched for T cells as described above. Whole splenocytes or purified T cells were then cultured at 1e6 cells/well in 200ul in 96-well plates. Both groups were cultured for 24 hours in the presence of recombinant IFNα (Pacific BioLabs; 50U/ml), recombinant IFNβ (Pacific BioLabs; 50U/ml), and recombinant IL-2 (Biolegend; 20ng/ml). Golgiplug (BD Biosciences) was added at 1:1000 after 20 hours of culture. For TCR stimulation positive control wells, 96-well plates were coated with 1ug/ml purified anti-CD3 and 2ug/ml anti-CD28 (Biolegend) for 24hours at 4 degrees C before plating cells. Negative controls were cultured in media alone.

2.4.9 *Statistical analysis*

For flow cytometry data, statistical analyses were performed with Prism software version 9.1 (GraphPad Software, San Diego, CA). Paired data were assessed with paired t tests. When comparing groups within datasets containing greater than two groups, Kruskal-Wallis followed by Dunn's test for multiple comparisons or one-way ANOVA followed by Tukey's test for multiple comparisons was used. Significance was defined by a p value less than .05.

2.4.10 *Bulk RNA-sequencing*

We performed bulk RNA-sequencing on 110-200 sorted CD4Tconv and Treg from the dLN of infected and uninfected mice and the VT of infected mice. Cells were not pooled between mice. 22 samples were sequenced: 4 from CD4+FoxP3+ from infected dLN; 4 from CD4+FoxP3+ from infected VT; 4 from CD4+FoxP3- from infected dLN; 4 from CD4+FoxP3- from infected VT; 3 CD4+FoxP3+ from uninfected dLN; 3 from CD4+FoxP3- from uninfected dLN. Briefly, as previously described[240], cells were sorted into SMART-seq v4 Ultra Low Input (Takara Bio USA, San Jose, California) lysis buffer and reverse transcription was performed followed by PCR amplification to generate full length amplified cDNA. Sequencing libraries were constructed using the NexteraXT DNA sample preparation kit (Illumina) to generate Illumina-compatible barcoded libraries. Libraries were pooled and quantified using a Qubit® Fluorometer (Life Technologies). Dual-index, single-read sequencing of the pooled libraries was carried out on a HiSeq2500 sequencer (Illumina) with 58-base reads, using HiSeq v4 Cluster and SBS kits (Illumina) with a target depth of 5 million reads per sample. FASTQs were aligned to a mouse reference genome, using STAR v.2.4.2a and gene counts were generated using htseq-count.

2.4.11 *Bulk RNA-seq analysis*

QC and metrics analysis was performed using the Picard family of tools (v1.134). The RNA-seq data were aligned to the mouse genome (reference sequence mm10) using STAR (v2.4.2a)[241] and gene expression quantification was performed using RSEM (v1.2.22)[242]. Genes with less than seven nonzero read counts were discarded, leaving 12,317 expressed genes for the analysis. Libraries (samples) with less than 2,000,000 reads; 9,000 detected genes; and an exon rate < 75% were also removed. Twenty-one of the 22 prepared libraries passed these quality criteria.

Raw count data from RSEM was imported into R. The *edgeR* Bioconductor package was used to calculate normalization factors[243], followed by the voom transformation from the *limma* Bioconductor package for normalization[244, 245]. Statistical analyses were performed with the *limma* R package. A linear model was fitted to each gene, and empirical Bayes moderated t-statistics were used to assess differences in expression[246]. We subsetted the whole dataset into one subset corresponding to the cell type Treg & the treatment HSV-2+, and looked at the constrast between vaginal tract and lymph node. Intraclass correlations were estimated to account for measures originating from the same mice. An absolute log2-fold change cutoff of 1 and a false discovery rate (FDR) cutoff of 5% were used to determine differentially expressed genes (DEGs). Gene set enrichment analysis (GSEA) was performed using the R function *Camera* implemented within the *limma* R package[247]. An FDR cut-off of 5% was used to determine significant gene sets.

2.4.12 *Single-cell RNA-sequencing*

Sorted cells from dLN and VT were processed using the 10X Genomics Platform with the 5' Chromium Single Cell V(D)J Enrichment Kit v2 following manufactures instructions. Sorted populations from each mouse (infected: n= 5; uninfected: n=3) were pooled with the following total cell numbers were loaded into the Chromium Controller: infected dLN CD4+FoxP3+: 20,000; infected VT CD4+FoxP3+: 2,855; infected dLN CD4+FoxP3-: 20,000; infected VT CD4+FoxP3-: 20,000; uninfected dLN CD4+FoxP3+: 20,000; uninfected dLN CD4+FoxP3-: 20,000; uninfected VT CD4+FoxP3-: 1,562. As per manufacturer's instructions, the target cell number for each population was calculated as half the number of cells loaded. cDNA was

generated within oil emulsion droplets made by the Chromium Controller. cDNA was purified using DynaBeads MyOne Silane magnetic beads (thomerFisher, #370002D). cDNA amplification was performed by 10 rounds of PCR using Chromium Single Cell 5' Reagent kit. Amplified cDNA was then purified with SRPIselect magnetic beads (Beckman Coulter). After cDNA was fragmented and size selected, library construction was performed by end repair, A-tailing, adaptor ligation and PCR (12 cycles). Prior to sequencing, quality of libraries was determined by using Aglient 2200 TapeStation with High Sensitivity D5000 Screen Tape (Agilent). Libraries were quantified by digital droplet PCR with Library Quantification Kit for Illumina TruSeq (BioRad, #1863040). Libraries were diluted to 3 nM and paired-end sequencing was performed on a NovaSeq 6000 sequencer (Illumina).

2.4.13 *Single-cell RNA-sequencing analysis*

As previously described[240], sequencing data were processed to per-cell read and unique molecular identifier (UMI) counts with Cell Ranger software (10x Genomics, Pleasanton, CA). The reads were converted from BCL to FASTQ, demultiplexed, filtered, aligned to mouse genome assembly GRCm38 (mm10), collapsed to UMIs, and assigned to cell barcodes. Default settings in Cell Ranger were used to call cells vs. background. Data from each sample were aggregated without normalizing.

The R package Seurat was used to analyze count data[216, 248-250]. Genes detected in fewer than 400 and greater than 35,000 cells were removed, as were cells that had fewer than 400 and greater than 5000 genes detected based on natural breaks in data visualization. Cells with greater than 5% mitochondrial reads were also removed. As previously described[240], the UMI counts were

log transformed and total UMIs and % mitochondrial reads per cells were regressed out. With UMAP, cells were projected on the first 50 principal component axes from 2000 highly variable genes identified using default cutoffs. Seurat objects were created for each sample and re-scaled using all genes. Each cell's expression of defined gene sets was summarized by the mean normalized expression across the set in each cell. To remove noise around 0 introduced by normalization, 0 values for each gene in each cell with a raw UMI count of 0 were restored. Differential expression was quantified among populations using the hurdle model in MAST, with total UMIs per cell as a covariate. MAST identifies DE genes that overlap with those found by other methods with high precision and low false positive rates [218, 251].

2.4.14 *Data availability*

The sequencing data from this publication have been deposited in the NCBI's Gene Expression Omnibus and are accessible through the series accession number GEO: (GSE189375).
All scripts used for data processing and figure generation are available at GitHub: https://github.com/Brianna-Traxinger/scRNAseq_vaginalTreg_HSV-2

2.5 ACKNOWLEDGEMENTS

We thank the members of the Lund and Prlic labs for their helpful input and discussions and the study participants. We used BioRender for the generation of some figures.

Chapter 3. TREGS IN HSV-2 MEMORY RESPONSES

3.1 INTRODUCTION

3.1.1 *HSV-2 pathogenesis*

HSV-2 is a common and globally pervasive STI, for which there is currently no vaccine HSV-2 is a large double-stranded *Herpesviridae* family member[252]. HSV-2 initially infects the vaginal epithelium through Nectin-1[209] and other receptors before ascending to the sensory nerve root ganglia, where it becomes latent[252]. HSV-2 periodically reactivates both randomly and in response to cytopathic factors such as ultraviolet exposure, sending infectious virus down the axon to exit at the nerve ending, causing lesions and viral shedding in the mucosa and skin[252]. HSV-2 is highly contagious, and even asymptomatic patients regularly shed infectious virus[252]. HSV-2, in addition to causing painful lesions, increases HIV susceptibility by three-fold, and vertical transfer of HSV-2 during childbirth accounts for 14,000 annual global cases of often-fatal neonatal HSV-2 cases[252-254]. A vaccine is urgently needed for HSV-2 and other mucosally acquired STIs.

3.1.2 *Tissue resident memory T cells in HSV-2*

Tissue-resident memory T cells (Trm) are T cells that traffic to non-lymphoid tissue sites and do not recirculate, express unique transcriptional profiles and are classically defined by expression of CD69 and CD103[204, 255, 256]. Trm in the vaginal mucosa have been shown to be indispensable for protection from HSV-2 and other infections and are known controllers of HSV-2 viral load during shedding events[204, 223, 235-237]. Encouragingly, a vaccine model in mice protects from HSV-2 infection by recruiting Trm to the site of infection[213]. However, HSV-2 vaccines have so far

been unsuccessful in humans[257-259], even in cases where HSV-2-specific antibodies or circulating memory T cells have been generated, suggesting that circulating memory cells are insufficient for protection and that blood represents a poor marker of HSV-2 immunity. Therefore, vaccine efforts for HSV-2 and STIs rely on eliciting potent Trm responses that are poised at the site of infection[259]. However, despite the protective properties of Trm in HSV-2[259], some patients experience frequent viral shedding and lesions, while others are asymptomatic[252]. Given that Tregs are known mediators of T cell responses and are found within HSV-2 lesions[260] in skin, we hypothesized that Tregs may influence Trm to be more protective or less protective against HSV-2.

3.1.3 *Tregs limit effector T cell responses in mucosal infection*

Tregs are known regulators of other T cells and have been shown to restrain immune responses during infection. This restraint often limit immune-mediated tissue pathology at the expense of efficient viral clearance, as has been shown in RSV, influenza, Mtb, and Leishmania infection, both in primary infection and memory responses[19, 40, 42, 48, 50, 51, 201, 202]. Tregs mediate this restraint through secreted factors such as inhibitory cytokines such as IL-10, GzmB-mediated inhibition or even killing[18], and through suppressive mechanisms such as CTLA-4[208]. Given this precedent, we hypothesized that vaginal Tregs established after primary HSV-2 infection could be poised to restrain aggressive Trm responses in the vagina, with unknown consequences to viral load and tissue pathology.

Tregs have also been implicated in memory responses to pathogens. During secondary infection with influenza in mice, antigen-specific Tregs accumulate in the lung-draining lymph node and

lung with accelerated kinetics compared to primary infection, where they control antigen-specific CD8+ T cell proliferation[39]. Likewise, Treg depletion before challenge with influenza results in an increased antigen-specific CD8+ responses, leading to aggressive chemokine responses and inflammation in the lung and airway[39]. However, the increased suppressive ability of antigen-experienced Tregs may eventually wane following loss of antigenic stimulation, possibly to prevent a chronic suppressive state that could leave to aberrant, generalized immunosuppression[261]. In support of this, Mtb-specific Tregs expand during primary Mtb infection but are subsequently culled during later stages of infection[50]. However, antigen-experienced Tregs maintained a long-lived preference for accumulation in non-lymphoid tissues, suggesting that constitutively suppressive Tregs may be specifically important in tissue compartments, where they prevent immune-mediated tissue damage[261]. Further studies are needed to assess whether non-lymphoid Treg phenotypes are a result of continual stimulation through antigen or cytokine and which roles these non-lymphoid memory Tregs perform during infection[261].

3.1.4 *Tregs promote tissue healing during injury and infection*

In addition to preventing T cell-mediated tissue damage from occurring, Tregs can also directly heal tissue. In muscle tissue injured by cardiotoxins, a transcriptionally distinct population of Tregs accumulate in the muscle within days of injury and potentiate muscle repair[30, 38]. Through expression of the IL-33R, these Tregs respond to fibro/adipogenic progenitor cell production of IL-33 alarmin by producing growth factor Areg, which directly promotes skeletal muscle repair. Likewise, lung Tregs in influenza infection produce Areg and limit acute lung damage and decreased blood oxygen concentration[44]. Notably, loss of Areg expression on these lung Tregs

did not alter Treg suppressive function or viral titer, suggesting that Tregs specifically heal tissue through production of Areg[44].

3.2 STUDY GOALS

We sought to understand the previously unstudied role of vaginal Tregs in secondary exposure to HSV-2 and define the kinetics of vaginal Treg populations after primary infection with HSV-2. We also interrogated how the Tregs that persist in the vagina influence tissue pathology, Trm responses, and tissue healing upon challenge with HSV-2.

3.3 RESULTS

3.3.1 *Tregs persist in the vaginal mucosa of mice immunized with thymidine kinase-deficient HSV-2*

The experiments in Chapter 2 employed wildtype HSV-2 (HSV-2 WT), which is lethal in within 7-14 days, precluding long-term experiments. Alternatively, thymidine kinase deficient HSV-2 (HSV-2 TK-) is an attenuated strain of HSV-2 that causes less severe disease, is non-lethal, and is cleared from the vaginal tissue, allowing for experiments at memory timepoints[239]. To study the role of Tregs in memory responses to HSV-2, we infected FoxP3DTR[26] mice with HSV-2 TK- and harvested the VT and dLN at days 0, 43, and 90 post-infection. By flow cytometry, we identified Tregs as CD4+ FoxP3+ and calculated the absolute number of Tregs and total CD4+ T cells in the dLN and VT. By day 43 post-HSV-2 TK- infection, Treg numbers

in the VT were significantly increased compared to baseline, as were total CD4+ T cells (

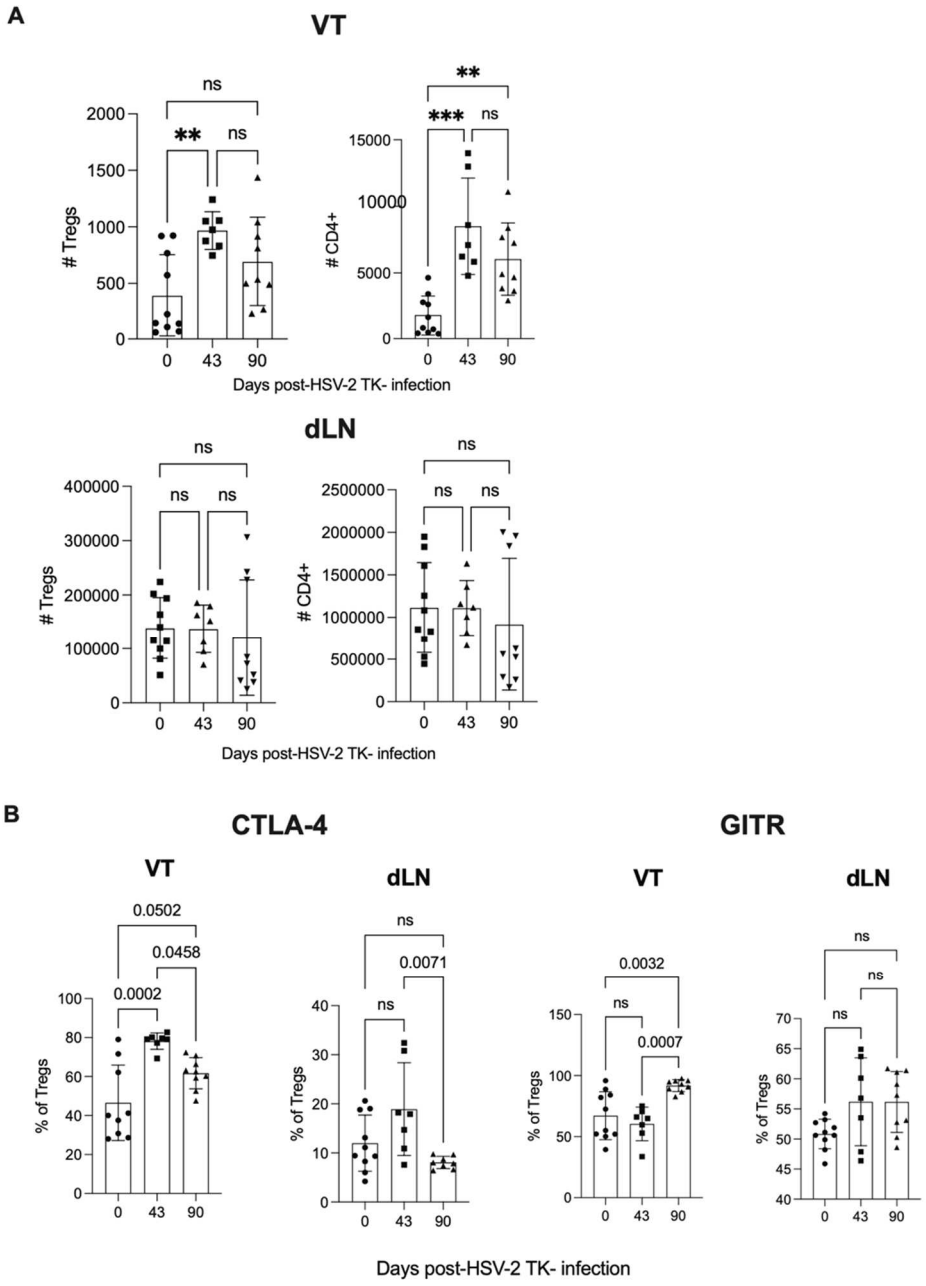

Figure 3.1A). By day 90, Treg numbers in the VT had diminished compared to day 43, but were maintained at a (non-significantly) higher number than at baseline, suggesting that a vaginal Treg population persists in the tissue after HSV-2 infection and that vaginal Tregs may

be important for secondary HSV-2 exposures (

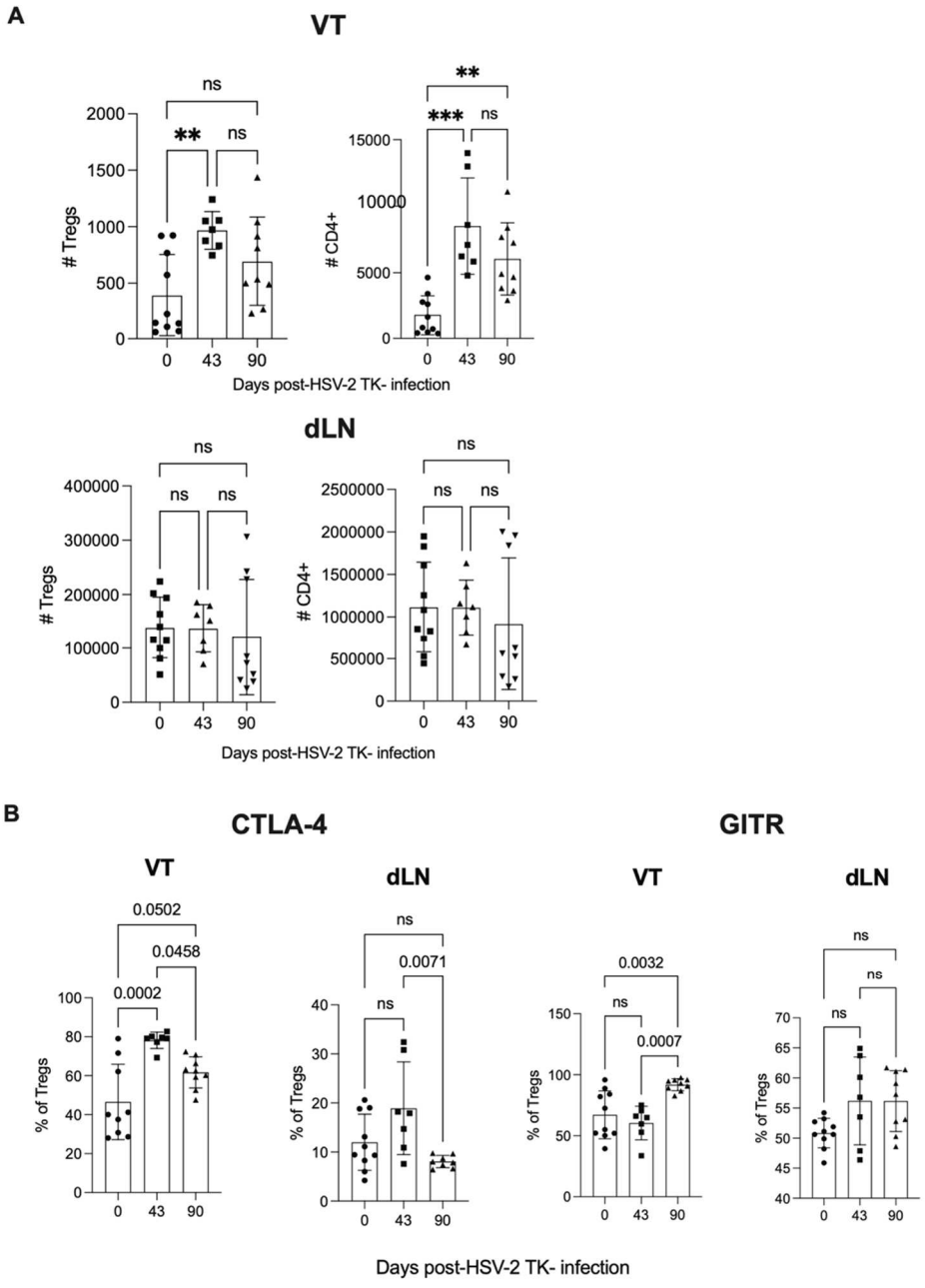

Figure 3.1A). Likewise, total CD4+ T cell numbers at day 90 in the VT decreased compared to day 43 but persisted at significantly higher numbers than uninfected mice (

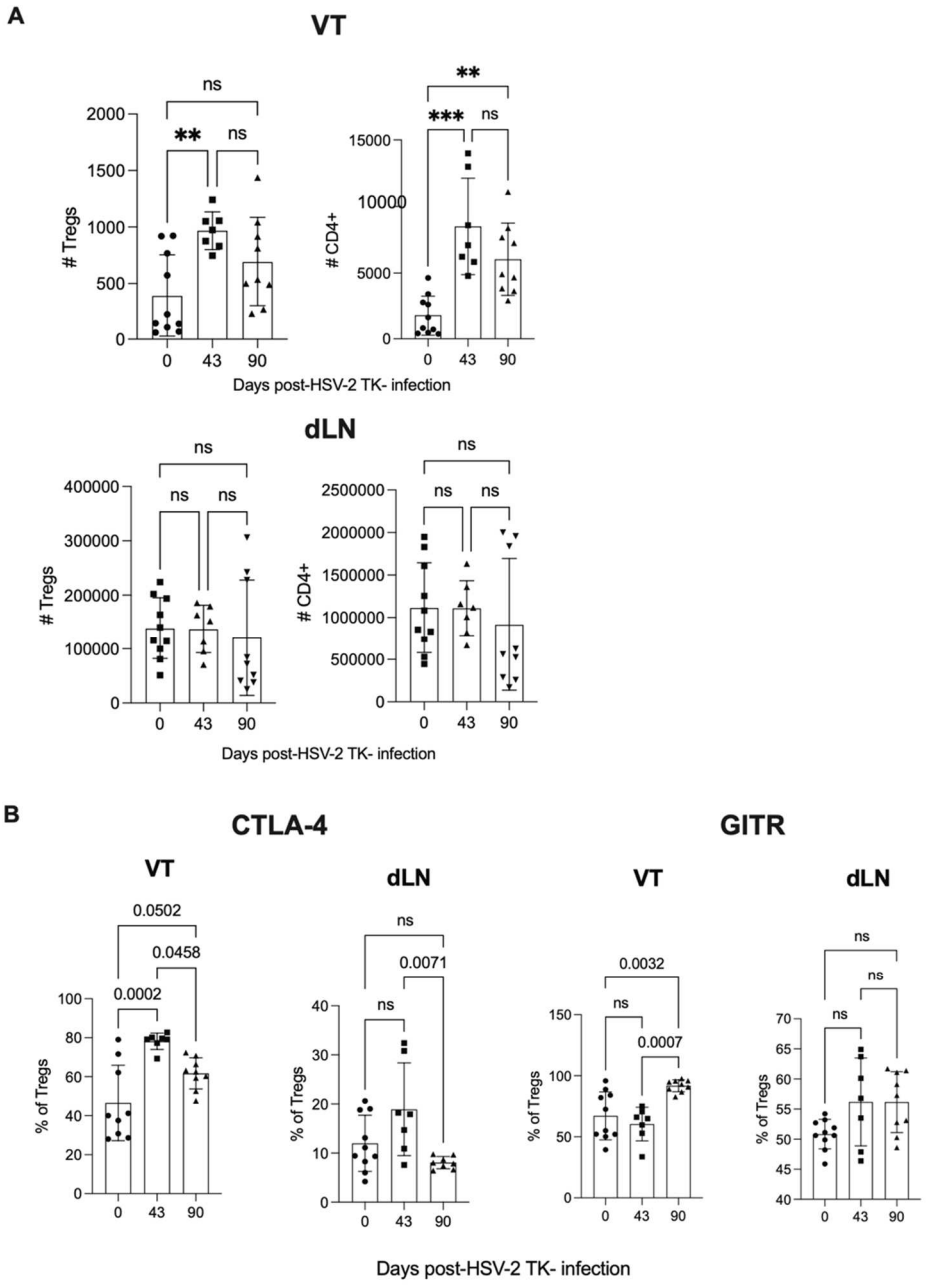

Figure 3.1A). In contrast, neither Treg nor CD4+ T cell numbers were significantly increased in the dLN at day 43 or day 90 compared to baseline, demonstrating that the dLN CD4+ and Treg compartment are relatively undynamic compared to the VT, suggesting a specific role for

CD4+ T cells and Tregs in the tissue at the site of HSV-2 infection (

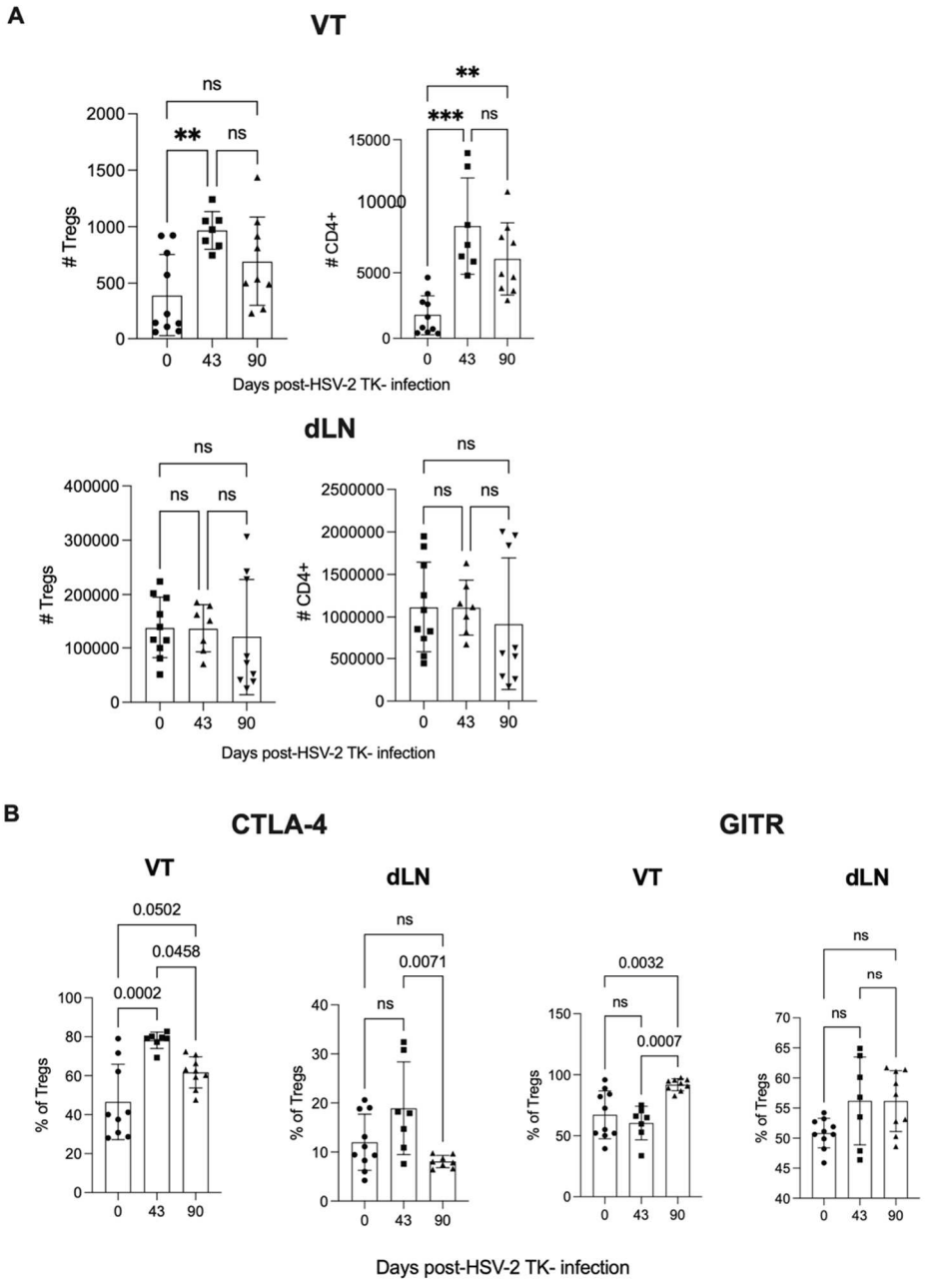

Figure 3.1A).

Additionally, the frequency of vaginal Tregs expressing CTLA-4 after infection remained significantly elevated at day 43 compared to uninfected mice and was nearly significantly

elevated at day 90 ($p = .0502$, Figure 3.1B). In contrast, CTLA-4 expression on dLN Tregs was not significantly increased at day 43 or day 90 (Figure 3.1B). These findings suggest that the pool of memory Tregs that persist in the vaginal tissue retain heightened activation potential. Interestingly, Tregs expressing GITR followed a similar pattern, although GITR expression was not significantly increased on vaginal Tregs until day 90 (Figure 3.1B). This could suggest that GITR+ Tregs are preferentially retained in the tissue long-term while GITR- Tregs decay, skewing the vaginal Treg pool towards highly activated tissue Tregs that are poised to respond to HSV-2 re-encounter.

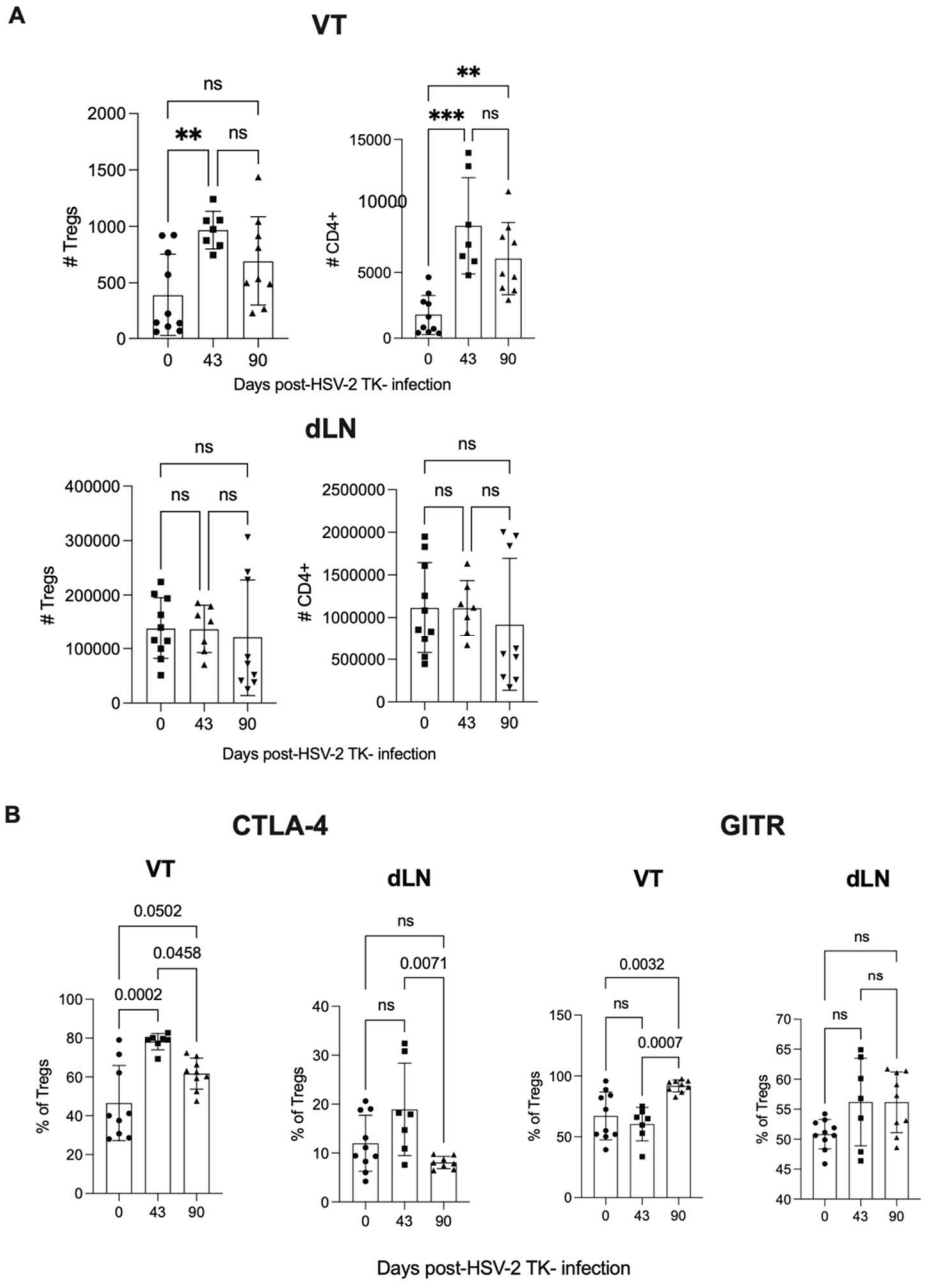

Figure 3.1. Tregs persist in the vaginal tissue after infection with HSV-2 TK-.

C57BL/6J mice were administered Depo provera s.c. and infected 5-7 days later ivag with HSV-2 TK-; uninfected controls received Depo provera only. On days 0, 43, and 90 post-infection, VT and dLN were harvested and prepared for flow cytometry. Tregs were identified as CD4+ FoxP3+. A) Top: Absolute number of Tregs (left) and total CD4+ T cells (right) in the VT. Bottom: Absolute number of Tregs (left) and total CD4+ T cells (right) in the dLN. Significance determined by Kruskal-Wallis test with Dunn's multiple comparison test, $p < .05$. **B)** Frequency of Tregs in the VT or dLN expressing CTLA-4 (left) or GITR (right). Significance determined by One-way ANOVA with Tukey's multiple comparison test, $p < .05$.

3.3.2 *Tregs restrain Granzyme B expression on vaginal CD8+ T cells during HSV-2 challenge*

Given that we observed that activated Tregs persist in the vaginal tissue up to 90 days post-infection with HSV-2 TK-, we hypothesized that these memory Tregs might function to rapidly respond during HSV-2 challenge, limiting the cytotoxic responses of vaginal CD8+ T cells. To test this, we infected FoxP3DTR mice with HSV-2TK- and challenged with HSV-2 WT 30 days later. We simultaneously administered i.p. DT or PBS control on days -1 and 0 of HSV-2 challenge to deplete Tregs. On day 3 post-challenge, we harvested the VT and dLN of both groups to compare CD8 responses in the presence or absence of Tregs. Although preliminary, we found that Treg depletion significantly ($p = .0051$) increased the frequency of vaginal CD8+ T cells expressing GzmB by approximately 4-fold compared to Treg-replete mice (Figure 3.2A-B). Interestingly, we did not observe a significant increase in GzmB+ expression on dLN CD8+ T cells, highlighting the importance of the tissue-localized Treg response at the site of infection (Figure 3.2A-B). However, further studies are needed to confirm this result, as well as to assess additional effects of Treg depletion on the overall CD4+ and CD8+ Trm compartment.

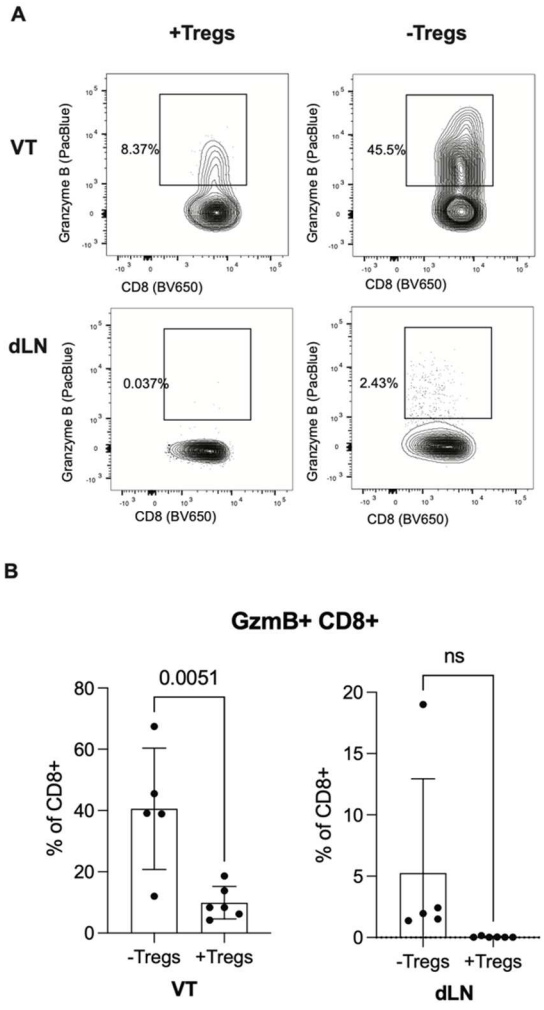

Figure 3.2. Tregs restrain Granzyme B production during HSV-2 challenge in vaginal CD8+ T cells

FoxP3^{DTR} mice were administered subcutaneous (s.c.) Depo provera in the neck ruff, and infected 5-7 days later with intravaginal (ivag.) infection HSV-2 TK-. On day 30 post-infection, mice we re-administered s.c. Depo provera in the neck ruff. 5-7 days later, mice were administered intraperitoneal (i.p.) diphtheria toxin (DT) or PBS mock on days -1 and 0 of ivag. HSV-2 WT challenge. Mice were harvested on day 3 post-infection and VT and dLN harvested for flow cytometry. **A)** Representative GzmB staining on CD8+ T cells in the VT (top) and dLN (bottom) in Treg-replete (left) and Treg-depleted (right) mice. **B)** GzmB+ CD8 frequency of total CD8+ T cells in the VT (left) and dLN (right) of Treg-replete or Treg-depleted mice. Significance determined by t test, $p < .05$.

3.3.3 *Vaginal tissue healing is delayed in mice depleted of Tregs during HSV-2 challenge*

In humans, HSV-2 infects the vaginal epithelium before ascending the dorsal root ganglia where it becomes latent; HSV-2 can then periodically reactivate, traveling back down the neurons to cause lesions and viral shedding in the vaginal mucosa and skin[238, 262]. Although there is currently no model of HSV-2 reactivation in mice, we circumvent this limitation by initially infecting mice with HSV-2 TK- and later challenging with HSV-2 WT. HSV-2 TK- generates protective immunity, preventing death in WT-challenged mice[263-266], allowing us to study immune responses to secondary HSV-2 exposure. Given that Tregs have been shown to limit tissue pathology by restraining effector immune responses to mucosal infection[19], we hypothesized that a loss of Tregs during HSV-2 challenge would lead to increased vaginal pathology. To test this, FoxP3^{DTR} mice were synchronized in the diestrus phase of the estrus cycle with a s.c. injection of depo provera 5-7 days before ivag. infection with HSV-2 TK-. At 30 days post-primary infection, mice were re-synchronized with depo provera 5-7 days before challenging with ivag. HSV-2 WT. On days -1 and 0 of challenge, mice were treated with intraperitoneal (i.p.) injection of diphtheria toxin, which selectively depletes Tregs within 2 days of treatment[26], or PBS control. The vaginal cavity was swabbed daily for subsequent PCR analysis of HSV-2 virus. On days 3, 7, 10, and 14 post-challenge, we harvested the VT and performed by Hematoxylin and Eosin (H&E) staining to assess vaginal pathology (Figure 3.3). Previously, we established a scoring rubric for HSV-2-mediated vaginal pathology (Figure 3.3A) based on H&E visualization of cellular infiltrate and loss of tissue integrity of the vaginal epithelium, lumen, muscularis, and lamina propria. Using this system, we blindly scored the vaginal pathology in the presence or absence of Tregs. Pathology scores were highest at day 3

post-challenge, with no significant difference in the scores between Treg-depleted and Treg-replete groups (Figure 3.3B). However, by day 7 post-challenge, Treg-depleted mice scored significantly higher than Treg-intact mice, suggesting that a loss of Tregs delays tissue healing after HSV-2 challenge. By day 10 post-challenge, pathology scores in both groups continue to decrease, and by day 14 post-challenge, vaginal pathology was nearly returned to baseline scores. At both days 10 and 14, Treg-depleted scores were not significantly elevated compared to Treg-replete mice, suggesting that Tregs have important *early* roles during the peak memory response to HSV-2. Mice treated with DT alone showed minor increased pathology compared to untreated mice, but significantly less than mice treated with both HSV-2 and DT (Figure 3.3B). Together, these data suggest that Tregs might prevent tissue damage during HSV-2 challenge.

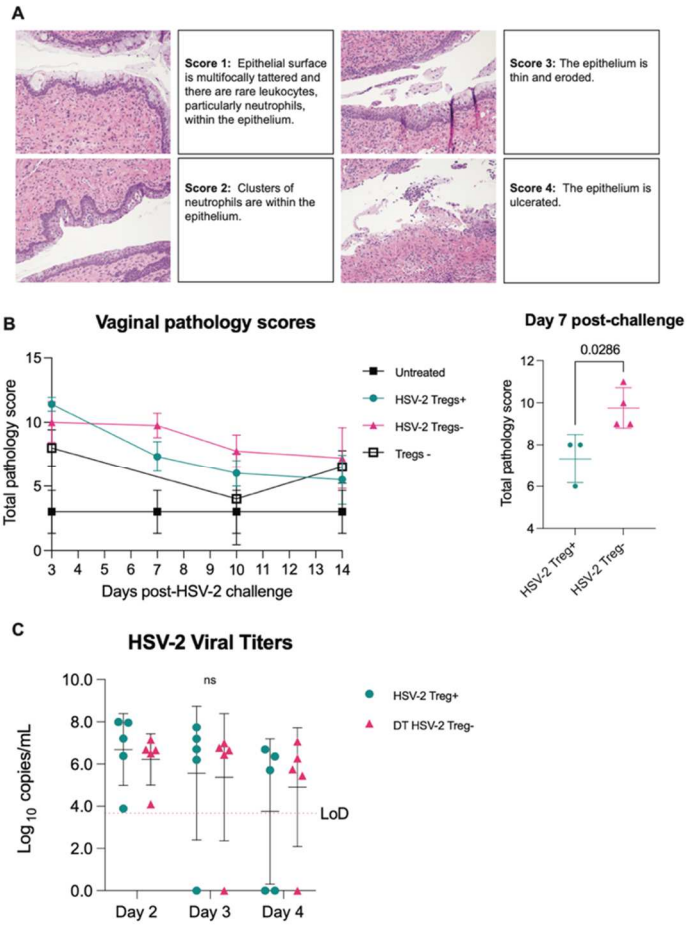

Figure 3.3. Treg depletion delays vaginal tissue healing after HSV-2 challenge.

A)Vaginal tissue pathology scoring system by Hematoxylin and Eosin (H&E) staining. Vaginal pathology is assessed by totaling discrete pathology scores within the lumen, muscularis, epithelium, and lamina propria, based on cellular infiltrate and loss of tissue integrity. Images shown are vaginal epithelium from FoxP3^{DTR} mice treated with HSV-2 WT or HSV-2 TK-. **B)** FoxP3^{DTR} mice were administered subcutaneous (s.c.) Depo provera in the neck ruff, and infected 5-7 days later with intravaginal (ivag.) infection HSV-2 TK-. On day 30 post-infection, mice were re-administered s.c. depo provera. 5-7 days later, mice were administered intraperitoneal (i.p.) diphtheria toxin (DT) or PBS mock on days -1 and 0 of ivag. HSV-2 WT challenge. Mice were harvested on days 3, 7, 10, and 14 post-challenge and vaginal sections were taken for H&E staining and pathology scoring. Left: total pathology scores after challenge and in untreated mice. Right: Total pathology scores on day 7 post-HSV-2 challenge. Significance determined by Mann-Whitney test, $p < .05$. **C)** FoxP3^{DTR} mice were administered s.c. Depo provera in the neck ruff, and infected 5-7 days later with intravaginal ivag. Infection with HSV-2 TK-. On day 30 post-infection, mice administered intraperitoneal (i.p.) DT or PBS mock on days -1 and 0 of ivag. HSV-2 WT challenge. On days 2, 3, and 4 post-challenge, the vaginal lumen was swabbed into titration buffer and HSV-2 viral load assessed by PCR. Significance determined by Mann-Whitney test, $p < .05$.

3.3.4 *Treg depletion during HSV-2 challenge does not affect vaginal viral titer*

Tissue Tregs have been shown to limit collateral damage to the host by limiting immune responses to several pathogens, often at the expense of efficient pathogen control[19, 50, 51, 201, 202, 267, 268]. Alternatively, Treg removal in other infections delays viral clearance[194, 195, 269 270, 271], suggesting that the role of Tregs during infection is highly context-dependent. Thus, we predicted that Treg removal during HSV-2 challenge might either 1) exacerbate viral clearance due to unrestrained effector responses or 2) delay viral clearance due to dysregulation of the immune response to HSV-2 without Tregs[194, 195]. However, when we assessed the vaginal viral load by PCR on days 2 through 4 post-challenge, viral titers were comparable between groups (Figure 3.3C) and virus was cleared below the level of detection by days 5-6 (data not shown). This finding shows that although vaginal tissue pathology is increased without Tregs during HSV-2 challenge, this increased pathology is not the result of increased viral replication, and Treg depletion does not affect vaginal viral load.

3.3.5 *Vaginal Tregs produce Areg early after primary HSV-2 infection*

Based on these findings, we hypothesized that vaginal Tregs may limit pathology by restraining excessive memory immune responses, and that Tregs may also directly contribute to tissue repair. As previously mentioned, Tregs in both muscle and lung have been shown to produce Areg to contribute to tissue repair during muscle damage and lung infection with influenza[30, 38, 44]. Therefore, we hypothesized that vaginal Tregs could contribute to vaginal healing post-HSV-2 lesion by producing Areg. To test this, we revisited data from an earlier experiment where we sorted CD4+GFP+ Tregs or CD4+GFP- CD4Tconv from the VT of FoxP3^{GFP} mice on day 7

post-HSV-2 infection, or from uninfected control mice. We then performed single-cell RNA-seq. We used the Seurat pipeline[216] to perform graph-based clustering of Tregs and CD4 Tconv in the VT and compared differentially expressed genes (DEG) between vaginal Tregs and CD4Tconv using Model-based Analysis of Single-cell Transcriptomics (MAST)[218]. Although we recovered insufficient Tregs from uninfected VT to sequence, we found that VT Tregs from infected mice differentially upregulated *Areg* compared to dLN Tregs from HSV-2-infected and uninfected mice (APPENDIX C, Figure 3.4A). To confirm this finding on the protein level, we treated C57BL/6J mice s.c. with depo provera 5-7 days before intravaginal infection to synchronize estrus cycle phases for consistent susceptibility to HSV-2 infection[209]. On days 0 and 5 post-WT HSV-2 primary infection, we stained for Areg in the dLN and VT[44]. Cell numbers at day 0 were low, precluding accurate quantification of Areg+ Tregs as a percentage of total Tregs. However, by day 5 post-infection, VT Tregs expressed Areg, although not significantly more than dLN Tregs or VT CD4 Tconv. (Figure 3.4B-D). Together, these results demonstrate that vaginal Tregs express Areg transcripts and protein after HSV-2 infection, suggesting that vaginal Tregs may have a unique role in Areg-mediated tissue repair after HSV-2 infection. However, further research is needed to confirm Areg production by Tregs after HSV-2 challenge and to functionally link Treg-produced Areg to vaginal tissue healing.

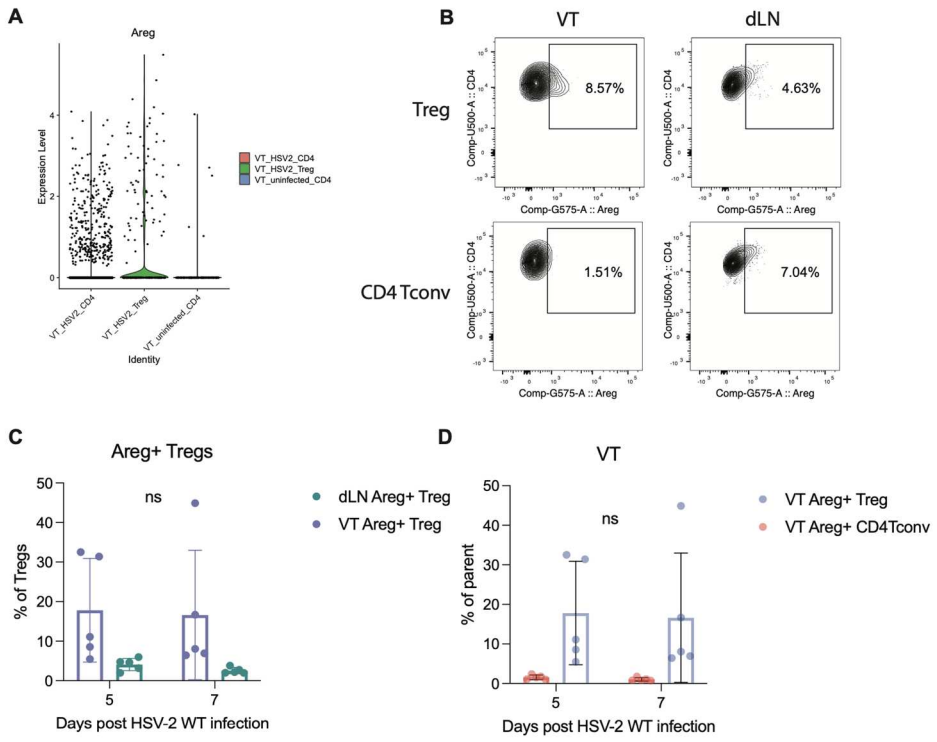

Figure 3.4. Tregs express Areg after primary infection with HSV-2 WT.

A) FoxP3^{GFP} mice were administered Depo provera s.c. and infected 5-7 days later ivag with WT HSV-2; uninfected controls received Depo provera only. On day 7 post-infection, VT were harvested and prepared for FACS to isolate CD4+ FoxP3+ Tregs and CD4+ FoxP3- CD4 Tconv. Single-cell RNA-sequencing was performed on VT Tregs and CD4 Tconv and analyzed with the Seurat pipeline in R. n = 5 HSV-2+ and n = 3 uninfected. Violin plots of *Areg* expression in vaginal Treg (HSV-2+) and CD4 Tconv (HSV-2 +/-) populations. **B)** C57BL/6J mice were administered Depo provera s.c. in the neck ruff, and infected 5-7 days later with intravaginal (ivag.) HSV-2 or PBS mock. On days 0 and 5 post-infection, VT and dLN were harvested for flow cytometry analysis. Representative staining for Areg on FoxP3+ Tregs (top) and CD4+ Tconv (bottom) on day 5 post-infection in VT (left) and dLN (right), C-D) quantified as a percentage of parent population. n=5. Significance determined by multiple paired t test, $p < .05$.

3.4 DISCUSSION

Previously, investigations of Tregs in viral infection, including memory Treg responses, have been sparse, while the vaginal Treg compartment has remained completely unstudied. We sought to define contributions of Tregs during HSV-2 secondary exposure or recurrence and to assess how Tregs might either augment or hinder immune responses to HSV-2 and the consequences of

this immunoregulation in the host tissue compartment. We first confirmed the establishment and persistence of an activated vaginal Treg population after HSV-2 infection, and then used a secondary HSV-2 infection model in mice to assess vaginal immunopathology and HSV-2 control in mice depleted of Tregs during viral challenge. We also used transcriptional analysis and flow cytometry to measure vaginal Treg production of Areg, a growth factor known to repair injured tissues.

Although vaginal Trm are known to be important for protection from and control of HSV-2, little consideration has been given to Treg-mediated regulation of Trm. Importantly, despite the presence of Trm in HSV-2 lesions in human vaginal tissue, HSV-2 symptoms are highly variable between infected people and higher Treg:CD4Tconv ratios are associated with higher viral shedding[260], suggesting that Tregs may influence Trm-mediated immunity to HSV-2. We hypothesized that Tregs could be a missing link between vaginal Trm and viral control. In support of this, our preliminary data found that Treg depletion at the time of HSV-2 challenge significantly increased the CD8+GzmB+ pool in the vagina, suggesting that memory vaginal Tregs restrain potent CTL responses during HSV-2 challenge, possibly to protect the local tissue from aggressive memory T cell responses. We further sought to investigate immune responses and tissue pathology when Tregs were removed during HSV-2 challenge in mice. Consistent with other infection models[19, 39, 40, 201], these experiments revealed that Treg ablation results in delayed tissue healing of HSV-2 lesions. However, unlike other infection models[19, 50, 51, 202], Treg removal did not improve viral clearance, suggesting that the pathology observed is not virus-mediated and that Tregs do not impede viral clearance during HSV-2 challenge. Together, these findings led us to conclude that vaginal Tregs limit collateral damage during HSV-2 challenge

without affecting viral load. We hypothesized that Tregs could exert this protective effect by restraining highly activated Trm and/or by actively contributing to lesion repair.

To test whether Tregs could be directly contributing to vaginal tissue healing through production of Areg, a growth factor secreted by muscle and lung Tregs to heal damaged tissue[30, 44], we revisited previous single-cell RNA seq analysis of vaginal Tregs and CD4Tconv after primary HSV-2 infection. This data revealed that vaginal Tregs from HSV-2-infected mice differentially express Areg transcripts compared to vaginal CD4 Tconv (from both infected and uninfected mice), suggesting that vaginal Tregs may acquire Areg transcripts after either localization in the tissue or in response to viral infection. Additionally, we confirmed Areg production in Tregs, and to a lesser degree in CD4 Tconv, in the mouse vagina after HSV-2 primary infection. This suggests a tissue-specific non-regulatory function for Tregs in promoting lesion healing after HSV-2 infection. Further studies are needed to confirm Treg Areg production in HSV-2 challenge and in human Tregs, as well as functional studies to test whether Areg specifically—instead of Tregs in general—are necessary for preventing tissue pathology after HSV-2 infection. For example, our Treg depletion experiments could be repeated with $Areg^{flox/flox44}$ mice crossed to $FoxP3^{Cre272}$ mice will produce offspring that lack Areg only on Tregs, revealing whether Treg-produced Areg is specifically responsible for the pathology discrepancies we observed. Alternatively, Areg could be one of several functions, such as production of inhibitory cytokines and restraint of CTL or antigen-specific Trm, that Tregs employ to limit local pathology. However, if true, the beneficial functions of Tregs in preserving delicate mucosal tissues must be considered in vaccine design or therapeutics, where Tregs have been classically considered a hindrance to pathogen or tumor clearance.

In addition to further Areg studies, experiments are ongoing to assess how conventional effector T cell responses are affected by Tregs during HSV-2 challenge. We are currently investigating how the number, activation status, and cytotoxic potential of both CD4+ and CD8+ T cells in the VT and dLN of Treg-depleted mice compare to Treg-replete mice during HSV-2 challenge. Although we have thus far found that Tregs restrain GzmB expression on vaginal CD8+ T cells during HSV-2 challenge, we are further assessing Treg-mediated control of Trm, such as whether Tregs preferentially limit HSV-2-specific Trm responses through the use of an HSV-2 tetramer that identifies CD8+ T cells that recognize glycoprotein B on HSV-2[273].

In summary, our work further defines the previously unstudied vaginal Treg compartment and identifies a role for Tregs in preventing excessive vaginal pathology during HSV-2 challenge, quantified through the development of a vaginal immunopathology scoring system, which has not been previously used to measure HSV-2 disease. We also found evidence that vaginal Tregs produce Areg in response to local infection, identifying a putative non-regulatory role for vaginal Tregs and linking this population to muscle and lung Tregs, which have been previously shown to promote tissue repair through Areg production[30, 38, 44]. Lastly, this work investigates the kinetics and functions memory Tregs during infection, a subject which has not been extensively studied. This work has important implications for mucosal therapeutics and vaccine development, as these interventions generally aim to boost host immunity at all costs. However, the Treg-mediated balance of immunity:immune restraint should be considered, as the protective effects of Tregs may outweigh the consequences of their immune restraint during mucosal infection.

3.5 MATERIALS AND METHODS

3.5.1 *Mice*

6-8 week-old female wildtype C57BL/6J (Jackson Laboratories, Bar Harbor, ME), FoxP3^{DTR26}, or FoxP3$^{GFP\ 214}$ (bred at Fred Hutch) mice were used for experimental groups. All animal experiments were approved by Fred Hutch IACUC and the study was conducted in strict compliance with the PHS Policy on Humane Care and Use of Laboratory Animals.

3.5.2 *Infections*

For primary infections, mice were injected subcutaneously in the neck ruff with 2 mg of medroxyprogesterone acetate (Depo-Provera) 5-7 days prior to intravaginal (ivag.) infection with 10^4 PFU of WT HSV-2 derived from a human clinical isolate or 10^5 PFU of HSV-2 TK-^{239}.
For memory infections, mice were injected subcutaneously in the neck ruff with 2 mg of medroxyprogesterone acetate (Depo-Provera) 5-7 days prior to intravaginal (ivag.) infection with 10^5 PFU of HSV-2 TK-. 30 days following infection, mice were again injected subcutaneously in the neck ruff with 2 mg of Depo Provera 5-7 days prior to ivag. infection with 10^4 PFU of WT HSV-2.

3.5.3 *Mouse tissue processing*

Vaginal tract (VT), including the vagina and cervix, was harvested and minced with scissors followed by a 30-minute incubation in RPMI containing collagenase D (2mg/ml; Sigma) and

DNAse (15ug/ml; Sigma) at 37 degrees C. Following incubation, collagenase reaction was quenched with 5mM EDTA in HBSS without calcium and magnesium and passed through 70um strainer to prepare a single-cell suspension. After harvesting, vaginal-draining lymph nodes (dLN), including the inguinal and iliac lymph nodes, were passed through 70um filter to prepare a single-cell suspension.

3.5.4 *Cell sorting and flow cytometry*

Cells were incubated in fixable viability dye (Invitrogen) and blocked for non-specific Fc binding in PBS for 30 minutes. Cells were then stained for surface proteins in FACS buffer (PBS containing .02% sodium azide and 2% fetal calf serum) for 20 minutes, fixed for 30 minutes with Foxp3 Transcription Factor Staining Buffer Set (eBioscience) fixative, followed by 2 washes with Foxp3 Transcription Factor Staining Buffer perm buffer and stained for 30 minutes with intracellular antibodies in perm buffer. Cells were acquired with the FACSymphony (BD Biosciences, San Jose, CA) and data analyzed with FlowJo software version 10.6.1 (Treestar, Ashland, OR).

Cell sorting for RNA-sequencing experiments was performed on the FACSAria (BD Biosciences, San Jose, CA). Tregs and CD4+ T_{conv} isolated from vaginal tissue and vaginal-draining lymph nodes were sorted from $FoxP3^{GFP}$ mice on CD4+ GFP+ and CD4+ GFP-, respectively. Tregs and CD4+T_{conv} from vaginal tissues were additionally sorted on intravascular label- population to exclude blood T cell contamination. To estimate total cell counts, $2x10^4$ AccuCheck Counting Beads (Thermo Fisher Scientific) were added to each sample prior to acquisition on the cytometer.

3.5.5 *Single-cell RNA-sequencing*

Sorted cells from VT were processed using the 10X Genomics Platform with the 5' Chromium Single Cell V(D)J Enrichment Kit v2 following manufactures instructions. Sorted populations from each mouse (infected: n= 5; uninfected: n=3) were pooled with the following total cell numbers were loaded into the Chromium Controller: infected VT CD4+FoxP3+: 2,855; infected VT CD4+FoxP3-: 20,000; uninfected VT CD4+FoxP3-: 1,562. As per manufacturer's instructions, the target cell number for each population was calculated as half the number of cells loaded. cDNA was generated within oil emulsion droplets made by the Chromium Controller. cDNA was purified using DynaBeads MyOne Silane magnetic beads (thomerFisher, #370002D). cDNA amplification was performed by 10 rounds of PCR using Chromium Single Cell 5' Reagent kit. Amplified cDNA was then purified with SRPIselect magnetic beads (Beckman Coulter). After cDNA was fragmented and size selected, library construction was performed by end repair, A-tailing, adaptor ligation and PCR (12 cycles). Prior to sequencing, quality of libraries was determined by using Aglient 2200 TapeStation with High Sensitivity D5000 Screen Tape (Agilent). Libraries were quantified by digital droplet PCR with Library Quantification Kit for Illumina TruSeq (BioRad, #1863040). Libraries were diluted to 3 nM and paired-end sequencing was performed on a NovaSeq 6000 sequencer (Illumina).

3.5.6 *Single-cell RNA-sequencing analysis*

As previously described[240], sequencing data were processed to per-cell read and unique molecular identifier (UMI) counts with Cell Ranger software (10x Genomics, Pleasanton, CA).

The reads were converted from BCL to FASTQ, demultiplexed, filtered, aligned to mouse genome assembly GRCm38 (mm10), collapsed to UMIs, and assigned to barcodes. Default settings in Cell Ranger were used to call cells vs. background. Data from each sample were aggregated without normalizing.

The R package Seurat was used to analyze count data[216, 248-250]. Genes detected in fewer than 400 and greater than 35,000 cells were removed, as were cells that had fewer than 400 and greater than 5000 genes detected based on natural breaks in data visualization. Cells with greater than 5% mitochondrial reads were also removed. As previously described[240], the UMI counts were log transformed and total UMIs and % mitochondrial reads per cells were regressed out. With UMAP, cells were projected on the first 50 principal component axes from 2000 highly variable genes identified using default cutoffs. Seurat objects were created for each sample and re-scaled using all genes. Each cell's expression of defined gene sets was summarized by the mean normalized expression across the set in each cell. To remove noise around 0 introduced by normalization, 0 values for each gene in each cell with a raw UMI count of 0 were restored. Differential expression was quantified among populations using the hurdle model in MAST, with total UMIs per cell as a covariate. MAST identifies DE genes that overlap with those found by other methods with high precision and low false positive rates [218, 251].

3.5.7 *Treg depletion*

Tregs were depleted from FoxP3DTR mice by administering 30mg/kg and 10mg/kg i.p. diphtheria toxin (DT)[26] on days -1 and 0, respectively, of HSV-2 WT challenge.

3.5.8 *Vaginal pathology scoring*

Vaginal tissues were fixed in 4% paraformaldehyde for 4 days and then paraffin embedded for sectioning. Tissues were sectioned into the lumen and stained with hematoxylin and eosin (H&E) and blindly scored for vaginal pathology by an animal pathologist. A scoring rubric was created by an animal pathologist for this project by comparing H&E-stained vaginal sections from mice with known, increasing levels of vaginal pathology (uninfected, infected with HSV-TK-, infected with HSV-2 WT). Experimental pathology scores were then obtained by blind scoring of vaginal slides, based on the established rubric. Total pathology scores are the sum of the scores from the epithelium, lamina propria, muscularis, and lumen compartments.

3.5.9 *HSV-2 quantification by PCR*

HSV-2 viral titers were quantified by PCR at UW Virology. DNA was extracted from 200 ul specimen using QIAamp 96 DNA blood kit and eluted into 100 ul of AE buffer (Qiagen). Real-time Taqman PCR detects HSV gB gene was applied to quantify HSV in the samples (Jerome paper). Each 30 ul PCR reaction contains 10 ul of purified DNA , 833 nM primers, 100 nM probe, 15 ul of 2x QuantiTect Multiplex PCR master mix, 0.03 units of UNG. To monitor PCR inhibition, EXO internal control was spiked into all the reactions. The thermocycling conditions are as following: 50ºC for 2 minutes, 95ºC for 15 minutes, followed by 45 cycles of 94ºC for 1 minute and 60ºC for 1 minute. The limit of detection is 3 viral copies/reaction.

3.5.10 *Statistical analysis*

For flow cytometry data, statistical analyses were performed with Prism software version 9.1 (GraphPad Software, San Diego, CA). Ordinal data were assessed with Mann-Whitney U test,

and parametric data were assessed with multiple paired T tests. Non-parametric multiple comparisons were assessed with the Kruskal-Wallis test followed by Dunn's multiple comparison test. Significance was defined by a p value less than .05.

3.6 ACKNOWLEDGEMENTS

We thank Amanda Koehne and the Fred Hutch Experimental Histopathology core for their help with immunohistochemistry and Meei-Li Huang and Tracy Santo at UW Virology for their help with performing HSV-2 quantification by PCR. We thank Irene Cruz Talavera for her help with this project, as well as members of the Lund and Prlic labs for their helpful discussions.

Chapter 4. CONCLUDING REMARKS

4.1 CONCLUSIONS AND IMPLICATIONS

Tregs were originally discovered and studied in the thymus, circulation, and secondary lymphoid organs, demonstrating their indispensable role in maintaining peripheral tolerance and preventing autoimmunity[26]. Building on this research, Tregs were later discovered in various non-lymphoid tissues, where they performed surprising, extra-regulatory roles and location-specific functions, demonstrating the dynamic and context-dependent nature of Tregs[30-32, 35]. More recently, Tregs have been described in mucosal barrier tissues such as the GI tract and lung, where they also carry out both classic immunoregulation and specialized, location-appropriate roles such as promoting oral tolerance and maintaining mucosal tissue integrity[44, 85]. However, the investigation of Tregs in the female reproductive tract has been limited. Additionally, while Tregs are well-studied in autoimmunity and cancer, the role of Tregs in anti-pathogen responses has only been investigated by a few groups, yielding varied and context-dependent results. Therefore, we sought to characterize the vaginal Treg compartment in both health and viral infection, combining two understudied areas of Treg biology.

We found that vaginal Tregs in both healthy mice and humans are relatively rare, but highly activated population compared to blood or dLN Tregs, where most of the population expressed activation and suppression markers such as CTLA-4, GITR, ICOS, CD39, and TIGIT. This suggests that tissue localization alone confers a distinct, activated phenotype on Tregs. Interestingly, we found that the expression of classical markers of tissue residency-CD69 and CD103- are difficult to interpret in vaginal Tregs and may not be necessary for vaginal tissue localization or retention. For example, we found that vaginal Tregs expressed little CD103, and

CD69 expression was dynamic, transiently increasing during acute activation and waning days later. Consistent with other literature suggesting that CD4+ Trm may not be constrained by CD69 and CD103 expression[206, 207], these findings suggest that CD69 and CD103 cannot be universally interpreted outside of a defined tissue and infection model.

We also investigated vaginal Tregs after HSV-2 infection. Other studies of Tregs in infection, including in mucosal sites, have revealed that Treg roles are extremely context-dependent, as varying models have yielded differing results. For example, Tregs restrain immune-mediated tissue damage in some infection, while also inhibiting efficient pathogen control[50, 51, 201, 202]. Conversely, other groups, including our own, have previously shown that Tregs limit viral-mediated disease[40, 194, 195]. In fact, our lab has shown that Tregs in the vaginal dLN are crucial for proper coordination of the immune response to primary HSV-2 infection, and that a loss of Tregs delays viral clearance and augments disease[194, 195]. However, the phenotype and role of Tregs in the vagina, at the site of HSV-2 infection, have not been studied until now. We found that HSV-2 infection increased the number of vaginal Tregs in mice, including highly activated CTLA-4+ and GITR+ Tregs, as well as induced ICOS expression on vaginal Tregs. Interestingly, we found that HSV-2 infection specifically induced GzmB on a subset of vaginal, but not dLN Tregs, and that we could reproduce this Treg GzmB acquisition ex vivo by stimulating either bulk splenocytes or T cells with inflammatory cytokines IFN-a, IFN-B, and IL-2. Together, these results suggest that vaginal Tregs further activate during local viral infection and acquire cytotoxic potential that could be used to restrain effector T cell responses, limit immunopathology, or for some additional, undefined role. GzmB+ Tregs in acute infection have important implications for clinical therapeutics or vaccines. GzmB+ Tregs could serve as a

marker of acute infection, and the dynamic role of Tregs in the mucosal tissue should be considered when designing mucosal vaccines, as Tregs may not simply hinder anti-pathogen immune responses, as previously thought, but also crucially prevent irrevocable tissue damage. Tregs must be leveraged in the clinic to harness the best balance of immunoregulatory and non-canonical functions.

Additionally, we studied memory Tregs—which are largely undefined-- in HSV-2 reinfection, demonstrating that vaginal the vaginal Treg population established after HSV-2 infection persists up to at least 90 days in mice. These Tregs are poised to respond to HSV-2 recurrence, where they limit vaginal pathology following HSV-2 challenge lesions. The increased pathology observed is not virus-mediated, as HSV-2 titers are comparable between Treg-depleted and Treg-intact mice, suggesting that Tregs instead limit collateral self-damage by the host immune system, although this subject requires further investigation. These findings relate to HSV-2 recurrence in humans, as HSV-2 becomes latent, causing periodic reactivations accompanied by viral shedding and lesions, which have been difficult to treat in some patients. Tregs could be a factor that influence why some HSV-2+ people experience painful lesions, while others remain asymptomatic. Lastly, we preliminarily showed that vaginal Tregs can produce Areg after HSV-2 infection, highlighting a potential shared role with lung and muscle Tregs[30, 44] and an important tissue-preserving function for vaginal Tregs. Again, these findings underscore that in addition to Trm, Tregs must be considered in mucosal vaccine design, as they may influence Trm responses in order to protect the mucosa, and that either blocking or augmenting Tregs may exacerbate one extreme at the expense of the other.

Although not specifically studied in this thesis, uterine, cervical, and vaginal Tregs likely have a large role in pregnancy. The mother's immune system must remain tolerant to both reproductive antigens as well as the semi-foreign fetus and circulating and placental Tregs are well-known mediators of this phenomenon[175]. However, given the tolerogenic requirements of the reproductive tissues, it is very likely that vaginal and uterine Tregs are indispensable for conception and gestation. If so, these Tregs have large implications for therapeutics relating to infertility, miscarriage, and preeclampsia.

In summary, this thesis characterizes for the first time vaginal Tregs in both health and viral infection, situating vaginal Tregs within the greater context of tissue and mucosal Tregs. This work makes several discoveries about the nuances of Tregs in the specialized tissues of the female GU tract: even within HSV-2 infection, Tregs within the vaginal tissue behave quite differently than Tregs in the dLN, as previously shown by our lab[194, 195]. Overall, this work further emphasizes that the phenotype and function of Tregs is highly dependent on context, including the location, infection, and time post-infection.

4.2 LIMITATIONS AND FUTURE DIRECTIONS

Our studies in both Chapter 2 and 3 are limited by low cell numbers in the vagina, a constraint that is inherent to this tissue compartment in addition to other mucosal tissues. Our work revealed that very few T cells in general are present in the VT in naïve mice, suggesting that antigenic stimuli or inflammation is necessary to initially draw T cells and Tregs to the vagina, consistent with other mucosal T cell literature[274]. After infection, T cell numbers are boosted into

the hundreds or sometimes thousands, but as Tregs make up only 10-20% of the vaginal T cell compartment, these numbers remain limiting for downstream analysis. For example, we were not able to recover sufficient Tregs from the VT of uninfected mice to perform bulk or single-cell RNA-seq on this population, leaving us unable to transcriptionally compare vaginal Tregs before and after infection.

Likewise, we attempted to perform TCR sequencing on vaginal Tregs to assess their antigen specificities and clonality to circulating Tregs, but we did not recover sufficient Tregs for adequate analysis. Further studies investigating the TCR repertoire of vaginal Tregs are needed, especially to determine if the vaginal Tregs that become hyper-activated and express GzmB after HSV-2 infection are potentially pathogen-specific. Alternatively, these Tregs could be self-reactive Tregs that have previously received a TCR signal and are able to quickly respond to HSV-2 infection in a cytokine-dependent, TCR-independent manner. Other studies have revealed that tissue Tregs have TCR repertoires that are non-overlapping with local CD4 Tconv or circulating Tregs, and that these TCR repertoires are highly clonal, suggesting expansion after specific antigenic stimulation[30, 32, 37, 50, 51, 200]. As an alternative approach, we are currently exploring Treg TCR usage during HSV-2 infection through the Nur77^{GFP} mouse reporter strain[275], which express GFP after TCR ligation through peptide:MHC complexes. These studies will reveal if GzmB+ Tregs during HSV-2 infection have recently experienced TCR activation or if they acquire this phenotype through inflammatory cytokines alone, as our data in Chapter 2 suggest.

The low cell numbers in vaginal Tregs also precluded some functional analyses. We found that in mouse, only vaginal Tregs expressed GzmB after infection, limiting the availability of GzmB+ Tregs to extremely small numbers. This prevented us from performing suppression or killing assays to test the functional capacity of GzmB+ Tregs to restrain or kill other T cells. This obstacle could be circumvented by a $GzmB^{flox/flox}$ mouse bred to $FoxP3^{Cre}$ [272]mice, which would yield offspring who lack GzmB only on Tregs and allow for targeted, functional experiments to determine how Tregs use GzmB. Tregs could limit or even kill other T and B cells with contact-dependent or contact-independent cytotoxic GzmB activity as has been shown in both mouse and human[18, 19]; alternatively, Treg GzmB could have non-apoptotic, extracellular activity[276-278]. Given the cytokine-dependent acquisition of GzmB we observed in Tregs from uninfected mice in Chapter 2, we hypothesize that vaginal Tregs may use GzmB in a non-targeted manner. However, we have not yet assessed vaginal Treg expression of perforin, which is necessary for targeted, contact-dependent killing[279] and could illuminate whether Tregs deploy contact-dependent or extracellular GzmB functions.

Although we were able to corroborate the highly activated phenotype observed in naïve mice to the vaginal Tregs in healthy women, at the time of this work we did not have access to vaginal biopsies from HSV-2+ women, preventing us from comparing human Treg production of GzmB after infection (we did not observe GzmB on Tregs from healthy human tissue). In the future, we hope to obtain HSV-2+ biopsies to compare mouse versus human Granzyme production in Tregs. However, studies are ongoing to stimulate Tregs from healthy human vaginal tissue to assess cytokine-dependent GzmB production, as well as production of Areg.

Our studies of Areg in mouse Tregs are promising, yet still preliminary. Going forward, we plan to measure vaginal Treg production of Areg through enzyme-linked immunoassays (ELISA) quantification of Areg in the vaginal lumen in mice with and without Tregs, as well as functional studies with $Areg^{flox/flox44}$ x $FoxP3^{Cre272}$ mice. While vaginal Tregs may heal tissue damage through Areg, it is likely that they also prevent tissue damage by restraining aggressive memory Trm responses during HSV-2 challenge. To test this, we are pursuing Treg depletion experiments during HSV-2 challenge where we will assess the effects of Treg ablation on both CD4+ and CD8+ T cells in the VT and dLN through flow cytometry analysis of effector T cell numbers, activation, HSV-2-specificity, and GzmB production.

Together, our novel investigation of the vaginal Treg compartment during health and disease provides a strong foundation for studying this unique and important barrier tissue Treg subset, while introducing many more exciting questions for future study.

4.3 FINAL THOUGHTS

Tregs in the female GU tract have previously been unstudied, while few (albeit prolific) research groups study general T cells the female reproductive tissues. This deficiency is representative of a larger theme of the lack of both bench and clinical research relating to women's health. Globally, women carry a higher burden than men of STIs and HIV[280, 281], as the vaginal mucosa is more permissive to infection, especially during the "window of vulnerability," where the GU tract becomes more immunosuppressive and tolerant to allow for conception and reproduction[183, 187]. Additionally, STI infections in women can lead to secondary complications with fertility and cancer[282, 283]. These inequities highlight the need for preventative strategies and vaccines for HIV

and STIs, which are dependent on a high volume of both bench and clinical research in GU tract immunology. Additionally, understanding GU tract immune responses, including Tregs, could potentially inform prevention, treatments, or cures for issues in women's health, including urinary tract infections, complications with menopause, viral-related cancers, sexual health, infertility, and miscarriage. Ultimately, the chronic under-investigation of the biology and immunology relating to women's health projects a general cultural and scientific devaluation of women and a dismissal of the emotional and physical pain that women disproportionately bear relating to sexual health and pregnancy.

Although women's health and the study of GU tract biology and immunology is inherently important, there is also much to be learned from GU tract immunology that can be extrapolated to other health problems. First, as STIs are more transmissible from male to female, interrupting the chain of infection in women with vaccines would disrupt this pattern, decreasing overall infections and infection-related cancers (such as human papilloma virus-derived oral and cervical cancers). Second, the GU tract is an extraordinary mucosal compartment that must simultaneously remain tolerant to foreign antigens and commensal bacteria, while also thwarting infections before they enter cells or invade the body. While other barrier mucosal surfaces are similarly tasked with this paradoxical challenge, the GU tract holds the added responsibility of allowing for conception and pregnancy on both an immunological and structural capacity. The immune responses that facilitate this exceptional and dynamic balance—if better understood—could be leveraged in conditions such as autoimmunity, where aberrant self-responses are extremely pathogenic, but many available treatments introduce the extreme opposite by causing

non-targeted, heavy immunosuppression. Specifically, GU tract Tregs may be the key for this dynamic immune balance and warrant aggressive study.

Although a small part of what could be a very vast field of study, this work proudly contributes to the collective understanding of immune cells within the female reproductive tissues and how Tregs may specifically be leveraged to maintain health and prevent disease.

BIBLIOGRAPHY

References.

1. Josefowicz SZ, Rudensky A. Control of regulatory T cell lineage commitment and maintenance. *Immunity* 2009; **30**(5)**:** 616-625.

2. Smigiel KS, Srivastava S, Stolley JM, Campbell DJ. Regulatory T-cell homeostasis: steady-state maintenance and modulation during inflammation. *Immunol Rev* 2014; **259**(1)**:** 40-59.

3. Sakaguchi S, Yamaguchi T, Nomura T, Ono M. Regulatory T cells and immune tolerance. *Cell* 2008; **133**(5)**:** 775-787.

4. Bennett CL, Christie J, Ramsdell F, Brunkow ME, Ferguson PJ, Whitesell L *et al.* The immune dysregulation, polyendocrinopathy, enteropathy, X-linked syndrome (IPEX) is caused by mutations of FOXP3. *Nat Genet* 2001; **27**(1)**:** 20-21.

5. Brunkow ME, Jeffery EW, Hjerrild KA, Paeper B, Clark LB, Yasayko SA *et al.* Disruption of a new forkhead/winged-helix protein, scurfin, results in the fatal lymphoproliferative disorder of the scurfy mouse. *Nat Genet* 2001; **27**(1)**:** 68-73.

6. Wildin RS, Ramsdell F, Peake J, Faravelli F, Casanova JL, Buist N *et al.* X-linked neonatal diabetes mellitus, enteropathy and endocrinopathy syndrome is the human equivalent of mouse scurfy. *Nat Genet* 2001; **27**(1)**:** 18-20.

7. Fontenot JD, Gavin MA, Rudensky AY. Foxp3 programs the development and function of CD4+CD25+ regulatory T cells. *Nat Immunol* 2003; **4**(4)**:** 330-336.

8. Hori S, Nomura T, Sakaguchi S. Control of regulatory T cell development by the transcription factor Foxp3. *Science* 2003; **299**(5609)**:** 1057-1061.

9. Khattri R, Cox T, Yasayko SA, Ramsdell F. An essential role for Scurfin in CD4+CD25+ T regulatory cells. *Nat Immunol* 2003; **4**(4)**:** 337-342.

10. Gavin MA, Rasmussen JP, Fontenot JD, Vasta V, Manganiello VC, Beavo JA *et al.* Foxp3-dependent programme of regulatory T-cell differentiation. *Nature* 2007; **445**(7129)**:** 771-775.

11. Lin W, Haribhai D, Relland LM, Truong N, Carlson MR, Williams CB *et al.* Regulatory T cell development in the absence of functional Foxp3. *Nat Immunol* 2007; **8**(4)**:** 359-368.

12. Hu W, Wang ZM, Feng Y, Schizas M, Hoyos BE, van der Veeken J *et al.* Regulatory T cells function in established systemic inflammation and reverse fatal autoimmunity. *Nat Immunol* 2021; **22**(9)**:** 1163-1174.

13. Williams LM, Rudensky AY. Maintenance of the Foxp3-dependent developmental program in mature regulatory T cells requires continued expression of Foxp3. *Nat Immunol* 2007; **8**(3)**:** 277-284.

14. Li MO, Wan YY, Flavell RA. T cell-produced transforming growth factor-beta1 controls T cell tolerance and regulates Th1- and Th17-cell differentiation. *Immunity* 2007; **26**(5)**:** 579-591.

15. Rubtsov YP, Rasmussen JP, Chi EY, Fontenot J, Castelli L, Ye X *et al.* Regulatory T cell-derived interleukin-10 limits inflammation at environmental interfaces. *Immunity* 2008; **28**(4)**:** 546-558.

16. Gondek DC, Lu LF, Quezada SA, Sakaguchi S, Noelle RJ. Cutting edge: contact-mediated suppression by CD4+CD25+ regulatory cells involves a granzyme B-dependent, perforin-independent mechanism. *J Immunol* 2005; **174**(4)**:** 1783-1786.

17. Grossman WJ, Verbsky JW, Barchet W, Colonna M, Atkinson JP, Ley TJ. Human T regulatory cells can use the perforin pathway to cause autologous target cell death. *Immunity* 2004; **21**(4)**:** 589-601.

18. Zhao DM, Thornton AM, DiPaolo RJ, Shevach EM. Activated CD4+CD25+ T cells selectively kill B lymphocytes. *Blood* 2006; **107**(10)**:** 3925-3932.

19. Loebbermann J, Thornton H, Durant L, Sparwasser T, Webster KE, Sprent J *et al.* Regulatory T cells expressing granzyme B play a critical role in controlling lung inflammation during acute viral infection. *Mucosal Immunol* 2012; **5**(2)**:** 161-172.

20. Wing K, Onishi Y, Prieto-Martin P, Yamaguchi T, Miyara M, Fehervari Z *et al.* CTLA-4 control over Foxp3+ regulatory T cell function. *Science* 2008; **322**(5899)**:** 271-275.

21. Bopp T, Becker C, Klein M, Klein-Hessling S, Palmetshofer A, Serfling E *et al.* Cyclic adenosine monophosphate is a key component of regulatory T cell-mediated suppression. *J Exp Med* 2007; **204**(6)**:** 1303-1310.

22. Borsellino G, Kleinewietfeld M, Di Mitri D, Sternjak A, Diamantini A, Giometto R *et al.* Expression of ectonucleotidase CD39 by Foxp3+ Treg cells: hydrolysis of extracellular ATP and immune suppression. *Blood* 2007; **110**(4)**:** 1225-1232.

23. Deaglio S, Dwyer KM, Gao W, Friedman D, Usheva A, Erat A *et al.* Adenosine generation catalyzed by CD39 and CD73 expressed on regulatory T cells mediates immune suppression. *J Exp Med* 2007; **204**(6)**:** 1257-1265.

24. Kobie JJ, Shah PR, Yang L, Rebhahn JA, Fowell DJ, Mosmann TR. T regulatory and primed uncommitted CD4 T cells express CD73, which suppresses effector CD4 T cells by converting 5'-adenosine monophosphate to adenosine. *J Immunol* 2006; **177**(10)**:** 6780-6786.

25. Pandiyan P, Zheng L, Ishihara S, Reed J, Lenardo MJ. CD4+CD25+Foxp3+ regulatory T cells induce cytokine deprivation-mediated apoptosis of effector CD4+ T cells. *Nat Immunol* 2007; **8**(12)**:** 1353-1362.

26. Kim JM, Rasmussen JP, Rudensky AY. Regulatory T cells prevent catastrophic autoimmunity throughout the lifespan of mice. *Nat Immunol* 2007; **8**(2)**:** 191-197.

27. Josefowicz SZ, Lu LF, Rudensky AY. Regulatory T cells: mechanisms of differentiation and function. *Annu Rev Immunol* 2012; **30:** 531-564.

28. Belkaid Y, Tarbell K. Regulatory T cells in the control of host-microorganism interactions (*). *Annu Rev Immunol* 2009; **27:** 551-589.

29. Richert-Spuhler LE, Lund JM. The Immune Fulcrum: Regulatory T Cells Tip the Balance Between Pro- and Anti-inflammatory Outcomes upon Infection. *Prog Mol Biol Transl Sci* 2015; **136:** 217-243.

30. Burzyn D, Kuswanto W, Kolodin D, Shadrach JL, Cerletti M, Jang Y *et al.* A special population of regulatory T cells potentiates muscle repair. *Cell* 2013; **155**(6)**:** 1282-1295.

31. Cipolletta D, Feuerer M, Li A, Kamei N, Lee J, Shoelson SE *et al.* PPAR-gamma is a major driver of the accumulation and phenotype of adipose tissue Treg cells. *Nature* 2012; **486**(7404)**:** 549-553.

32. Sanchez Rodriguez R, Pauli ML, Neuhaus IM, Yu SS, Arron ST, Harris HW *et al.* Memory regulatory T cells reside in human skin. *J Clin Invest* 2014; **124**(3)**:** 1027-1036.

33. Kalekar LA, Cohen JN, Prevel N, Sandoval PM, Mathur AN, Moreau JM *et al.* Regulatory T cells in skin are uniquely poised to suppress profibrotic immune responses. *Sci Immunol* 2019; **4**(39).

34. Ali N, Zirak B, Rodriguez RS, Pauli ML, Truong HA, Lai K *et al.* Regulatory T Cells in Skin Facilitate Epithelial Stem Cell Differentiation. *Cell* 2017; **169**(6)**:** 1119-1129 e1111.

35. Li C, DiSpirito JR, Zemmour D, Spallanzani RG, Kuswanto W, Benoist C *et al.* TCR Transgenic Mice Reveal Stepwise, Multi-site Acquisition of the Distinctive Fat-Treg Phenotype. *Cell* 2018; **174**(2)**:** 285-299 e212.

36. Vasanthakumar A, Moro K, Xin A, Liao Y, Gloury R, Kawamoto S *et al.* The transcriptional regulators IRF4, BATF and IL-33 orchestrate development and maintenance of adipose tissue-resident regulatory T cells. *Nat Immunol* 2015; **16**(3)**:** 276-285.

37. Feuerer M, Herrero L, Cipolletta D, Naaz A, Wong J, Nayer A *et al.* Lean, but not obese, fat is enriched for a unique population of regulatory T cells that affect metabolic parameters. *Nat Med* 2009; **15**(8)**:** 930-939.

38. Kuswanto W, Burzyn D, Panduro M, Wang KK, Jang YC, Wagers AJ *et al.* Poor Repair of Skeletal Muscle in Aging Mice Reflects a Defect in Local, Interleukin-33-Dependent Accumulation of Regulatory T Cells. *Immunity* 2016; **44**(2)**:** 355-367.

39. Brincks EL, Roberts AD, Cookenham T, Sell S, Kohlmeier JE, Blackman MA *et al.* Antigen-specific memory regulatory CD4+Foxp3+ T cells control memory responses to influenza virus infection. *J Immunol* 2013; **190**(7)**:** 3438-3446.

40. Durant LR, Makris S, Voorburg CM, Loebbermann J, Johansson C, Openshaw PJ. Regulatory T cells prevent Th2 immune responses and pulmonary eosinophilia during respiratory syncytial virus infection in mice. *J Virol* 2013; **87**(20)**:** 10946-10954.

41. Leon B, Bradley JE, Lund FE, Randall TD, Ballesteros-Tato A. FoxP3+ regulatory T cells promote influenza-specific Tfh responses by controlling IL-2 availability. *Nat Commun* 2014; **5:** 3495.

42. Belkaid Y. Regulatory T cells and infection: a dangerous necessity. *Nat Rev Immunol* 2007; **7**(11)**:** 875-888.

43. Sell S, McKinstry KK, Strutt TM. Mouse Models Reveal Role of T-Cytotoxic and T-Reg Cells in Immune Response to Influenza: Implications for Vaccine Design. *Viruses* 2019; **11**(1).

44. Arpaia N, Green JA, Moltedo B, Arvey A, Hemmers S, Yuan S *et al.* A Distinct Function of Regulatory T Cells in Tissue Protection. *Cell* 2015; **162**(5)**:** 1078-1089.

45. Betts RJ, Prabhu N, Ho AW, Lew FC, Hutchinson PE, Rotzschke O *et al.* Influenza A virus infection results in a robust, antigen-responsive, and widely disseminated Foxp3+ regulatory T cell response. *J Virol* 2012; **86**(5)**:** 2817-2825.

46. D'Alessio FR, Tsushima K, Aggarwal NR, West EE, Willett MH, Britos MF *et al.* CD4+CD25+Foxp3+ Tregs resolve experimental lung injury in mice and are present in humans with acute lung injury. *J Clin Invest* 2009; **119**(10)**:** 2898-2913.

47. Ichikawa T, Hirahara K, Kokubo K, Kiuchi M, Aoki A, Morimoto Y *et al.* CD103(hi) Treg cells constrain lung fibrosis induced by CD103(lo) tissue-resident pathogenic CD4 T cells. *Nat Immunol* 2019; **20**(11)**:** 1469-1480.

48. Veiga-Parga T, Sehrawat S, Rouse BT. Role of regulatory T cells during virus infection. *Immunol Rev* 2013; **255**(1)**:** 182-196.

49. Botta D, Fuller MJ, Marquez-Lago TT, Bachus H, Bradley JE, Weinmann AS *et al.* Dynamic regulation of T follicular regulatory cell responses by interleukin 2 during influenza infection. *Nat Immunol* 2017; **18**(11)**:** 1249-1260.

50. Shafiani S, Dinh C, Ertelt JM, Moguche AO, Siddiqui I, Smigiel KS *et al.* Pathogen-specific Treg cells expand early during mycobacterium tuberculosis infection but are later eliminated in response to Interleukin-12. *Immunity* 2013; **38**(6)**:** 1261-1270.

51. Shafiani S, Tucker-Heard G, Kariyone A, Takatsu K, Urdahl KB. Pathogen-specific regulatory T cells delay the arrival of effector T cells in the lung during early tuberculosis. *J Exp Med* 2010; **207**(7)**:** 1409-1420.

52. Vick SC, Frutoso M, Mair F, Konecny AJ, Greene E, Wolf CR *et al.* A differential regulatory T cell signature distinguishes the immune landscape of COVID-19 hospitalized patients from those hospitalized with other respiratory viral infections. *medRxiv* 2021.

53. Sadeghi A, Tahmasebi S, Mahmood A, Kuznetsova M, Valizadeh H, Taghizadieh A *et al.* Th17 and Treg cells function in SARS-CoV2 patients compared with healthy controls. *J Cell Physiol* 2021; **236**(4)**:** 2829-2839.

54. Szabo PA, Dogra P, Gray JI, Wells SB, Connors TJ, Weisberg SP *et al.* Longitudinal profiling of respiratory and systemic immune responses reveals myeloid cell-driven lung inflammation in severe COVID-19. *Immunity* 2021; **54**(4)**:** 797-814 e796.

55. Delacher M, Simon M, Sanderink L, Hotz-Wagenblatt A, Wuttke M, Schambeck K *et al.* Single-cell chromatin accessibility landscape identifies tissue repair program in human regulatory T cells. *Immunity* 2021; **54**(4)**:** 702-720 e717.

56. Delacher M, Imbusch CD, Weichenhan D, Breiling A, Hotz-Wagenblatt A, Trager U *et al.* Genome-wide DNA-methylation landscape defines specialization of regulatory T cells in tissues. *Nat Immunol* 2017; **18**(10)**:** 1160-1172.

57. Delacher M, Imbusch CD, Hotz-Wagenblatt A, Mallm JP, Bauer K, Simon M *et al.* Precursors for Nonlymphoid-Tissue Treg Cells Reside in Secondary Lymphoid Organs and Are Programmed by the Transcription Factor BATF. *Immunity* 2020; **52**(2)**:** 295-312 e211.

58. DiSpirito JR, Zemmour D, Ramanan D, Cho J, Zilionis R, Klein AM *et al.* Molecular diversification of regulatory T cells in nonlymphoid tissues. *Sci Immunol* 2018; **3**(27).

59. Miragaia RJ, Gomes T, Chomka A, Jardine L, Riedel A, Hegazy AN *et al.* Single-Cell Transcriptomics of Regulatory T Cells Reveals Trajectories of Tissue Adaptation. *Immunity* 2019; **50**(2)**:** 493-504 e497.

60. Szabo PA, Levitin HM, Miron M, Snyder ME, Senda T, Yuan J *et al.* Single-cell transcriptomics of human T cells reveals tissue and activation signatures in health and disease. *Nat Commun* 2019; **10**(1)**:** 4706.

61. Munoz-Rojas AR, Mathis D. Tissue regulatory T cells: regulatory chameleons. *Nat Rev Immunol* 2021.

62. Liu Q, Dwyer GK, Zhao Y, Li H, Mathews LR, Chakka AB *et al.* IL-33-mediated IL-13 secretion by ST2+ Tregs controls inflammation after lung injury. *JCI Insight* 2019; **4**(6).

63. Harb H, Benamar M, Lai PS, Contini P, Griffith JW, Crestani E *et al.* Notch4 signaling limits regulatory T-cell-mediated tissue repair and promotes severe lung inflammation in viral infections. *Immunity* 2021; **54**(6)**:** 1186-1199 e1187.

64. Dial CF, Tune MK, Doerschuk CM, Mock JR. Foxp3(+) Regulatory T Cell Expression of Keratinocyte Growth Factor Enhances Lung Epithelial Proliferation. *Am J Respir Cell Mol Biol* 2017; **57**(2)**:** 162-173.

65. Noval Rivas M, Chatila TA. Regulatory T cells in allergic diseases. *J Allergy Clin Immunol* 2016; **138**(3)**:** 639-652.

66. Singh R, Alape D, de Lima A, Ascanio J, Majid A, Gangadharan SP. Regulatory T Cells in Respiratory Health and Diseases. *Pulm Med* 2019; **2019:** 1907807.

67. Chatila TA, Blaeser F, Ho N, Lederman HM, Voulgaropoulos C, Helms C *et al.* JM2, encoding a fork head-related protein, is mutated in X-linked autoimmunity-allergic disregulation syndrome. *J Clin Invest* 2000; **106**(12)**:** R75-81.

68. Verbsky JW, Chatila TA. Immune dysregulation, polyendocrinopathy, enteropathy, X-linked (IPEX) and IPEX-related disorders: an evolving web of heritable autoimmune diseases. *Curr Opin Pediatr* 2013; **25**(6)**:** 708-714.

69. Lin W, Truong N, Grossman WJ, Haribhai D, Williams CB, Wang J *et al.* Allergic dysregulation and hyperimmunoglobulinemia E in Foxp3 mutant mice. *J Allergy Clin Immunol* 2005; **116**(5)**:** 1106-1115.

70. Kearley J, Barker JE, Robinson DS, Lloyd CM. Resolution of airway inflammation and hyperreactivity after in vivo transfer of CD4+CD25+ regulatory T cells is interleukin 10 dependent. *J Exp Med* 2005; **202**(11)**:** 1539-1547.

71. Lewkowich IP, Herman NS, Schleifer KW, Dance MP, Chen BL, Dienger KM *et al.* CD4+CD25+ T cells protect against experimentally induced asthma and alter pulmonary dendritic cell phenotype and function. *J Exp Med* 2005; **202**(11)**:** 1549-1561.

72. Josefowicz SZ, Niec RE, Kim HY, Treuting P, Chinen T, Zheng Y *et al.* Extrathymically generated regulatory T cells control mucosal TH2 inflammation. *Nature* 2012; **482**(7385)**:** 395-399.

73. Hartl D, Koller B, Mehlhorn AT, Reinhardt D, Nicolai T, Schendel DJ *et al.* Quantitative and functional impairment of pulmonary CD4+CD25hi regulatory T cells in pediatric asthma. *J Allergy Clin Immunol* 2007; **119**(5)**:** 1258-1266.

74. Beura LK, Hamilton SE, Bi K, Schenkel JM, Odumade OA, Casey KA *et al.* Normalizing the environment recapitulates adult human immune traits in laboratory mice. *Nature* 2016; **532**(7600)**:** 512-516.

75. Thome JJ, Bickham KL, Ohmura Y, Kubota M, Matsuoka N, Gordon C *et al.* Early-life compartmentalization of human T cell differentiation and regulatory function in mucosal and lymphoid tissues. *Nat Med* 2016; **22**(1)**:** 72-77.

76. Goulding J, Snelgrove R, Saldana J, Didierlaurent A, Cavanagh M, Gwyer E *et al.* Respiratory infections: do we ever recover? *Proc Am Thorac Soc* 2007; **4**(8)**:** 618-625.

77. Wissinger E, Goulding J, Hussell T. Immune homeostasis in the respiratory tract and its impact on heterologous infection. *Semin Immunol* 2009; **21**(3)**:** 147-155.

78. Snyder ME, Farber DL. Human lung tissue resident memory T cells in health and disease. *Curr Opin Immunol* 2019; **59:** 101-108.

79. Shevyrev D, Tereshchenko V. Treg Heterogeneity, Function, and Homeostasis. *Front Immunol* 2019; **10:** 3100.

80. Stolley JM, Johnston TS, Soerens AG, Beura LK, Rosato PC, Joag V *et al.* Retrograde migration supplies resident memory T cells to lung-draining LN after influenza infection. *J Exp Med* 2020; **217**(8).

81. Takamura S. Persistence in Temporary Lung Niches: A Survival Strategy of Lung-Resident Memory CD8(+) T Cells. *Viral Immunol* 2017; **30**(6)**:** 438-450.

82. Masopust D, Soerens AG. Tissue-Resident T Cells and Other Resident Leukocytes. *Annu Rev Immunol* 2019; **37:** 521-546.

83. Pabst O, Mowat AM. Oral tolerance to food protein. *Mucosal Immunol* 2012; **5**(3)**:** 232-239.

84. Hadis U, Wahl B, Schulz O, Hardtke-Wolenski M, Schippers A, Wagner N *et al.* Intestinal tolerance requires gut homing and expansion of FoxP3+ regulatory T cells in the lamina propria. *Immunity* 2011; **34**(2)**:** 237-246.

85. Tanoue T, Atarashi K, Honda K. Development and maintenance of intestinal regulatory T cells. *Nat Rev Immunol* 2016; **16**(5)**:** 295-309.

86. Atarashi K, Tanoue T, Shima T, Imaoka A, Kuwahara T, Momose Y *et al.* Induction of colonic regulatory T cells by indigenous Clostridium species. *Science* 2011; **331**(6015)**:** 337-341.

87. Sakaguchi S, Sakaguchi N, Asano M, Itoh M, Toda M. Immunologic self-tolerance maintained by activated T cells expressing IL-2 receptor alpha-chains (CD25). Breakdown of a single mechanism of self-tolerance causes various autoimmune diseases. *J Immunol* 1995; **155**(3)**:** 1151-1164.

88. Sharma R, Sung SS, Fu SM, Ju ST. Regulation of multi-organ inflammation in the regulatory T cell-deficient scurfy mice. *J Biomed Sci* 2009; **16:** 20.

89. Mayer CT, Ghorbani P, Kuhl AA, Stuve P, Hegemann M, Berod L *et al.* Few Foxp3(+) regulatory T cells are sufficient to protect adult mice from lethal autoimmunity. *Eur J Immunol* 2014; **44**(10)**:** 2990-3002.

90. Mottet C, Uhlig HH, Powrie F. Cutting edge: cure of colitis by CD4+CD25+ regulatory T cells. *J Immunol* 2003; **170**(8)**:** 3939-3943.

91. Whibley N, Tucci A, Powrie F. Regulatory T cell adaptation in the intestine and skin. *Nat Immunol* 2019; **20**(4)**:** 386-396.

92. Picca CC, Larkin J, 3rd, Boesteanu A, Lerman MA, Rankin AL, Caton AJ. Role of TCR specificity in CD4+ CD25+ regulatory T-cell selection. *Immunol Rev* 2006; **212:** 74-85.

93. Hsieh CS, Lee HM, Lio CW. Selection of regulatory T cells in the thymus. *Nat Rev Immunol* 2012; **12**(3)**:** 157-167.

94. Lee HM, Bautista JL, Scott-Browne J, Mohan JF, Hsieh CS. A broad range of self-reactivity drives thymic regulatory T cell selection to limit responses to self. *Immunity* 2012; **37**(3)**:** 475-486.

95. Savage PA, Klawon DEJ, Miller CH. Regulatory T Cell Development. *Annu Rev Immunol* 2020; **38:** 421-453.

96. Thornton AM, Korty PE, Tran DQ, Wohlfert EA, Murray PE, Belkaid Y *et al.* Expression of Helios, an Ikaros transcription factor family member, differentiates thymic-derived from peripherally induced Foxp3+ T regulatory cells. *Journal of immunology* 2010; **184**(7)**:** 3433-3441.

97. Singh K, Hjort M, Thorvaldson L, Sandler S. Concomitant analysis of Helios and Neuropilin-1 as a marker to detect thymic derived regulatory T cells in naive mice. *Sci Rep* 2015; **5:** 7767.

98. Chen W, Jin W, Hardegen N, Lei KJ, Li L, Marinos N *et al.* Conversion of peripheral CD4+CD25- naive T cells to CD4+CD25+ regulatory T cells by TGF-beta induction of transcription factor Foxp3. *J Exp Med* 2003; **198**(12)**:** 1875-1886.

99. Kretschmer K, Apostolou I, Hawiger D, Khazaie K, Nussenzweig MC, von Boehmer H. Inducing and expanding regulatory T cell populations by foreign antigen. *Nat Immunol* 2005; **6**(12)**:** 1219-1227.

100. Selvaraj RK, Geiger TL. A kinetic and dynamic analysis of Foxp3 induced in T cells by TGF-beta. *J Immunol* 2007; **179**(2)**:** 11 p following 1390.

101. Zheng SG, Wang JH, Gray JD, Soucier H, Horwitz DA. Natural and induced CD4+CD25+ cells educate CD4+CD25- cells to develop suppressive activity: the role of IL-2, TGF-beta, and IL-10. *J Immunol* 2004; **172**(9)**:** 5213-5221.

102. Pratama A, Schnell A, Mathis D, Benoist C. Developmental and cellular age direct conversion of CD4+ T cells into RORgamma+ or Helios+ colon Treg cells. *J Exp Med* 2020; **217**(1).

103. Sefik E, Geva-Zatorsky N, Oh S, Konnikova L, Zemmour D, McGuire AM *et al.* MUCOSAL IMMUNOLOGY. Individual intestinal symbionts induce a distinct population of RORgamma(+) regulatory T cells. *Science* 2015; **349**(6251)**:** 993-997.

104. Nutsch K, Chai JN, Ai TL, Russler-Germain E, Feehley T, Nagler CR *et al.* Rapid and Efficient Generation of Regulatory T Cells to Commensal Antigens in the Periphery. *Cell Rep* 2016; **17**(1)**:** 206-220.

105. Weiss JM, Bilate AM, Gobert M, Ding Y, Curotto de Lafaille MA, Parkhurst CN *et al.* Neuropilin 1 is expressed on thymus-derived natural regulatory T cells, but not mucosa-generated induced Foxp3+ T reg cells. *J Exp Med* 2012; **209**(10)**:** 1723-1742, S1721.

106. Cebula A, Seweryn M, Rempala GA, Pabla SS, McIndoe RA, Denning TL *et al.* Thymus-derived regulatory T cells contribute to tolerance to commensal microbiota. *Nature* 2013; **497**(7448)**:** 258-262.

107. Ramanan D, Sefik E, Galvan-Pena S, Wu M, Yang L, Yang Z *et al.* An Immunologic Mode of Multigenerational Transmission Governs a Gut Treg Setpoint. *Cell* 2020; **181**(6)**:** 1276-1290 e1213.

108. Campbell C, Dikiy S, Bhattarai SK, Chinen T, Matheis F, Calafiore M *et al.* Extrathymically Generated Regulatory T Cells Establish a Niche for Intestinal Border-Dwelling Bacteria and Affect Physiologic Metabolite Balance. *Immunity* 2018; **48**(6)**:** 1245-1257 e1249.

109. Kim KS, Hong SW, Han D, Yi J, Jung J, Yang BG *et al.* Dietary antigens limit mucosal immunity by inducing regulatory T cells in the small intestine. *Science* 2016; **351**(6275)**:** 858-863.

110. Abdel-Gadir A, Stephen-Victor E, Gerber GK, Noval Rivas M, Wang S, Harb H *et al.* Microbiota therapy acts via a regulatory T cell MyD88/RORgammat pathway to suppress food allergy. *Nat Med* 2019; **25**(7)**:** 1164-1174.

111. Cosovanu C, Neumann C. The Many Functions of Foxp3(+) Regulatory T Cells in the Intestine. *Front Immunol* 2020; **11:** 600973.

112. Ohnmacht C, Park JH, Cording S, Wing JB, Atarashi K, Obata Y *et al.* MUCOSAL IMMUNOLOGY. The microbiota regulates type 2 immunity through RORgammat(+) T cells. *Science* 2015; **349**(6251)**:** 989-993.

113. Knoop KA, McDonald KG, Coughlin PE, Kulkarni DH, Gustafsson JK, Rusconi B *et al.* Synchronization of mothers and offspring promotes tolerance and limits allergy. *JCI Insight* 2020; **5**(15).

114. Knoop KA, McDonald KG, Hsieh CS, Tarr PI, Newberry RD. Regulatory T Cells Developing Peri-Weaning Are Continually Required to Restrain Th2 Systemic Responses Later in Life. *Front Immunol* 2020; **11:** 603059.

115. Al Nabhani Z, Dulauroy S, Marques R, Cousu C, Al Bounny S, Dejardin F *et al.* A Weaning Reaction to Microbiota Is Required for Resistance to Immunopathologies in the Adult. *Immunity* 2019; **50**(5)**:** 1276-1288 e1275.

116. Yang BH, Hagemann S, Mamareli P, Lauer U, Hoffmann U, Beckstette M *et al.* Foxp3(+) T cells expressing RORgammat represent a stable regulatory T-cell effector lineage with enhanced suppressive capacity during intestinal inflammation. *Mucosal Immunol* 2016; **9**(2)**:** 444-457.

117. Xu M, Pokrovskii M, Ding Y, Yi R, Au C, Harrison OJ *et al.* c-MAF-dependent regulatory T cells mediate immunological tolerance to a gut pathobiont. *Nature* 2018; **554**(7692)**:** 373-377.

118. Neumann C, Blume J, Roy U, Teh PP, Vasanthakumar A, Beller A *et al.* c-Maf-dependent Treg cell control of intestinal TH17 cells and IgA establishes host-microbiota homeostasis. *Nat Immunol* 2019; **20**(4)**:** 471-481.

119. Lochner M, Peduto L, Cherrier M, Sawa S, Langa F, Varona R *et al.* In vivo equilibrium of proinflammatory IL-17+ and regulatory IL-10+ Foxp3+ RORgamma t+ T cells. *J Exp Med* 2008; **205**(6)**:** 1381-1393.

120. Glocker EO, Kotlarz D, Boztug K, Gertz EM, Schaffer AA, Noyan F *et al.* Inflammatory bowel disease and mutations affecting the interleukin-10 receptor. *N Engl J Med* 2009; **361**(21)**:** 2033-2045.

121. Glocker EO, Kotlarz D, Klein C, Shah N, Grimbacher B. IL-10 and IL-10 receptor defects in humans. *Ann N Y Acad Sci* 2011; **1246:** 102-107.

122. Kamanaka M, Kim ST, Wan YY, Sutterwala FS, Lara-Tejero M, Galan JE *et al.* Expression of interleukin-10 in intestinal lymphocytes detected by an interleukin-10 reporter knockin tiger mouse. *Immunity* 2006; **25**(6)**:** 941-952.

123. Kryczek I, Wu K, Zhao E, Wei S, Vatan L, Szeliga W *et al.* IL-17+ regulatory T cells in the microenvironments of chronic inflammation and cancer. *Journal of immunology* 2011; **186**(7)**:** 4388-4395.

124. Ayyoub M, Deknuydt F, Raimbaud I, Dousset C, Leveque L, Bioley G *et al.* Human memory FOXP3+ Tregs secrete IL-17 ex vivo and constitutively express the T(H)17 lineage-specific transcription factor RORgamma t. *Proc Natl Acad Sci U S A* 2009; **106**(21)**:** 8635-8640.

125. Lochner M, Berard M, Sawa S, Hauer S, Gaboriau-Routhiau V, Fernandez TD *et al.* Restricted microbiota and absence of cognate TCR antigen leads to an unbalanced generation of Th17 cells. *J Immunol* 2011; **186**(3)**:** 1531-1537.

126. Lathrop SK, Bloom SM, Rao SM, Nutsch K, Lio CW, Santacruz N *et al.* Peripheral education of the immune system by colonic commensal microbiota. *Nature* 2011; **478**(7368)**:** 250-254.

127. Shinde R, McGaha TL. The Aryl Hydrocarbon Receptor: Connecting Immunity to the Microenvironment. *Trends Immunol* 2018; **39**(12)**:** 1005-1020.

128. Ye J, Qiu J, Bostick JW, Ueda A, Schjerven H, Li S *et al.* The Aryl Hydrocarbon Receptor Preferentially Marks and Promotes Gut Regulatory T Cells. *Cell Rep* 2017; **21**(8)**:** 2277-2290.

129. Mezrich JD, Fechner JH, Zhang X, Johnson BP, Burlingham WJ, Bradfield CA. An interaction between kynurenine and the aryl hydrocarbon receptor can generate regulatory T cells. *J Immunol* 2010; **185**(6)**:** 3190-3198.

130. Coombes JL, Siddiqui KR, Arancibia-Carcamo CV, Hall J, Sun CM, Belkaid Y *et al.* A functionally specialized population of mucosal CD103+ DCs induces Foxp3+ regulatory T cells via a TGF-beta and retinoic acid-dependent mechanism. *J Exp Med* 2007; **204**(8)**:** 1757-1764.

131. Mucida D, Park Y, Kim G, Turovskaya O, Scott I, Kronenberg M *et al.* Reciprocal TH17 and regulatory T cell differentiation mediated by retinoic acid. *Science* 2007; **317**(5835)**:** 256-260.

132. Sun CM, Hall JA, Blank RB, Bouladoux N, Oukka M, Mora JR *et al.* Small intestine lamina propria dendritic cells promote de novo generation of Foxp3 T reg cells via retinoic acid. *J Exp Med* 2007; **204**(8)**:** 1775-1785.

133. Kang SW, Kim SH, Lee N, Lee WW, Hwang KA, Shin MS *et al.* 1,25-Dihyroxyvitamin D3 promotes FOXP3 expression via binding to vitamin D response elements in its conserved noncoding sequence region. *J Immunol* 2012; **188**(11)**:** 5276-5282.

134. Yamaguchi T, Hirota K, Nagahama K, Ohkawa K, Takahashi T, Nomura T *et al.* Control of immune responses by antigen-specific regulatory T cells expressing the folate receptor. *Immunity* 2007; **27**(1)**:** 145-159.

135. Arpaia N, Campbell C, Fan X, Dikiy S, van der Veeken J, deRoos P *et al.* Metabolites produced by commensal bacteria promote peripheral regulatory T-cell generation. *Nature* 2013; **504**(7480)**:** 451-455.

136. Furusawa Y, Obata Y, Fukuda S, Endo TA, Nakato G, Takahashi D *et al.* Commensal microbe-derived butyrate induces the differentiation of colonic regulatory T cells. *Nature* 2013; **504**(7480)**:** 446-450.

137. Smith PM, Howitt MR, Panikov N, Michaud M, Gallini CA, Bohlooly YM *et al.* The microbial metabolites, short-chain fatty acids, regulate colonic Treg cell homeostasis. *Science* 2013; **341**(6145)**:** 569-573.

138. Danne C, Ryzhakov G, Martinez-Lopez M, Ilott NE, Franchini F, Cuskin F *et al.* A Large Polysaccharide Produced by Helicobacter hepaticus Induces an Anti-inflammatory Gene Signature in Macrophages. *Cell Host Microbe* 2017; **22**(6)**:** 733-745 e735.

139. Round JL, Mazmanian SK. Inducible Foxp3+ regulatory T-cell development by a commensal bacterium of the intestinal microbiota. *Proc Natl Acad Sci U S A* 2010; **107**(27)**:** 12204-12209.

140. Shen Y, Giardino Torchia ML, Lawson GW, Karp CL, Ashwell JD, Mazmanian SK. Outer membrane vesicles of a human commensal mediate immune regulation and disease protection. *Cell Host Microbe* 2012; **12**(4)**:** 509-520.

141. Verma R, Lee C, Jeun EJ, Yi J, Kim KS, Ghosh A *et al.* Cell surface polysaccharides of Bifidobacterium bifidum induce the generation of Foxp3(+) regulatory T cells. *Sci Immunol* 2018; **3**(28).

142. Campbell C, McKenney PT, Konstantinovsky D, Isaeva OI, Schizas M, Verter J *et al.* Bacterial metabolism of bile acids promotes generation of peripheral regulatory T cells. *Nature* 2020; **581**(7809)**:** 475-479.

143. Hang S, Paik D, Yao L, Kim E, Trinath J, Lu J *et al.* Bile acid metabolites control TH17 and Treg cell differentiation. *Nature* 2019; **576**(7785)**:** 143-148.

144. Li W, Hang S, Fang Y, Bae S, Zhang Y, Zhang M *et al.* A bacterial bile acid metabolite modulates Treg activity through the nuclear hormone receptor NR4A1. *Cell Host Microbe* 2021; **29**(9)**:** 1366-1377 e1369.

145. Wohlfert EA, Grainger JR, Bouladoux N, Konkel JE, Oldenhove G, Ribeiro CH *et al.* GATA3 controls Foxp3(+) regulatory T cell fate during inflammation in mice. *J Clin Invest* 2011; **121**(11)**:** 4503-4515.

146. Schiering C, Krausgruber T, Chomka A, Frohlich A, Adelmann K, Wohlfert EA *et al.* The alarmin IL-33 promotes regulatory T-cell function in the intestine. *Nature* 2014; **513**(7519)**:** 564-568.

147. Rudra D, deRoos P, Chaudhry A, Niec RE, Arvey A, Samstein RM *et al.* Transcription factor Foxp3 and its protein partners form a complex regulatory network. *Nat Immunol* 2012; **13**(10)**:** 1010-1019.

148. Wang Y, Su MA, Wan YY. An essential role of the transcription factor GATA-3 for the function of regulatory T cells. *Immunity* 2011; **35**(3)**:** 337-348.

149. Biton M, Haber AL, Rogel N, Burgin G, Beyaz S, Schnell A *et al.* T Helper Cell Cytokines Modulate Intestinal Stem Cell Renewal and Differentiation. *Cell* 2018; **175**(5)**:** 1307-1320 e1322.

150. Corthesy B. Multi-faceted functions of secretory IgA at mucosal surfaces. *Front Immunol* 2013; **4:** 185.

151. Kawamoto S, Maruya M, Kato LM, Suda W, Atarashi K, Doi Y *et al.* Foxp3(+) T cells regulate immunoglobulin a selection and facilitate diversification of bacterial species responsible for immune homeostasis. *Immunity* 2014; **41**(1)**:** 152-165.

152. Cong Y, Feng T, Fujihashi K, Schoeb TR, Elson CO. A dominant, coordinated T regulatory cell-IgA response to the intestinal microbiota. *Proc Natl Acad Sci U S A* 2009; **106**(46)**:** 19256-19261.

153. Tsuji M, Komatsu N, Kawamoto S, Suzuki K, Kanagawa O, Honjo T *et al.* Preferential generation of follicular B helper T cells from Foxp3+ T cells in gut Peyer's patches. *Science* 2009; **323**(5920)**:** 1488-1492.

154. Sun B, Liu M, Cui M, Li T. Granzyme B-expressing treg cells are enriched in colorectal cancer and present the potential to eliminate autologous T conventional cells. *Immunol Lett* 2020; **217:** 7-14.

155. Zhang X, Kelaria S, Kerstetter J, Wang J. The functional and prognostic implications of regulatory T cells in colorectal carcinoma. *J Gastrointest Oncol* 2015; **6**(3)**:** 307-313.

156. Chang LY, Lin YC, Mahalingam J, Huang CT, Chen TW, Kang CW *et al.* Tumor-derived chemokine CCL5 enhances TGF-beta-mediated killing of CD8(+) T cells in colon cancer by T-regulatory cells. *Cancer Res* 2012; **72**(5)**:** 1092-1102.

157. Betts G, Jones E, Junaid S, El-Shanawany T, Scurr M, Mizen P *et al.* Suppression of tumour-specific CD4(+) T cells by regulatory T cells is associated with progression of human colorectal cancer. *Gut* 2012; **61**(8)**:** 1163-1171.

158. Colombo MP, Piconese S. Regulatory-T-cell inhibition versus depletion: the right choice in cancer immunotherapy. *Nat Rev Cancer* 2007; **7**(11)**:** 880-887.

159. Zou W. Regulatory T cells, tumour immunity and immunotherapy. *Nat Rev Immunol* 2006; **6**(4)**:** 295-307.

160. Tokuno K, Hazama S, Yoshino S, Yoshida S, Oka M. Increased prevalence of regulatory T-cells in the peripheral blood of patients with gastrointestinal cancer. *Anticancer Res* 2009; **29**(5)**:** 1527-1532.

161. Terme M, Pernot S, Marcheteau E, Sandoval F, Benhamouda N, Colussi O *et al.* VEGFA-VEGFR pathway blockade inhibits tumor-induced regulatory T-cell proliferation in colorectal cancer. *Cancer Res* 2013; **73**(2)**:** 539-549.

162. Khazaie K, Bonertz A, Beckhove P. Current developments with peptide-based human tumor vaccines. *Curr Opin Oncol* 2009; **21**(6)**:** 524-530.

163. Curiel TJ. Regulatory T cells and treatment of cancer. *Curr Opin Immunol* 2008; **20**(2)**:** 241-246.

164. Ward-Hartstonge KA, McCall JL, McCulloch TR, Kamps AK, Girardin A, Cretney E *et al.* Inclusion of BLIMP-1(+) effector regulatory T cells improves the Immunoscore in a cohort of New Zealand colorectal cancer patients: a pilot study. *Cancer Immunol Immunother* 2017; **66**(4)**:** 515-522.

165. Chung AY, Li Q, Blair SJ, De Jesus M, Dennis KL, LeVea C *et al.* Oral interleukin-10 alleviates polyposis via neutralization of pathogenic T-regulatory cells. *Cancer Res* 2014; **74**(19)**:** 5377-5385.

166. Dennis KL, Wang Y, Blatner NR, Wang S, Saadalla A, Trudeau E *et al.* Adenomatous polyps are driven by microbe-instigated focal inflammation and are controlled by IL-10-producing T cells. *Cancer Res* 2013; **73**(19)**:** 5905-5913.

167. Olguin JE, Medina-Andrade I, Rodriguez T, Rodriguez-Sosa M, Terrazas LI. Relevance of Regulatory T Cells during Colorectal Cancer Development. *Cancers (Basel)* 2020; **12**(7).

168. Szeponik L, Ahlmanner F, Sundstrom P, Rodin W, Gustavsson B, Bexe Lindskog E *et al.* Intratumoral regulatory T cells from colon cancer patients comprise several activated effector populations. *BMC Immunol* 2021; **22**(1)**:** 58.

169. Osman A, Yan B, Li Y, Pavelko KD, Quandt J, Saadalla A *et al.* TCF-1 controls Treg cell functions that regulate inflammation, CD8(+) T cell cytotoxicity and severity of colon cancer. *Nat Immunol* 2021; **22**(9)**:** 1152-1162.

170. Iwasaki A. Exploiting Mucosal Immunity for Antiviral Vaccines. *Annu Rev Immunol* 2016; **34:** 575-608.

171. Park JY, Chung H, DiPalma DT, Tai X, Park JH. Immune quiescence in the oral mucosa is maintained by a uniquely large population of highly activated Foxp3(+) regulatory T cells. *Mucosal Immunol* 2018; **11**(4)**:** 1092-1102.

172. Bhattacharjee A, Hand TW. Role of nutrition, infection, and the microbiota in the efficacy of oral vaccines. *Clin Sci (Lond)* 2018; **132**(11)**:** 1169-1177.

173. Williams WB, Liao HX, Moody MA, Kepler TB, Alam SM, Gao F *et al.* HIV-1 VACCINES. Diversion of HIV-1 vaccine-induced immunity by gp41-microbiota cross-reactive antibodies. *Science* 2015; **349**(6249)**:** aab1253.

174. Price DN, Kusewitt DF, Lino CA, McBride AA, Muttil P. Oral Tolerance to Environmental Mycobacteria Interferes with Intradermal, but Not Pulmonary, Immunization against Tuberculosis. *PLoS Pathog* 2016; **12**(5)**:** e1005614.

175. Aluvihare VR, Kallikourdis M, Betz AG. Regulatory T cells mediate maternal tolerance to the fetus. *Nat Immunol* 2004; **5**(3)**:** 266-271.

176. Quinn KH, Lacoursiere DY, Cui L, Bui J, Parast MM. The unique pathophysiology of early-onset severe preeclampsia: role of decidual T regulatory cells. *J Reprod Immunol* 2011; **91**(1-2)**:** 76-82.

177. Santner-Nanan B, Peek MJ, Khanam R, Richarts L, Zhu E, Fazekas de St Groth B *et al.* Systemic increase in the ratio between Foxp3+ and IL-17-producing CD4+ T cells in healthy pregnancy but not in preeclampsia. *J Immunol* 2009; **183**(11)**:** 7023-7030.

178. Sasaki Y, Darmochwal-Kolarz D, Suzuki D, Sakai M, Ito M, Shima T *et al.* Proportion of peripheral blood and decidual CD4(+) CD25(bright) regulatory T cells in pre-eclampsia. *Clin Exp Immunol* 2007; **149**(1)**:** 139-145.

179. Guerin LR, Moldenhauer LM, Prins JR, Bromfield JJ, Hayball JD, Robertson SA. Seminal fluid regulates accumulation of FOXP3+ regulatory T cells in the preimplantation mouse uterus through expanding the FOXP3+ cell pool and CCL19-mediated recruitment. *Biol Reprod* 2011; **85**(2)**:** 397-408.

180. Moldenhauer LM, Diener KR, Thring DM, Brown MP, Hayball JD, Robertson SA. Cross-presentation of male seminal fluid antigens elicits T cell activation to initiate the female immune response to pregnancy. *J Immunol* 2009; **182**(12)**:** 8080-8093.

181. Robertson SA, Guerin LR, Bromfield JJ, Branson KM, Ahlstrom AC, Care AS. Seminal fluid drives expansion of the CD4+CD25+ T regulatory cell pool and induces tolerance to paternal alloantigens in mice. *Biol Reprod* 2009; **80**(5)**:** 1036-1045.

182. Care AS, Bourque SL, Morton JS, Hjartarson EP, Robertson SA, Davidge ST. Reduction in Regulatory T Cells in Early Pregnancy Causes Uterine Artery Dysfunction in Mice. *Hypertension* 2018; **72**(1)**:** 177-187.

183. Vojtech L, Zhang M, Dave V, Levy C, Hughes SM, Wang R *et al.* Extracellular vesicles in human semen modulate antigen-presenting cell function and decrease downstream antiviral T cell responses. *PLoS One* 2019; **14**(10)**:** e0223901.

184. Wira CR, Fahey JV. A new strategy to understand how HIV infects women: identification of a window of vulnerability during the menstrual cycle. *AIDS* 2008; **22**(15)**:** 1909-1917.

185. Wira CR, Fahey JV, Ghosh M, Patel MV, Hickey DK, Ochiel DO. Sex hormone regulation of innate immunity in the female reproductive tract: the role of epithelial cells in balancing reproductive potential with protection against sexually transmitted pathogens. *Am J Reprod Immunol* 2010; **63**(6)**:** 544-565.

186. Wira CR, Fahey JV, Rodriguez-Garcia M, Shen Z, Patel MV. Regulation of mucosal immunity in the female reproductive tract: the role of sex hormones in immune protection against sexually transmitted pathogens. *Am J Reprod Immunol* 2014; **72**(2)**:** 236-258.

187. Hughes SM, Pandey U, Johnston C, Marrazzo J, Hladik F, Micks E. Impact of the menstrual cycle and ethinyl estradiol/etonogestrel contraceptive vaginal ring on granulysin and other mucosal immune mediators. *Am J Reprod Immunol* 2021**:** e13412.

188. Robertson SA, Green ES, Care AS, Moldenhauer LM, Prins JR, Hull ML *et al.* Therapeutic Potential of Regulatory T Cells in Preeclampsia-Opportunities and Challenges. *Front Immunol* 2019; **10:** 478.

189. Ma B, Forney LJ, Ravel J. Vaginal microbiome: rethinking health and disease. *Annu Rev Microbiol* 2012; **66:** 371-389.

190. Campisciano G, Zanotta N, Licastro D, De Seta F, Comar M. In vivo microbiome and associated immune markers: New insights into the pathogenesis of vaginal dysbiosis. *Sci Rep* 2018; **8**(1)**:** 2307.

191. Eslami S, Hadjati J, Motevaseli E, Mirzaei R, Farashi Bonab S, Ansaripour B *et al.* Lactobacillus crispatus strain SJ-3C-US induces human dendritic cells (DCs) maturation and confers an anti-inflammatory phenotype to DCs. *APMIS* 2016; **124**(8)**:** 697-710.

192. Schellenberg JJ, Card CM, Ball TB, Mungai JN, Irungu E, Kimani J *et al.* Bacterial vaginosis, HIV serostatus and T-cell subset distribution in a cohort of East African commercial sex workers: retrospective analysis. *AIDS* 2012; **26**(3)**:** 387-393.

193. Amabebe E, Anumba DOC. The Vaginal Microenvironment: The Physiologic Role of Lactobacilli. *Front Med (Lausanne)* 2018; **5:** 181.

194. Soerens AG, Da Costa A, Lund JM. Regulatory T cells are essential to promote proper CD4 T-cell priming upon mucosal infection. *Mucosal Immunol* 2016; **9**(6)**:** 1395-1406.

195. Lund JM, Hsing L, Pham TT, Rudensky AY. Coordination of early protective immunity to viral infection by regulatory T cells. *Science* 2008; **320**(5880)**:** 1220-1224.

196. Nemati M, Malla N, Yadav M, Khorramdelazad H, Jafarzadeh A. Humoral and T cell-mediated immune response against trichomoniasis. *Parasite Immunol* 2018; **40**(3).

197. Ssemaganda A, Cholette F, Perner M, Kambaran C, Adhiambo W, Wambugu PM *et al.* Endocervical Regulatory T Cells Are Associated With Decreased Genital Inflammation and Lower HIV Target Cell Abundance. *Front Immunol* 2021.

198. Stary G, Olive A, Radovic-Moreno AF, Gondek D, Alvarez D, Basto PA *et al.* VACCINES. A mucosal vaccine against Chlamydia trachomatis generates two waves of protective memory T cells. *Science* 2015; **348**(6241)**:** aaa8205.

199. Mathur AN, Zirak B, Boothby IC, Tan M, Cohen JN, Mauro TM *et al.* Treg-Cell Control of a CXCL5-IL-17 Inflammatory Axis Promotes Hair-Follicle-Stem-Cell Differentiation During Skin-Barrier Repair. *Immunity* 2019; **50**(3)**:** 655-667 e654.

200. Kolodin D, van Panhuys N, Li C, Magnuson AM, Cipolletta D, Miller CM *et al.* Antigen- and cytokine-driven accumulation of regulatory T cells in visceral adipose tissue of lean mice. *Cell Metab* 2015; **21**(4)**:** 543-557.

201. Suvas S, Azkur AK, Kim BS, Kumaraguru U, Rouse BT. CD4+CD25+ regulatory T cells control the severity of viral immunoinflammatory lesions. *J Immunol* 2004; **172**(7)**:** 4123-4132.

202. Belkaid Y, Piccirillo CA, Mendez S, Shevach EM, Sacks DL. CD4+CD25+ regulatory T cells control Leishmania major persistence and immunity. *Nature* 2002; **420**(6915)**:** 502-507.

203. Mendez S, Reckling SK, Piccirillo CA, Sacks D, Belkaid Y. Role for CD4(+) CD25(+) regulatory T cells in reactivation of persistent leishmaniasis and control of concomitant immunity. *J Exp Med* 2004; **200**(2)**:** 201-210.

204. Gebhardt T, Wakim LM, Eidsmo L, Reading PC, Heath WR, Carbone FR. Memory T cells in nonlymphoid tissue that provide enhanced local immunity during infection with herpes simplex virus. *Nat Immunol* 2009; **10**(5)**:** 524-530.

205. Pattacini L, Woodward Davis A, Czartoski J, Mair F, Presnell S, Hughes SM *et al.* A pro-inflammatory CD8+ T-cell subset patrols the cervicovaginal tract. *Mucosal Immunol* 2019; **12**(5)**:** 1118-1129.

206. Turner DL, Farber DL. Mucosal resident memory CD4 T cells in protection and immunopathology. *Front Immunol* 2014; **5:** 331.

207. Woodward Davis AS, Vick SC, Pattacini L, Voillet V, Hughes SM, Lentz GM *et al.* The human memory T cell compartment changes across tissues of the female reproductive tract. *Mucosal Immunol* 2021; **14**(4)**:** 862-872.

208. Vignali DA, Collison LW, Workman CJ. How regulatory T cells work. *Nat Rev Immunol* 2008; **8**(7)**:** 523-532.

209. Linehan MM, Richman S, Krummenacher C, Eisenberg RJ, Cohen GH, Iwasaki A. In vivo role of nectin-1 in entry of herpes simplex virus type 1 (HSV-1) and HSV-2 through the vaginal mucosa. *J Virol* 2004; **78**(5)**:** 2530-2536.

210. Anderson KG, Mayer-Barber K, Sung H, Beura L, James BR, Taylor JJ *et al.* Intravascular staining for discrimination of vascular and tissue leukocytes. *Nat Protoc* 2014; **9**(1)**:** 209-222.

211. Galkina E, Thatte J, Dabak V, Williams MB, Ley K, Braciale TJ. Preferential migration of effector CD8+ T cells into the interstitium of the normal lung. *J Clin Invest* 2005; **115**(12)**:** 3473-3483.

212. Han Y, Guo Q, Zhang M, Chen Z, Cao X. CD69+ CD4+ CD25- T cells, a new subset of regulatory T cells, suppress T cell proliferation through membrane-bound TGF-beta 1. *J Immunol* 2009; **182**(1)**:** 111-120.

213. Shin H, Iwasaki A. A vaccine strategy that protects against genital herpes by establishing local memory T cells. *Nature* 2012; **491**(7424)**:** 463-467.

214. Fontenot JD, Rasmussen JP, Williams LM, Dooley JL, Farr AG, Rudensky AY. Regulatory T cell lineage specification by the forkhead transcription factor foxp3. *Immunity* 2005; **22**(3)**:** 329-341.

215. Levine AG, Mendoza A, Hemmers S, Moltedo B, Niec RE, Schizas M *et al.* Stability and function of regulatory T cells expressing the transcription factor T-bet. *Nature* 2017; **546**(7658)**:** 421-425.

216. Stuart T, Butler A, Hoffman P, Hafemeister C, Papalexi E, Mauck WM, 3rd *et al.* Comprehensive Integration of Single-Cell Data. *Cell* 2019; **177**(7)**:** 1888-1902 e1821.

217. Becht E, McInnes L, Healy J, Dutertre CA, Kwok IWH, Ng LG *et al.* Dimensionality reduction for visualizing single-cell data using UMAP. *Nat Biotechnol* 2018.

218. Finak G, McDavid A, Yajima M, Deng J, Gersuk V, Shalek AK *et al.* MAST: a flexible statistical framework for assessing transcriptional changes and characterizing heterogeneity in single-cell RNA sequencing data. *Genome Biol* 2015; **16:** 278.

219. Malarkannan S. NKG7 makes a better killer. *Nat Immunol* 2020; **21**(10)**:** 1139-1140.

220. Ng SS, De Labastida Rivera F, Yan J, Corvino D, Das I, Zhang P *et al.* The NK cell granule protein NKG7 regulates cytotoxic granule exocytosis and inflammation. *Nat Immunol* 2020; **21**(10)**:** 1205-1218.

221. Kohlmeier JE, Cookenham T, Roberts AD, Miller SC, Woodland DL. Type I interferons regulate cytolytic activity of memory CD8(+) T cells in the lung airways during respiratory virus challenge. *Immunity* 2010; **33**(1)**:** 96-105.

222. Mackay LK, Wakim L, van Vliet CJ, Jones CM, Mueller SN, Bannard O *et al.* Maintenance of T cell function in the face of chronic antigen stimulation and repeated reactivation for a latent virus infection. *J Immunol* 2012; **188**(5)**:** 2173-2178.

223. Davé VA, Cardozo-Ojeda EF, Mair F, Erickson J, Woodward-Davis AS, Koehne A *et al.* Cervicovaginal Tissue Residence Confers a Distinct Differentiation Program upon Memory CD8 T Cells. *J Immunol* 2021.

224. Lund J, Sato A, Akira S, Medzhitov R, Iwasaki A. Toll-like receptor 9-mediated recognition of Herpes simplex virus-2 by plasmacytoid dendritic cells. *J Exp Med* 2003; **198**(3)**:** 513-520.

225. Lund JM, Linehan MM, Iijima N, Iwasaki A. Cutting Edge: Plasmacytoid dendritic cells provide innate immune protection against mucosal viral infection in situ. *J Immunol* 2006; **177**(11)**:** 7510-7514.

226. Cao X, Cai SF, Fehniger TA, Song J, Collins LI, Piwnica-Worms DR *et al.* Granzyme B and perforin are important for regulatory T cell-mediated suppression of tumor clearance. *Immunity* 2007; **27**(4)**:** 635-646.

227. Sula Karreci E, Eskandari SK, Dotiwala F, Routray SK, Kurdi AT, Assaker JP *et al.* Human regulatory T cells undergo self-inflicted damage via granzyme pathways upon activation. *JCI Insight* 2017; **2**(21).

228. Salti SM, Hammelev EM, Grewal JL, Reddy ST, Zemple SJ, Grossman WJ *et al.* Granzyme B regulates antiviral CD8+ T cell responses. *J Immunol* 2011; **187**(12)**:** 6301-6309.

229. Efimova OV, Kelley TW. Induction of granzyme B expression in T-cell receptor/CD28-stimulated human regulatory T cells is suppressed by inhibitors of the PI3K-mTOR pathway. *BMC Immunol* 2009; **10:** 59.

230. Grossman WJ, Verbsky JW, Tollefsen BL, Kemper C, Atkinson JP, Ley TJ. Differential expression of granzymes A and B in human cytotoxic lymphocyte subsets and T regulatory cells. *Blood* 2004; **104**(9)**:** 2840-2848.

231. Maurice NJ, Taber AK, Prlic M. The Ugly Duckling Turned to Swan: A Change in Perception of Bystander-Activated Memory CD8 T Cells. *J Immunol* 2021; **206**(3)**:** 455-462.

232. Milligan GN, Bernstein DI. Interferon-gamma enhances resolution of herpes simplex virus type 2 infection of the murine genital tract. *Virology* 1997; **229**(1)**:** 259-268.

233. Nakanishi Y, Lu B, Gerard C, Iwasaki A. CD8(+) T lymphocyte mobilization to virus-infected tissue requires CD4(+) T-cell help. *Nature* 2009; **462**(7272)**:** 510-513.

234. Chu T, Tyznik AJ, Roepke S, Berkley AM, Woodward-Davis A, Pattacini L *et al.* Bystander-activated memory CD8 T cells control early pathogen load in an innate-like, NKG2D-dependent manner. *Cell Rep* 2013; **3**(3)**:** 701-708.

235. Roychoudhury P, Swan DA, Duke E, Corey L, Zhu J, Davé V *et al.* Tissue-resident T cell-derived cytokines eliminate herpes simplex virus-2-infected cells. *J Clin Invest* 2020; **130**(6)**:** 2903-2919.

236. Iijima N, Iwasaki A. T cell memory. A local macrophage chemokine network sustains protective tissue-resident memory CD4 T cells. *Science* 2014; **346**(6205)**:** 93-98.

237. Schiffer JT. Mucosal HSV-2 Specific CD8+ T-Cells Represent Containment of Prior Viral Shedding Rather than a Correlate of Future Protection. *Front Immunol* 2013; **4:** 209.

238. Schiffer JT, Corey L. Rapid host immune response and viral dynamics in herpes simplex virus-2 infection. *Nat Med* 2013; **19**(3)**:** 280-290.

239. Jones CA, Taylor TJ, Knipe DM. Biological properties of herpes simplex virus 2 replication-defective mutant strains in a murine nasal infection model. *Virology* 2000; **278**(1)**:** 137-150.

240. Woodward Davis AS, Roozen HN, Dufort MJ, DeBerg HA, Delaney MA, Mair F *et al.* The human tissue-resident CCR5(+) T cell compartment maintains protective and functional properties during inflammation. *Sci Transl Med* 2019; **11**(521).

241. Dobin A, Davis CA, Schlesinger F, Drenkow J, Zaleski C, Jha S *et al.* STAR: ultrafast universal RNA-seq aligner. *Bioinformatics* 2013; **29**(1)**:** 15-21.

242. Li B, Dewey CN. RSEM: accurate transcript quantification from RNA-Seq data with or without a reference genome. *BMC Bioinformatics* 2011; **12:** 323.

243. Robinson MD, McCarthy DJ, Smyth GK. edgeR: a Bioconductor package for differential expression analysis of digital gene expression data. *Bioinformatics* 2010; **26**(1)**:** 139-140.

244. Law CW, Chen Y, Shi W, Smyth GK. voom: Precision weights unlock linear model analysis tools for RNA-seq read counts. *Genome Biol* 2014; **15**(2)**:** R29.

245. Ritchie ME, Phipson B, Wu D, Hu Y, Law CW, Shi W *et al.* limma powers differential expression analyses for RNA-sequencing and microarray studies. *Nucleic Acids Res* 2015; **43**(7)**:** e47.

246. Smyth GK. Linear models and empirical bayes methods for assessing differential expression in microarray experiments. *Stat Appl Genet Mol Biol* 2004; **3:** Article3.

247. Wu D, Smyth GK. Camera: a competitive gene set test accounting for inter-gene correlation. *Nucleic Acids Res* 2012; **40**(17)**:** e133.

248. Hao Y, Hao S, Andersen-Nissen E, Mauck WM, 3rd, Zheng S, Butler A *et al.* Integrated analysis of multimodal single-cell data. *Cell* 2021; **184**(13)**:** 3573-3587 e3529.

249. Butler A, Hoffman P, Smibert P, Papalexi E, Satija R. Integrating single-cell transcriptomic data across different conditions, technologies, and species. *Nat Biotechnol* 2018; **36**(5)**:** 411-420.

250. Satija R, Farrell JA, Gennert D, Schier AF, Regev A. Spatial reconstruction of single-cell gene expression data. *Nat Biotechnol* 2015; **33**(5)**:** 495-502.

251. Wang T, Li B, Nelson CE, Nabavi S. Comparative analysis of differential gene expression analysis tools for single-cell RNA sequencing data. *BMC Bioinformatics* 2019; **20**(1)**:** 40.

252. Gupta R, Warren T, Wald A. Genital herpes. *Lancet* 2007; **370**(9605)**:** 2127-2137.

253. Looker KJ, Magaret AS, May MT, Turner KME, Vickerman P, Newman LM *et al.* First estimates of the global and regional incidence of neonatal herpes infection. *Lancet Glob Health* 2017; **5**(3)**:** e300-e309.

254. Freeman EE, Weiss HA, Glynn JR, Cross PL, Whitworth JA, Hayes RJ. Herpes simplex virus 2 infection increases HIV acquisition in men and women: systematic review and meta-analysis of longitudinal studies. *Aids* 2006; **20**(1)**:** 73-83.

255. Kumar BV, Ma W, Miron M, Granot T, Guyer RS, Carpenter DJ *et al.* Human Tissue-Resident Memory T Cells Are Defined by Core Transcriptional and Functional Signatures in Lymphoid and Mucosal Sites. *Cell Rep* 2017; **20**(12)**:** 2921-2934.

256. Mackay LK, Minnich M, Kragten NA, Liao Y, Nota B, Seillet C *et al.* Hobit and Blimp1 instruct a universal transcriptional program of tissue residency in lymphocytes. *Science* 2016; **352**(6284)**:** 459-463.

257. Awasthi S, Friedman HM. Status of prophylactic and therapeutic genital herpes vaccines. *Curr Opin Virol* 2014; **6:** 6-12.

258. Hofstetter AM, Rosenthal SL, Stanberry LR. Current thinking on genital herpes. *Curr Opin Infect Dis* 2014; **27**(1)**:** 75-83.

259. Dropulic LK, Cohen JI. The challenge of developing a herpes simplex virus 2 vaccine. *Expert Rev Vaccines* 2012; **11**(12)**:** 1429-1440.

260. Milman N, Zhu J, Johnston C, Cheng A, Magaret A, Koelle DM *et al.* In Situ Detection of Regulatory T Cells in Human Genital Herpes Simplex Virus Type 2 (HSV-2) Reactivation and Their Influence on Spontaneous HSV-2 Reactivation. *J Infect Dis* 2016; **214**(1)**:** 23-31.

261. van der Veeken J, Gonzalez AJ, Cho H, Arvey A, Hemmers S, Leslie CS *et al.* Memory of Inflammation in Regulatory T Cells. *Cell* 2016; **166**(4)**:** 977-990.

262. Gilden DH, Mahalingam R, Cohrs RJ, Tyler KL. Herpesvirus infections of the nervous system. *Nat Clin Pract Neurol* 2007; **3**(2)**:** 82-94.

263. Harandi AM, Svennerholm B, Holmgren J, Eriksson K. Differential roles of B cells and IFN-gamma-secreting CD4(+) T cells in innate and adaptive immune control of genital herpes simplex virus type 2 infection in mice. *J Gen Virol* 2001; **82**(Pt 4)**:** 845-853.

264. Parr MB, Parr EL. The role of gamma interferon in immune resistance to vaginal infection by herpes simplex virus type 2 in mice. *Virology* 1999; **258**(2)**:** 282-294.

265. McDermott MR, Brais LJ, Evelegh MJ. Mucosal and systemic antiviral antibodies in mice inoculated intravaginally with herpes simplex virus type 2. *J Gen Virol* 1990; **71 (Pt 7):** 1497-1504.

266. Parr MB, Parr EL. Protective immunity against HSV-2 in the mouse vagina. *J Reprod Immunol* 1997; **36**(1-2)**:** 77-92.

267. Sarangi PP, Sehrawat S, Suvas S, Rouse BT. IL-10 and natural regulatory T cells: two independent anti-inflammatory mechanisms in herpes simplex virus-induced ocular immunopathology. *J Immunol* 2008; **180**(9)**:** 6297-6306.

268. Sehrawat S, Suvas S, Sarangi PP, Suryawanshi A, Rouse BT. In vitro-generated antigen-specific CD4+ CD25+ Foxp3+ regulatory T cells control the severity of herpes simplex virus-induced ocular immunoinflammatory lesions. *J Virol* 2008; **82**(14)**:** 6838-6851.

269. Pandiyan P, Conti HR, Zheng L, Peterson AC, Mathern DR, Hernández-Santos N *et al.* CD4(+)CD25(+)Foxp3(+) regulatory T cells promote Th17 cells in vitro and enhance host resistance in mouse Candida albicans Th17 cell infection model. *Immunity* 2011; **34**(3)**:** 422-434.

270. Fulton RB, Meyerholz DK, Varga SM. Foxp3+ CD4 regulatory T cells limit pulmonary immunopathology by modulating the CD8 T cell response during respiratory syncytial virus infection. *J Immunol* 2010; **185**(4)**:** 2382-2392.

271. Ruckwardt TJ, Bonaparte KL, Nason MC, Graham BS. Regulatory T cells promote early influx of CD8+ T cells in the lungs of respiratory syncytial virus-infected mice and diminish immunodominance disparities. *J Virol* 2009; **83**(7)**:** 3019-3028.

272. Zhou X, Jeker LT, Fife BT, Zhu S, Anderson MS, McManus MT *et al.* Selective miRNA disruption in T reg cells leads to uncontrolled autoimmunity. *J Exp Med* 2008; **205**(9)**:** 1983-1991.

273. Mueller SN, Heath W, McLain JD, Carbone FR, Jones CM. Characterization of two TCR transgenic mouse lines specific for herpes simplex virus. *Immunol Cell Biol* 2002; **80**(2)**:** 156-163.

274. Iijima N, Iwasaki A. Tissue instruction for migration and retention of TRM cells. *Trends Immunol* 2015; **36**(9)**:** 556-564.

275. Moran AE, Holzapfel KL, Xing Y, Cunningham NR, Maltzman JS, Punt J *et al.* T cell receptor signal strength in Treg and iNKT cell development demonstrated by a novel fluorescent reporter mouse. *J Exp Med* 2011; **208**(6)**:** 1279-1289.

276. Bhela S, Kempsell C, Manohar M, Dominguez-Villar M, Griffin R, Bhatt P *et al.* Nonapoptotic and extracellular activity of granzyme B mediates resistance to regulatory T cell (Treg) suppression by HLA-DR-CD25hiCD127lo Tregs in multiple sclerosis and in response to IL-6. *J Immunol* 2015; **194**(5)**:** 2180-2189.

277. Chamberlain CM, Ang LS, Boivin WA, Cooper DM, Williams SJ, Zhao H *et al.* Perforin-independent extracellular granzyme B activity contributes to abdominal aortic aneurysm. *Am J Pathol* 2010; **176**(2)**:** 1038-1049.

278. Boivin WA, Cooper DM, Hiebert PR, Granville DJ. Intracellular versus extracellular granzyme B in immunity and disease: challenging the dogma. *Lab Invest* 2009; **89**(11)**:** 1195-1220.

279. Voskoboinik I, Whisstock JC, Trapani JA. Perforin and granzymes: function, dysfunction and human pathology. *Nat Rev Immunol* 2015; **15**(6)**:** 388-400.

280. Newman L, Rowley J, Vander Hoorn S, Wijesooriya NS, Unemo M, Low N *et al.* Global Estimates of the Prevalence and Incidence of Four Curable Sexually Transmitted Infections in 2012 Based on Systematic Review and Global Reporting. *PLoS One* 2015; **10**(12)**:** e0143304.

281. Panchanadeswaran S, Johnson SC, Mayer KH, Srikrishnan AK, Sivaran S, Zelaya CE *et al.* Gender differences in the prevalence of sexually transmitted infections and genital symptoms in an urban setting in southern India. *Sex Transm Infect* 2006; **82**(6)**:** 491-495.

282. Tsevat DG, Wiesenfeld HC, Parks C, Peipert JF. Sexually transmitted diseases and infertility. *Am J Obstet Gynecol* 2017; **216**(1)**:** 1-9.

283. Burd EM. Human papillomavirus and cervical cancer. *Clin Microbiol Rev* 2003; **16**(1)**:** 1-17.

APPENDIX A

Table A.1. Genes co-clustered with PPARγ in VAT Treg, per Cipolletta et al., *Nature* 2021.

Genes Co-clustered with Pparg in VAT Treg (Cipolletta et al. *Nature* 2012)
Ablim3
Adam8
Alcam
Alox8
Anxa1
Ar
Areg
Atf3
Bcl2a1c
Cabyr
Car5b
Cass4
Ccr1
Ccr2
Ccr3
Ccr5
Ccrl2
Cd200r4
Cdkn1a
Cnnm2
Cobll1
Coq10b
Cpm
Crem
Crisp1
Csf2
Csrnp1
Ctla2a
Ctla2b
Ctsh
Cxcl10

Genes Co-clustered with Pparg in VAT Treg (Cipolletta et al. *Nature* 2012)
Cxcl2
Cxcl3
Cxcr6
Cyp11a1
Cysltr1
Cysltr2
Dennd4a
Dgat1
Dusp1
Egln3
Ehd4
Ell2
Enkur
Evi5
Fam183b
Fgl2
Fos
Fosb
Fosl2
Frmd5
Gadd45b
Gem
Gla
Gm10008
Gm5068
Gna15
Gp49a
Hip1
Hpgd
Hspa1a
Id2
Ier3
Ifrd1
Il10
Il18rap
Il1rl1
Il5
Itga1

Genes Co-clustered with Pparg in VAT Treg (Cipolletta et al. *Nature* 2012)
Jag1
Junb
Jup
Kcna4
Kdm6b
Klf4
Klrg1
Lgals3
Lilrb4
Lmna
Lpcat2
Lrrn4
Ltb4r1
Lyn
Mmp25
Mmp9
Mt1
Mt2
Muc1
Myadm
Myd116
Nebl
Nfil3
Nfkbid
Npnt
Nr4a2
Nr4a3
Olfr1259
Padi2
Pcsk1
Pcyt1a
Phlda1
Plin2
Plk2
Plod2
Pparg
Raph1
Rassf6

Genes Co-clustered with Pparg in VAT Treg (Cipolletta et al. *Nature* 2012)
Rgs2
Rnf128
Rora
Ryk
S100a4
S100a6
Serpinb6a
Sik1
Slc15a3
Spty2d1
Sytl3
Tc2n
Tmbim1
Tnfaip3
Tnfrsf10b
Ttc39c
Zeb2

APPENDIX B

Table B.1. Differentially expressed genes in vaginal Tregs compared to dLN Tregs.

List of DEG in Treg populations in HSV-2-infected and uninfected mice in Figure 2.7. DEG were determined by log2FC > .5 and FDR <.01.

gene	p_val	avg_log2FC	pct.1	pct.2	p_val_adj	cluster
mt-Atp8	2.28E-263	-1.566156162	0.958	0.996	3.28E-259	VT_HSV2_Treg
mt-Atp6	2.18E-81	0.878797555	0.973	0.989	3.13E-77	VT_HSV2_Treg
Ly6a	2.46E-73	1.87922106	0.795	0.407	3.54E-69	VT_HSV2_Treg
Uba52	2.76E-70	-0.823184463	0.909	0.991	3.98E-66	VT_HSV2_Treg
S100a6	1.15E-57	2.242003989	0.64	0.275	1.65E-53	VT_HSV2_Treg
Lgals1	5.41E-55	1.784252271	0.75	0.531	7.79E-51	VT_HSV2_Treg
Rps29	4.82E-54	-0.579940135	0.973	0.997	6.95E-50	VT_HSV2_Treg
Gzmb	1.01E-50	2.428181935	0.473	0.111	1.45E-46	VT_HSV2_Treg
Ctla2a	6.19E-49	2.099430206	0.398	0.111	8.91E-45	VT_HSV2_Treg
Ccr7	2.31E-42	-1.804917465	0.273	0.684	3.32E-38	VT_HSV2_Treg
Pabpc1	1.00E-41	-0.715108537	0.833	0.951	1.45E-37	VT_HSV2_Treg
Clic1	3.76E-41	0.834369288	0.867	0.774	5.42E-37	VT_HSV2_Treg
AW112010	6.07E-41	1.149138201	0.811	0.689	8.74E-37	VT_HSV2_Treg
S100a10	8.29E-41	1.198226435	0.83	0.743	1.19E-36	VT_HSV2_Treg
Rps28	1.93E-39	-0.53682418	0.973	0.994	2.78E-35	VT_HSV2_Treg
Aldoa	6.11E-36	0.955983596	0.822	0.726	8.80E-32	VT_HSV2_Treg
Cxcr3	1.15E-35	1.08006394	0.394	0.102	1.66E-31	VT_HSV2_Treg
Gm10076	1.60E-35	-0.818340428	0.265	0.584	2.31E-31	VT_HSV2_Treg
H2-D1	7.84E-35	0.52588104	0.932	0.99	1.13E-30	VT_HSV2_Treg
Vim	1.71E-34	1.44636344	0.727	0.599	2.46E-30	VT_HSV2_Treg
mt-Nd4l	2.01E-34	-0.677787725	0.898	0.983	2.90E-30	VT_HSV2_Treg
Actg1	2.31E-34	0.853903125	0.977	0.99	3.33E-30	VT_HSV2_Treg
Sh3bgrl3	7.54E-33	0.744096258	0.909	0.863	1.09E-28	VT_HSV2_Treg
Btg1	2.93E-31	-0.877606271	0.803	0.952	4.21E-27	VT_HSV2_Treg
Srgn	3.26E-31	0.684060132	0.924	0.963	4.70E-27	VT_HSV2_Treg
S100a13	3.52E-31	0.87313147	0.652	0.484	5.07E-27	VT_HSV2_Treg
Gimap7	1.11E-30	1.043516886	0.61	0.318	1.61E-26	VT_HSV2_Treg
S100a11	1.58E-30	1.036973547	0.686	0.438	2.28E-26	VT_HSV2_Treg
Glrx	2.63E-30	1.215710426	0.549	0.33	3.79E-26	VT_HSV2_Treg
Lgals3	2.81E-30	1.598597107	0.295	0.06	4.04E-26	VT_HSV2_Treg
Vps37b	2.90E-30	-1.133775372	0.568	0.807	4.17E-26	VT_HSV2_Treg

gene	p_val	avg_log2FC	pct.1	pct.2	p_val_adj	cluster
Gm28727	4.41E-30	-0.851720602	0.125	0.429	6.35E-26	VT_HSV2_Treg
Gimap4	2.90E-29	0.879708488	0.705	0.47	4.17E-25	VT_HSV2_Treg
mt-Nd2	5.87E-29	-0.747505121	0.761	0.93	8.45E-25	VT_HSV2_Treg
Sdf4	7.84E-29	0.929735036	0.811	0.721	1.13E-24	VT_HSV2_Treg
Ccr2	6.17E-28	0.936320554	0.341	0.086	8.89E-24	VT_HSV2_Treg
Pglyrp1	6.57E-28	0.975786997	0.591	0.376	9.46E-24	VT_HSV2_Treg
S100a4	6.92E-28	1.370774931	0.477	0.191	9.97E-24	VT_HSV2_Treg
mt-Cytb	1.25E-27	-0.595010754	0.951	0.992	1.80E-23	VT_HSV2_Treg
Anxa2	1.27E-27	1.347380282	0.436	0.198	1.83E-23	VT_HSV2_Treg
Cmtm7	3.87E-27	0.94241608	0.58	0.334	5.58E-23	VT_HSV2_Treg
Fxyd5	7.17E-27	0.612672496	0.871	0.896	1.03E-22	VT_HSV2_Treg
Aes	9.56E-27	0.642606006	0.716	0.573	1.38E-22	VT_HSV2_Treg
Actb	1.13E-26	0.670950742	0.992	0.998	1.63E-22	VT_HSV2_Treg
Ifi27l2a	6.46E-26	0.910864655	0.943	0.936	9.31E-22	VT_HSV2_Treg
Gclm	5.49E-25	-0.577413197	0.504	0.745	7.90E-21	VT_HSV2_Treg
Prelid1	1.39E-24	0.677650549	0.712	0.597	2.00E-20	VT_HSV2_Treg
Tnfrsf18	2.08E-24	0.818826575	0.769	0.705	2.99E-20	VT_HSV2_Treg
Crip1	3.21E-24	1.000164194	0.807	0.742	4.63E-20	VT_HSV2_Treg
Rsrp1	3.98E-24	-1.109390973	0.424	0.676	5.73E-20	VT_HSV2_Treg
Cox8a	6.55E-24	0.605185677	0.886	0.861	9.43E-20	VT_HSV2_Treg
Gmfg	1.11E-23	0.754371149	0.712	0.537	1.60E-19	VT_HSV2_Treg
Cd52	1.93E-23	0.740498462	0.939	0.923	2.78E-19	VT_HSV2_Treg
Arhgdib	7.39E-22	0.503883417	0.875	0.911	1.06E-17	VT_HSV2_Treg
Amd1	8.64E-22	-0.875004369	0.212	0.492	1.24E-17	VT_HSV2_Treg
Gm8186	9.47E-22	-0.705605219	0.42	0.648	1.36E-17	VT_HSV2_Treg
Pkm	1.24E-21	0.62359182	0.795	0.727	1.79E-17	VT_HSV2_Treg
Gm8730	1.28E-21	-0.666215616	0.261	0.492	1.84E-17	VT_HSV2_Treg
Selplg	1.29E-21	0.645826845	0.799	0.672	1.85E-17	VT_HSV2_Treg
Ctla4	4.10E-21	0.595445765	0.807	0.879	5.91E-17	VT_HSV2_Treg
Ptprcap	5.43E-21	0.686877638	0.803	0.706	7.81E-17	VT_HSV2_Treg
Pla2g16	7.89E-21	0.666531133	0.617	0.416	1.14E-16	VT_HSV2_Treg
Nsg2	1.47E-20	-0.735019939	0.125	0.396	2.12E-16	VT_HSV2_Treg
Mrpl33	1.76E-20	0.677745229	0.625	0.422	2.53E-16	VT_HSV2_Treg
Cfl1	1.81E-20	0.518159868	0.951	0.953	2.61E-16	VT_HSV2_Treg
Ppib	1.85E-20	0.599056802	0.837	0.721	2.67E-16	VT_HSV2_Treg
Tpi1	3.58E-20	0.959674342	0.489	0.284	5.16E-16	VT_HSV2_Treg
Hilpda	3.64E-20	1.00612355	0.428	0.212	5.24E-16	VT_HSV2_Treg
Tmsb4x	3.71E-20	0.519885238	0.981	0.999	5.35E-16	VT_HSV2_Treg

gene	p_val	avg_log2FC	pct.1	pct.2	p_val_adj	cluster
Isg20	4.74E-20	0.931606964	0.424	0.237	6.83E-16	VT_HSV2_Treg
Vcpkmt	6.24E-20	0.675245369	0.356	0.134	8.99E-16	VT_HSV2_Treg
Npc2	7.22E-20	0.535651727	0.826	0.772	1.04E-15	VT_HSV2_Treg
Chmp4b	1.02E-19	0.540772234	0.75	0.627	1.47E-15	VT_HSV2_Treg
Ubl5	1.08E-19	0.512472556	0.773	0.74	1.55E-15	VT_HSV2_Treg
Myl6	1.29E-19	0.534452824	0.89	0.902	1.85E-15	VT_HSV2_Treg
Rpl9-ps6	3.10E-19	-0.674769128	0.409	0.632	4.46E-15	VT_HSV2_Treg
Arpc1b	3.92E-19	0.521489501	0.814	0.778	5.64E-15	VT_HSV2_Treg
Rps27rt	6.06E-19	-0.663757034	0.667	0.838	8.72E-15	VT_HSV2_Treg
Pfn1	1.65E-18	0.509210629	0.985	0.989	2.37E-14	VT_HSV2_Treg
Capg	1.95E-18	0.747630752	0.64	0.56	2.82E-14	VT_HSV2_Treg
H2-Q7	2.12E-18	0.531986507	0.826	0.778	3.05E-14	VT_HSV2_Treg
Tagln2	2.89E-18	0.784547342	0.64	0.456	4.16E-14	VT_HSV2_Treg
Irf1	3.23E-18	0.758944654	0.636	0.445	4.65E-14	VT_HSV2_Treg
Ldha	3.41E-18	0.643067175	0.875	0.845	4.91E-14	VT_HSV2_Treg
Lrig1	8.70E-18	-0.760867704	0.087	0.318	1.25E-13	VT_HSV2_Treg
Gstp1	1.03E-17	0.600335872	0.765	0.707	1.48E-13	VT_HSV2_Treg
Cd47	1.14E-17	0.55940253	0.712	0.634	1.64E-13	VT_HSV2_Treg
Dnaja1	1.38E-17	-0.693251212	0.723	0.887	1.99E-13	VT_HSV2_Treg
Phf11b	1.85E-17	0.721911219	0.447	0.236	2.66E-13	VT_HSV2_Treg
Nkg7	2.03E-17	1.232051754	0.273	0.097	2.92E-13	VT_HSV2_Treg
Tspo	2.97E-17	0.59375819	0.72	0.604	4.28E-13	VT_HSV2_Treg
Pkp3	4.04E-17	0.746664603	0.485	0.305	5.82E-13	VT_HSV2_Treg
Acot7	4.61E-17	0.712726611	0.394	0.186	6.64E-13	VT_HSV2_Treg
Impdh2	4.70E-17	-0.564681176	0.277	0.513	6.78E-13	VT_HSV2_Treg
Pnrc1	4.73E-17	-0.59738052	0.845	0.945	6.82E-13	VT_HSV2_Treg
Abracl	7.74E-17	0.526402933	0.75	0.696	1.12E-12	VT_HSV2_Treg
Socs2	1.23E-16	0.855779339	0.299	0.135	1.77E-12	VT_HSV2_Treg
Smc4	1.88E-16	-0.666717162	0.432	0.66	2.70E-12	VT_HSV2_Treg
Rpl10-ps3	3.86E-16	-0.573180246	0.254	0.448	5.56E-12	VT_HSV2_Treg
Lamtor4	6.50E-16	0.67723004	0.47	0.252	9.36E-12	VT_HSV2_Treg
Dusp10	7.39E-16	-0.90065386	0.311	0.56	1.06E-11	VT_HSV2_Treg
Scand1	8.21E-16	0.622229547	0.697	0.549	1.18E-11	VT_HSV2_Treg
Zbp1	2.42E-15	0.62265998	0.489	0.284	3.49E-11	VT_HSV2_Treg
Psme2	6.72E-15	0.530732174	0.814	0.743	9.68E-11	VT_HSV2_Treg
Txn1	6.86E-15	0.687555281	0.636	0.473	9.88E-11	VT_HSV2_Treg
Gimap5	7.25E-15	0.672058533	0.58	0.362	1.04E-10	VT_HSV2_Treg
Gm10263	9.31E-15	-0.541428688	0.227	0.435	1.34E-10	VT_HSV2_Treg

gene	p_val	avg_log2FC	pct.1	pct.2	p_val_adj	cluster
Vamp8	1.12E-14	0.567633202	0.61	0.457	1.61E-10	VT_HSV2_Treg
Prr13	1.65E-14	0.622155722	0.674	0.507	2.38E-10	VT_HSV2_Treg
Ifi47	5.25E-14	0.604747157	0.591	0.367	7.57E-10	VT_HSV2_Treg
Tigit	5.56E-14	0.750540167	0.572	0.388	8.01E-10	VT_HSV2_Treg
Junb	6.62E-14	-0.561740821	0.89	0.965	9.54E-10	VT_HSV2_Treg
Pycard	8.03E-14	0.785124596	0.508	0.34	1.16E-09	VT_HSV2_Treg
Arl5a	8.24E-14	0.592990772	0.428	0.215	1.19E-09	VT_HSV2_Treg
Ppp1ca	1.50E-13	0.504237732	0.731	0.673	2.17E-09	VT_HSV2_Treg
Atox1	3.38E-13	0.584591341	0.629	0.465	4.87E-09	VT_HSV2_Treg
Hspe1	3.58E-13	-0.512767889	0.561	0.733	5.16E-09	VT_HSV2_Treg
Ephx1	4.73E-13	-0.624910041	0.121	0.324	6.81E-09	VT_HSV2_Treg
Cd83	5.09E-13	-0.988253193	0.11	0.303	7.33E-09	VT_HSV2_Treg
Srsf7	5.22E-13	-0.547245047	0.485	0.669	7.51E-09	VT_HSV2_Treg
Rtp4	6.36E-13	0.54317102	0.383	0.18	9.16E-09	VT_HSV2_Treg
Gm9493	6.65E-13	-0.520196227	0.659	0.777	9.58E-09	VT_HSV2_Treg
Ctsa	7.90E-13	0.522050945	0.466	0.288	1.14E-08	VT_HSV2_Treg
Nr4a3	9.12E-13	-0.853658662	0.311	0.503	1.31E-08	VT_HSV2_Treg
Hint1	9.67E-13	0.505389885	0.788	0.744	1.39E-08	VT_HSV2_Treg
Ctsd	1.23E-12	0.509551728	0.477	0.313	1.78E-08	VT_HSV2_Treg
mt-Nd4	1.60E-12	-0.515208563	0.701	0.831	2.30E-08	VT_HSV2_Treg
Mfsd10	1.65E-12	0.53873435	0.311	0.136	2.37E-08	VT_HSV2_Treg
Ifrd1	1.67E-12	-0.697255019	0.549	0.701	2.40E-08	VT_HSV2_Treg
Prkca	1.92E-12	-0.789224045	0.394	0.582	2.76E-08	VT_HSV2_Treg
Eprs	2.04E-12	-0.861647458	0.201	0.394	2.94E-08	VT_HSV2_Treg
Arpc5	2.06E-12	0.51110178	0.644	0.566	2.97E-08	VT_HSV2_Treg
Ndufb7	2.19E-12	0.567145032	0.606	0.484	3.15E-08	VT_HSV2_Treg
Sdcbp2	2.88E-12	0.574611919	0.371	0.179	4.15E-08	VT_HSV2_Treg
Gna15	4.14E-12	0.548030737	0.314	0.142	5.96E-08	VT_HSV2_Treg
Igtp	4.30E-12	0.658669394	0.572	0.387	6.20E-08	VT_HSV2_Treg
Krtcap2	4.70E-12	0.545022185	0.686	0.56	6.78E-08	VT_HSV2_Treg
Tmem234	5.41E-12	0.542801316	0.625	0.479	7.79E-08	VT_HSV2_Treg
Gm9843	9.19E-12	-0.539397717	0.705	0.809	1.32E-07	VT_HSV2_Treg
Inpp4b	9.29E-12	-0.573319551	0.364	0.573	1.34E-07	VT_HSV2_Treg
Slfn2	1.13E-11	0.538438219	0.617	0.48	1.63E-07	VT_HSV2_Treg
mt-Nd5	1.18E-11	-0.516914047	0.617	0.769	1.71E-07	VT_HSV2_Treg
Grap	3.52E-11	0.633980874	0.534	0.371	5.07E-07	VT_HSV2_Treg
Rilpl2	3.94E-11	0.747537405	0.515	0.382	5.68E-07	VT_HSV2_Treg
Dnajc15	4.99E-11	0.695010599	0.424	0.247	7.19E-07	VT_HSV2_Treg

gene	p_val	avg_log2FC	pct.1	pct.2	p_val_adj	cluster
Rel	6.93E-11	-0.662333594	0.337	0.51	9.99E-07	VT_HSV2_Treg
Nr4a2	8.69E-11	-0.893899109	0.174	0.357	1.25E-06	VT_HSV2_Treg
Nfkbia	1.27E-10	0.587271055	0.841	0.829	1.83E-06	VT_HSV2_Treg
Ddit4	1.43E-10	0.677152784	0.409	0.254	2.06E-06	VT_HSV2_Treg
Plp2	1.47E-10	0.607577971	0.485	0.339	2.12E-06	VT_HSV2_Treg
Dnajb1	1.57E-10	-0.68021254	0.447	0.602	2.26E-06	VT_HSV2_Treg
Il21r	1.99E-10	-0.711424164	0.352	0.486	2.87E-06	VT_HSV2_Treg
Rgs10	2.18E-10	-0.572449046	0.58	0.741	3.14E-06	VT_HSV2_Treg
Icos	2.59E-10	0.525443955	0.686	0.589	3.74E-06	VT_HSV2_Treg
Dctpp1	3.59E-10	0.541071557	0.28	0.123	5.18E-06	VT_HSV2_Treg
mt-Nd3	3.88E-10	-0.513001748	0.614	0.752	5.59E-06	VT_HSV2_Treg
Batf	4.40E-10	0.627999009	0.538	0.351	6.34E-06	VT_HSV2_Treg
Tmem64	4.66E-10	-0.625358715	0.223	0.404	6.72E-06	VT_HSV2_Treg
Tnfrsf9	5.83E-10	0.821842837	0.61	0.462	8.39E-06	VT_HSV2_Treg
Evl	1.00E-09	-0.56119851	0.129	0.299	1.44E-05	VT_HSV2_Treg
Gpr132	1.01E-09	-0.62014694	0.371	0.52	1.45E-05	VT_HSV2_Treg
Pigx	1.08E-09	0.564867448	0.473	0.293	1.56E-05	VT_HSV2_Treg
Dusp1	1.13E-09	-0.68024868	0.587	0.762	1.63E-05	VT_HSV2_Treg
Gpr183	1.43E-09	0.67346948	0.322	0.178	2.06E-05	VT_HSV2_Treg
Psmb9	1.48E-09	0.504206806	0.595	0.501	2.13E-05	VT_HSV2_Treg
Ctsb	1.85E-09	0.585863554	0.572	0.458	2.66E-05	VT_HSV2_Treg
Hmgb2	1.92E-09	0.705242404	0.712	0.56	2.77E-05	VT_HSV2_Treg
1810058I24Rik	2.04E-09	0.538821085	0.473	0.301	2.93E-05	VT_HSV2_Treg
Cd48	2.42E-09	0.516127515	0.545	0.409	3.48E-05	VT_HSV2_Treg
Tox	2.48E-09	-0.53968879	0.201	0.372	3.58E-05	VT_HSV2_Treg
Id2	4.29E-09	0.565464962	0.383	0.21	6.18E-05	VT_HSV2_Treg
Dgat1	4.94E-09	0.584498539	0.447	0.292	7.12E-05	VT_HSV2_Treg
Ptp4a1	7.73E-09	-0.530474056	0.212	0.367	0.00011131	VT_HSV2_Treg
Pim3	8.85E-09	-0.576519597	0.17	0.325	0.00012741	VT_HSV2_Treg
Ostf1	9.67E-09	0.549860516	0.508	0.359	0.00013936	VT_HSV2_Treg
Tnfrsf4	1.10E-08	0.645138254	0.811	0.821	0.00015913	VT_HSV2_Treg
Gm5424	1.29E-08	0.537019613	0.428	0.295	0.00018513	VT_HSV2_Treg
Calm2	1.74E-08	-0.510170322	0.67	0.793	0.0002502	VT_HSV2_Treg
Tcp11l2	2.54E-08	-0.602578529	0.223	0.381	0.00036613	VT_HSV2_Treg
Rgcc	3.06E-08	-0.758260227	0.227	0.392	0.00044007	VT_HSV2_Treg
Ndufb9	3.52E-08	0.512564832	0.606	0.444	0.00050686	VT_HSV2_Treg
Fam110a	1.20E-07	0.591071915	0.394	0.235	0.00172897	VT_HSV2_Treg
Mrpl57	1.29E-07	0.562206715	0.333	0.21	0.00185154	VT_HSV2_Treg

gene	p_val	avg_log2FC	pct.1	pct.2	p_val_adj	cluster
Hist1h2ap	1.30E-07	-0.835554	0.152	0.267	0.00186986	VT_HSV2_Treg
Foxp1	4.12E-07	-0.521482138	0.292	0.433	0.0059301	VT_HSV2_Treg
Crem	7.38E-07	-0.73721665	0.564	0.647	0.01062386	VT_HSV2_Treg
Tsc22d3	1.73E-06	-0.532094843	0.47	0.621	0.02487433	VT_HSV2_Treg
Dut	2.04E-06	0.753445102	0.299	0.22	0.02932747	VT_HSV2_Treg
Ctsz	2.09E-06	0.511250626	0.345	0.224	0.03009681	VT_HSV2_Treg
Pja1	2.21E-06	-0.525704729	0.159	0.29	0.03177574	VT_HSV2_Treg
Spty2d1	3.69E-06	-0.64076766	0.231	0.341	0.05309321	VT_HSV2_Treg
Chd2	4.55E-06	-0.529456601	0.303	0.393	0.06548286	VT_HSV2_Treg
Nrp1	4.99E-06	-0.526853506	0.163	0.289	0.07183938	VT_HSV2_Treg
Zfp36	5.58E-06	0.678311056	0.64	0.608	0.08041373	VT_HSV2_Treg
Klf2	6.56E-06	-0.534640356	0.379	0.507	0.09448395	VT_HSV2_Treg
Neurl3	2.03E-05	-0.513102256	0.227	0.354	0.29170901	VT_HSV2_Treg
Areg	3.03E-05	0.828945086	0.254	0.26	0.43599407	VT_HSV2_Treg
Cstb	6.39E-05	-0.745442875	0.383	0.407	0.920601	VT_HSV2_Treg
Mif	6.66E-05	0.559550752	0.754	0.707	0.95912067	VT_HSV2_Treg
Sap18	0.00016371	-0.652819582	0.708	0.788	1	VT_HSV2_Treg
Cebpb	0.00050459	-0.510269836	0.33	0.415	1	VT_HSV2_Treg
Cdk11b	0.00054474	-0.548095872	0.273	0.365	1	VT_HSV2_Treg
mt-Co2	1.65E-205	0.620712077	1	0.992	2.38E-201	LN_uninfected_Treg
Ly6a	1.91E-200	-2.152693307	0.217	0.685	2.76E-196	LN_uninfected_Treg
mt-Atp8	5.02E-197	0.642715961	0.998	0.986	7.24E-193	LN_uninfected_Treg
Rsrp1	1.52E-189	1.357650403	0.804	0.49	2.19E-185	LN_uninfected_Treg
mt-Cytb	3.06E-151	0.680211134	0.998	0.978	4.40E-147	LN_uninfected_Treg
Gimap7	5.36E-128	-1.219060352	0.165	0.539	7.72E-124	LN_uninfected_Treg
mt-Co3	3.40E-114	0.556154743	0.994	0.983	4.90E-110	LN_uninfected_Treg
Gimap4	2.25E-112	-1.048111974	0.331	0.667	3.24E-108	LN_uninfected_Treg
Ly6e	1.70E-101	-0.609428039	0.969	0.981	2.45E-97	LN_uninfected_Treg
Gimap6	1.61E-99	-0.635103696	0.643	0.896	2.33E-95	LN_uninfected_Treg
mt-Nd4l	7.51E-96	0.575288339	0.993	0.959	1.08E-91	LN_uninfected_Treg
Nr4a3	5.39E-92	1.104429263	0.621	0.338	7.76E-88	LN_uninfected_Treg
Ifngr1	1.12E-90	-0.796695754	0.69	0.85	1.61E-86	LN_uninfected_Treg
Gimap3	1.36E-86	-0.673111532	0.657	0.857	1.96E-82	LN_uninfected_Treg
H3f3b	7.63E-85	0.536370632	0.997	0.975	1.10E-80	LN_uninfected_Treg
Samhd1	7.66E-85	-0.778870359	0.658	0.847	1.10E-80	LN_uninfected_Treg
Dnaja1	3.70E-82	0.794674281	0.927	0.815	5.33E-78	LN_uninfected_Treg
Ifi47	5.10E-78	-0.992485389	0.244	0.543	7.34E-74	LN_uninfected_Treg
Il7r	1.98E-77	-0.912614111	0.351	0.624	2.85E-73	LN_uninfected_Treg

gene	p_val	avg_log2FC	pct.1	pct.2	p_val_adj	cluster
Nr4a2	1.34E-76	1.118446024	0.462	0.207	1.94E-72	LN_uninfected_Treg
Gbp2	1.00E-73	-1.22345126	0.131	0.385	1.44E-69	LN_uninfected_Treg
Igtp	9.26E-73	-0.894835903	0.265	0.557	1.33E-68	LN_uninfected_Treg
Rel	1.66E-72	0.994970382	0.586	0.396	2.39E-68	LN_uninfected_Treg
mt-Nd2	2.71E-72	0.600361948	0.951	0.88	3.90E-68	LN_uninfected_Treg
Rgcc	2.56E-70	0.995001075	0.498	0.244	3.69E-66	LN_uninfected_Treg
Junb	1.04E-66	0.581631392	0.987	0.929	1.50E-62	LN_uninfected_Treg
Selplg	1.95E-66	-0.729876098	0.578	0.799	2.81E-62	LN_uninfected_Treg
mt-Nd4	6.56E-66	0.60186603	0.876	0.758	9.44E-62	LN_uninfected_Treg
mt-Nd1	9.42E-66	0.510057541	0.932	0.857	1.36E-61	LN_uninfected_Treg
mt-Nd3	3.43E-65	0.647027739	0.805	0.669	4.95E-61	LN_uninfected_Treg
Ms4a6b	2.90E-63	-0.682468594	0.591	0.793	4.17E-59	LN_uninfected_Treg
Rheb	5.03E-62	0.759192561	0.574	0.4	7.24E-58	LN_uninfected_Treg
Clk1	1.18E-61	0.715714754	0.646	0.452	1.70E-57	LN_uninfected_Treg
H2afz	3.52E-61	0.606458141	0.953	0.911	5.07E-57	LN_uninfected_Treg
Ly6c1	7.74E-59	-1.193043554	0.112	0.307	1.11E-54	LN_uninfected_Treg
Rtp4	8.96E-59	-0.656094769	0.091	0.314	1.29E-54	LN_uninfected_Treg
Spty2d1	3.84E-58	0.922401074	0.428	0.224	5.53E-54	LN_uninfected_Treg
Gimap5	1.38E-56	-0.753004837	0.254	0.52	1.99E-52	LN_uninfected_Treg
Zfp36l1	1.71E-55	0.690819046	0.814	0.654	2.47E-51	LN_uninfected_Treg
Acp5	7.60E-55	-0.698610146	0.196	0.443	1.09E-50	LN_uninfected_Treg
Cd83	1.88E-53	1.091800656	0.382	0.182	2.71E-49	LN_uninfected_Treg
Crem	4.67E-53	0.89926201	0.714	0.557	6.72E-49	LN_uninfected_Treg
Amd1	1.04E-52	0.708791159	0.551	0.38	1.50E-48	LN_uninfected_Treg
Gpr18	1.31E-52	-0.63001937	0.101	0.318	1.89E-48	LN_uninfected_Treg
mt-Nd5	6.28E-52	0.538249013	0.805	0.704	9.05E-48	LN_uninfected_Treg
Tgif1	1.30E-50	0.699780334	0.697	0.518	1.87E-46	LN_uninfected_Treg
Fth1	2.74E-50	0.590773977	0.994	0.983	3.95E-46	LN_uninfected_Treg
Npc2	2.06E-49	-0.58229288	0.717	0.844	2.96E-45	LN_uninfected_Treg
Ecm1	2.67E-49	-0.979858686	0.288	0.496	3.84E-45	LN_uninfected_Treg
Cd74	1.26E-46	0.61239536	0.404	0.231	1.82E-42	LN_uninfected_Treg
Gpr183	2.28E-46	-0.592490273	0.093	0.298	3.29E-42	LN_uninfected_Treg
Ms4a4b	1.32E-45	-0.644491928	0.634	0.794	1.91E-41	LN_uninfected_Treg
H2-T22	2.37E-45	-0.527406343	0.632	0.795	3.41E-41	LN_uninfected_Treg
Irf7	1.76E-44	-0.627500282	0.211	0.43	2.53E-40	LN_uninfected_Treg
Sap18	6.26E-44	0.796507227	0.814	0.745	9.02E-40	LN_uninfected_Treg
Satb1	1.48E-43	-0.582057706	0.243	0.481	2.13E-39	LN_uninfected_Treg
Pim3	3.48E-43	0.732862941	0.39	0.227	5.02E-39	LN_uninfected_Treg

gene	p_val	avg_log2FC	pct.1	pct.2	p_val_adj	cluster
Zbp1	1.95E-42	-0.630106895	0.198	0.415	2.80E-38	LN_uninfected_Treg
Ninj1	5.12E-42	0.647804923	0.363	0.215	7.38E-38	LN_uninfected_Treg
Dynll1	1.20E-41	0.504658034	0.797	0.685	1.72E-37	LN_uninfected_Treg
Slc25a3	2.06E-41	0.521235581	0.911	0.876	2.96E-37	LN_uninfected_Treg
Serinc3	2.43E-40	-0.596307345	0.481	0.674	3.49E-36	LN_uninfected_Treg
Nrp1	5.98E-40	0.649939829	0.361	0.187	8.61E-36	LN_uninfected_Treg
Gbp7	7.79E-40	-0.505643966	0.148	0.358	1.12E-35	LN_uninfected_Treg
Itgb1	4.04E-39	0.660265261	0.373	0.226	5.82E-35	LN_uninfected_Treg
Klf4	8.68E-39	0.783262159	0.291	0.123	1.25E-34	LN_uninfected_Treg
Ifrd1	3.78E-38	0.654061864	0.745	0.626	5.44E-34	LN_uninfected_Treg
Nr4a1	5.15E-38	0.545415599	0.65	0.468	7.41E-34	LN_uninfected_Treg
Rgs10	1.40E-37	0.551465278	0.772	0.68	2.01E-33	LN_uninfected_Treg
Tgfb1	2.43E-36	0.523271721	0.588	0.468	3.49E-32	LN_uninfected_Treg
Gmfg	3.70E-36	-0.635028234	0.451	0.663	5.33E-32	LN_uninfected_Treg
Apobec3	1.33E-34	-0.547021099	0.277	0.496	1.91E-30	LN_uninfected_Treg
Hopx	1.86E-34	0.700844968	0.619	0.539	2.68E-30	LN_uninfected_Treg
Mxd4	4.10E-34	0.555643609	0.4	0.276	5.91E-30	LN_uninfected_Treg
Slfn2	4.08E-33	-0.579221093	0.397	0.596	5.87E-29	LN_uninfected_Treg
Tob2	8.28E-33	0.598862722	0.437	0.292	1.19E-28	LN_uninfected_Treg
Eprs	9.67E-33	0.767449263	0.438	0.314	1.39E-28	LN_uninfected_Treg
Ahnak	1.49E-32	0.508999881	0.386	0.229	2.14E-28	LN_uninfected_Treg
Mrps6	2.40E-32	0.557793184	0.444	0.362	3.46E-28	LN_uninfected_Treg
Mxd1	2.47E-32	-0.558128091	0.302	0.489	3.56E-28	LN_uninfected_Treg
Phlda1	1.76E-31	0.589950017	0.43	0.274	2.54E-27	LN_uninfected_Treg
Tox	1.93E-31	0.552613561	0.427	0.282	2.78E-27	LN_uninfected_Treg
Ikzf2	3.49E-31	0.532228889	0.675	0.589	5.03E-27	LN_uninfected_Treg
Smarca5	1.13E-30	0.507522657	0.459	0.355	1.62E-26	LN_uninfected_Treg
Jun	1.24E-30	-0.652611766	0.294	0.466	1.79E-26	LN_uninfected_Treg
Skil	2.00E-30	0.540069709	0.367	0.21	2.88E-26	LN_uninfected_Treg
Ccs	3.07E-30	-0.527317839	0.282	0.467	4.42E-26	LN_uninfected_Treg
Cstb	6.75E-30	0.951330491	0.452	0.352	9.72E-26	LN_uninfected_Treg
Txnip	6.85E-30	-0.612534563	0.23	0.388	9.87E-26	LN_uninfected_Treg
Tbc1d4	1.10E-29	0.610134079	0.295	0.151	1.59E-25	LN_uninfected_Treg
Ythdc1	1.30E-29	0.519265712	0.528	0.42	1.87E-25	LN_uninfected_Treg
Lrig1	2.21E-28	0.524180313	0.374	0.218	3.19E-24	LN_uninfected_Treg
Odc1	1.07E-27	0.512443383	0.597	0.46	1.54E-23	LN_uninfected_Treg
Isg20	3.15E-26	-0.525643064	0.17	0.345	4.53E-22	LN_uninfected_Treg
Rora	3.82E-26	0.530745147	0.395	0.285	5.50E-22	LN_uninfected_Treg

gene	p_val	avg_log2FC	pct.1	pct.2	p_val_adj	cluster
Dusp1	1.01E-23	0.57441941	0.791	0.701	1.45E-19	LN_uninfected_Treg
Bcl2a1b	2.65E-23	0.591383961	0.466	0.379	3.82E-19	LN_uninfected_Treg
Cdk11b	5.26E-21	0.618767068	0.409	0.299	7.58E-17	LN_uninfected_Treg
Bcl2a1d	8.83E-20	0.535563694	0.254	0.174	1.27E-15	LN_uninfected_Treg
Cwc25	3.08E-18	0.536720892	0.304	0.2	4.43E-14	LN_uninfected_Treg
Hist1h2ap	6.17E-16	0.521466757	0.288	0.224	8.89E-12	LN_uninfected_Treg
Hilpda	4.68E-14	-0.538254146	0.177	0.286	6.74E-10	LN_uninfected_Treg
S100a6	8.05E-06	-0.768245724	0.272	0.336	0.11593066	LN_uninfected_Treg
mt-Co2	1.31E-155	-0.578312713	0.994	0.998	1.89E-151	LN_HSV2_Treg
Rsrp1	9.42E-132	-1.208653113	0.503	0.758	1.36E-127	LN_HSV2_Treg
Ly6a	6.57E-100	1.035824334	0.665	0.287	9.47E-96	LN_HSV2_Treg
mt-Cytb	1.17E-89	-0.574304925	0.983	0.992	1.68E-85	LN_HSV2_Treg
Gimap6	3.35E-84	0.584621699	0.909	0.666	4.83E-80	LN_HSV2_Treg
Gimap3	2.95E-77	0.653596594	0.87	0.672	4.25E-73	LN_HSV2_Treg
H3f3b	1.01E-74	-0.515294252	0.979	0.992	1.45E-70	LN_HSV2_Treg
Ifngr1	1.14E-73	0.757481841	0.862	0.702	1.64E-69	LN_HSV2_Treg
Samhd1	5.92E-69	0.718719141	0.861	0.672	8.53E-65	LN_HSV2_Treg
Gimap7	8.56E-69	0.802883301	0.525	0.219	1.23E-64	LN_HSV2_Treg
Nr4a3	1.42E-64	-0.981361753	0.343	0.584	2.05E-60	LN_HSV2_Treg
Ly6c1	3.51E-62	1.18346905	0.332	0.119	5.06E-58	LN_HSV2_Treg
Il7r	9.81E-62	0.771463654	0.641	0.373	1.41E-57	LN_HSV2_Treg
Gimap4	3.95E-60	0.724250926	0.66	0.376	5.69E-56	LN_HSV2_Treg
Gbp2	1.46E-54	1.093546028	0.386	0.161	2.11E-50	LN_HSV2_Treg
Gm9843	2.24E-54	0.502045821	0.891	0.744	3.22E-50	LN_HSV2_Treg
Nr4a2	6.28E-54	-0.988245617	0.213	0.427	9.04E-50	LN_HSV2_Treg
Rgcc	3.30E-51	-0.881527264	0.247	0.465	4.75E-47	LN_HSV2_Treg
Rel	1.64E-50	-0.903492122	0.407	0.556	2.36E-46	LN_HSV2_Treg
Rheb	6.97E-50	-0.70692743	0.397	0.555	1.00E-45	LN_HSV2_Treg
Dnaja1	7.55E-50	-0.676714345	0.832	0.903	1.09E-45	LN_HSV2_Treg
Gm9493	1.69E-49	0.54524028	0.859	0.71	2.44E-45	LN_HSV2_Treg
Gpr18	1.93E-47	0.617328143	0.332	0.119	2.78E-43	LN_HSV2_Treg
Capg	9.54E-47	-0.61399301	0.477	0.623	1.37E-42	LN_HSV2_Treg
Ifi47	2.02E-46	0.786422247	0.535	0.286	2.91E-42	LN_HSV2_Treg
Igtp	5.66E-46	0.673916499	0.554	0.302	8.16E-42	LN_HSV2_Treg
Clk1	8.53E-46	-0.65626018	0.457	0.62	1.23E-41	LN_HSV2_Treg
BC021614	9.29E-46	-0.585461076	0.212	0.374	1.34E-41	LN_HSV2_Treg
Ahnak	1.11E-44	-0.683263277	0.2	0.386	1.60E-40	LN_HSV2_Treg
Spty2d1	4.02E-44	-0.828302444	0.223	0.404	5.79E-40	LN_HSV2_Treg

gene	p_val	avg_log2FC	pct.1	pct.2	p_val_adj	cluster
mt-Nd3	4.82E-44	-0.55716579	0.679	0.782	6.94E-40	LN_HSV2_Treg
Satb1	4.30E-43	0.584105042	0.501	0.258	6.20E-39	LN_HSV2_Treg
Fth1	6.35E-43	-0.558025997	0.989	0.989	9.15E-39	LN_HSV2_Treg
Ecm1	2.27E-42	0.879867602	0.511	0.303	3.27E-38	LN_HSV2_Treg
H2afz	5.34E-42	-0.538457071	0.917	0.944	7.70E-38	LN_HSV2_Treg
mt-Nd4	1.02E-41	-0.507830623	0.769	0.855	1.47E-37	LN_HSV2_Treg
Ms4a6b	2.94E-41	0.559798298	0.792	0.616	4.23E-37	LN_HSV2_Treg
Tgif1	7.75E-41	-0.647751932	0.516	0.676	1.12E-36	LN_HSV2_Treg
Crem	2.75E-38	-0.781113837	0.556	0.696	3.96E-34	LN_HSV2_Treg
Acp5	4.23E-38	0.603846896	0.443	0.225	6.09E-34	LN_HSV2_Treg
Zfp36l1	1.26E-37	-0.618922456	0.668	0.786	1.82E-33	LN_HSV2_Treg
Jun	2.65E-37	0.708216666	0.493	0.297	3.82E-33	LN_HSV2_Treg
Irf7	3.74E-37	0.573801165	0.441	0.23	5.39E-33	LN_HSV2_Treg
Dynll1	4.00E-37	-0.506076931	0.683	0.785	5.76E-33	LN_HSV2_Treg
Flna	2.49E-36	-0.518758874	0.219	0.356	3.58E-32	LN_HSV2_Treg
S100a11	4.41E-36	-0.588379638	0.364	0.516	6.35E-32	LN_HSV2_Treg
Phlda1	1.15E-35	-0.640919551	0.254	0.424	1.66E-31	LN_HSV2_Treg
Selplg	1.02E-34	0.52122624	0.799	0.605	1.46E-30	LN_HSV2_Treg
Cd83	2.03E-33	-0.939835599	0.195	0.349	2.93E-29	LN_HSV2_Treg
Sap18	3.62E-33	-0.687588763	0.752	0.801	5.21E-29	LN_HSV2_Treg
Ms4a4b	3.88E-33	0.528270536	0.811	0.642	5.60E-29	LN_HSV2_Treg
Nr4a1	6.70E-33	-0.578829546	0.465	0.63	9.65E-29	LN_HSV2_Treg
Il2rb	1.47E-32	0.534941529	0.742	0.593	2.11E-28	LN_HSV2_Treg
Tgfb1	1.68E-32	-0.53420403	0.463	0.577	2.41E-28	LN_HSV2_Treg
Txnip	1.49E-31	0.675043736	0.4	0.241	2.14E-27	LN_HSV2_Treg
Itgb1	4.67E-31	-0.605114955	0.222	0.358	6.73E-27	LN_HSV2_Treg
Odc1	9.27E-31	-0.573753889	0.444	0.591	1.34E-26	LN_HSV2_Treg
Gimap5	1.75E-30	0.533229926	0.508	0.293	2.53E-26	LN_HSV2_Treg
Ninj1	2.37E-30	-0.570993168	0.22	0.343	3.41E-26	LN_HSV2_Treg
Socs3	3.27E-29	0.524036643	0.477	0.288	4.70E-25	LN_HSV2_Treg
Serinc3	3.85E-29	0.520052555	0.679	0.501	5.55E-25	LN_HSV2_Treg
Amd1	5.18E-29	-0.547780647	0.411	0.51	7.46E-25	LN_HSV2_Treg
Ikzf2	1.10E-28	-0.525928272	0.585	0.667	1.59E-24	LN_HSV2_Treg
Pim3	1.91E-28	-0.635602031	0.238	0.363	2.75E-24	LN_HSV2_Treg
Nrp1	2.71E-28	-0.557088299	0.191	0.337	3.91E-24	LN_HSV2_Treg
Cd74	6.07E-28	-0.670777678	0.247	0.373	8.74E-24	LN_HSV2_Treg
Klf2	6.15E-27	0.554062676	0.605	0.429	8.86E-23	LN_HSV2_Treg
Crip1	1.28E-26	-0.541010827	0.718	0.765	1.85E-22	LN_HSV2_Treg

gene	p_val	avg_log2FC	pct.1	pct.2	p_val_adj	cluster
Ccs	2.13E-26	0.503979066	0.471	0.302	3.07E-22	LN_HSV2_Treg
Gem	2.02E-25	-0.569751388	0.191	0.326	2.90E-21	LN_HSV2_Treg
Bcl2a1b	2.93E-25	-0.639332288	0.364	0.465	4.22E-21	LN_HSV2_Treg
Hopx	5.84E-25	-0.632402657	0.542	0.608	8.41E-21	LN_HSV2_Treg
Mxd1	1.29E-24	0.500262318	0.493	0.322	1.87E-20	LN_HSV2_Treg
Mrps6	1.54E-24	-0.511171993	0.364	0.433	2.22E-20	LN_HSV2_Treg
Klf4	4.20E-24	-0.617637518	0.132	0.266	6.05E-20	LN_HSV2_Treg
Rora	3.60E-23	-0.521511372	0.276	0.387	5.18E-19	LN_HSV2_Treg
Cstb	3.94E-22	-0.8363459	0.346	0.443	5.67E-18	LN_HSV2_Treg
Tob2	1.80E-21	-0.515371498	0.302	0.413	2.60E-17	LN_HSV2_Treg
S100a4	2.11E-21	-0.608927899	0.153	0.25	3.04E-17	LN_HSV2_Treg
Sertad1	1.17E-20	-0.503233572	0.362	0.485	1.69E-16	LN_HSV2_Treg
Ifrd1	1.57E-20	-0.524143309	0.641	0.721	2.26E-16	LN_HSV2_Treg
Areg	2.83E-20	-0.597528511	0.185	0.308	4.08E-16	LN_HSV2_Treg
Eprs	2.60E-18	-0.613058104	0.335	0.41	3.75E-14	LN_HSV2_Treg
Cdk11b	3.51E-14	-0.518529328	0.304	0.393	5.05E-10	LN_HSV2_Treg

APPENDIX C

Table C.1. Differentially expressed genes in vaginal Tregs compared to vaginal CD4 Tconv.

List of DEG in vaginal Treg and CD4 Tconv populations in HSV-2-infected and uninfected mice. DEG were determined by log2FC >.5 and FDR <.01.

gene	p_val	avg_log2FC	pct.1	pct.2	p_val_adj	cluster
Eef2	1.10E-299	1.172481975	0.986	0.905	1.58E-295	VT_HSV2_CD4
mt-Atp6	3.73E-163	-0.97803199	0.993	0.984	5.37E-159	VT_HSV2_CD4
Gnai2	7.24E-120	-0.724846453	0.813	0.804	1.04E-115	VT_HSV2_CD4
Gnb1	1.12E-109	-0.849222231	0.411	0.519	1.62E-105	VT_HSV2_CD4
Ikzf2	2.88E-103	-1.329575845	0.152	0.341	4.15E-99	VT_HSV2_CD4
Aes	2.07E-97	-0.688257545	0.712	0.723	2.98E-93	VT_HSV2_CD4
Pabpc1	1.56E-93	0.694705452	0.976	0.859	2.24E-89	VT_HSV2_CD4
Rps27rt	1.88E-83	-0.994471101	0.558	0.663	2.71E-79	VT_HSV2_CD4
Grb2	3.29E-72	-0.691513751	0.394	0.473	4.73E-68	VT_HSV2_CD4
Hspa8	9.04E-71	0.594123961	0.991	0.96	1.30E-66	VT_HSV2_CD4
Capg	1.31E-69	-0.954301906	0.483	0.471	1.89E-65	VT_HSV2_CD4
Ppp2ca	4.41E-65	-0.600863354	0.448	0.489	6.35E-61	VT_HSV2_CD4
Arl5a	6.35E-62	-0.65142278	0.141	0.253	9.15E-58	VT_HSV2_CD4
Ifitm3	9.80E-61	2.562300315	0.616	0.121	1.41E-56	VT_HSV2_CD4
Il2ra	2.83E-58	-0.885994743	0.271	0.329	4.08E-54	VT_HSV2_CD4
Ifitm2	4.40E-57	2.693931308	0.588	0.097	6.34E-53	VT_HSV2_CD4
Ube2s	6.04E-52	-0.730207224	0.547	0.616	8.70E-48	VT_HSV2_CD4
Alyref	3.66E-50	-0.500883927	0.227	0.271	5.27E-46	VT_HSV2_CD4
Laptm5	4.36E-50	0.79270558	0.965	0.848	6.29E-46	VT_HSV2_CD4
Gramd3	8.11E-50	0.72519226	0.701	0.244	1.17E-45	VT_HSV2_CD4
Tnfrsf9	4.40E-49	-1.051255197	0.375	0.339	6.34E-45	VT_HSV2_CD4
Ass1	1.63E-48	-0.713278554	0.395	0.444	2.35E-44	VT_HSV2_CD4
Taf10	1.66E-47	-0.502001697	0.406	0.43	2.40E-43	VT_HSV2_CD4
Rps26-ps1	5.92E-47	-0.571936138	0.412	0.438	8.53E-43	VT_HSV2_CD4
Ifitm1	1.07E-45	2.626230365	0.365	0.022	1.54E-41	VT_HSV2_CD4
Ctla4	1.79E-45	-0.692148557	0.784	0.552	2.58E-41	VT_HSV2_CD4
Gimap7	2.02E-42	-0.580340742	0.473	0.402	2.91E-38	VT_HSV2_CD4
Gm5424	1.20E-41	-0.588890631	0.282	0.329	1.73E-37	VT_HSV2_CD4
Ptma	2.14E-41	-0.506001133	0.987	0.992	3.08E-37	VT_HSV2_CD4
Arid5a	2.77E-41	0.739108366	0.755	0.358	3.99E-37	VT_HSV2_CD4
Gzmb	8.41E-41	-1.113011217	0.411	0.259	1.21E-36	VT_HSV2_CD4

gene	p_val	avg_log2FC	pct.1	pct.2	p_val_adj	cluster
Malat1	2.46E-40	-0.965748233	0.988	0.945	3.55E-36	VT_HSV2_CD4
Gpx1	1.29E-39	-0.667099616	0.691	0.651	1.86E-35	VT_HSV2_CD4
Tnfrsf18	1.39E-37	-0.53376321	0.755	0.547	2.00E-33	VT_HSV2_CD4
Zfp36l2	6.97E-36	0.695314201	0.854	0.545	1.00E-31	VT_HSV2_CD4
Lax1	8.37E-36	0.716298957	0.5	0.111	1.21E-31	VT_HSV2_CD4
Izumo1r	1.73E-35	-1.045268044	0.272	0.426	2.49E-31	VT_HSV2_CD4
H2afz	3.90E-35	-0.523083783	0.893	0.836	5.62E-31	VT_HSV2_CD4
Lck	8.38E-35	0.68213684	0.935	0.745	1.21E-30	VT_HSV2_CD4
Plac8	1.52E-34	1.961601184	0.477	0.107	2.18E-30	VT_HSV2_CD4
Ctsw	7.74E-33	1.153542199	0.646	0.206	1.12E-28	VT_HSV2_CD4
Rnf19a	8.66E-33	0.561698615	0.461	0.123	1.25E-28	VT_HSV2_CD4
Slfn2	3.50E-32	0.812650543	0.913	0.616	5.05E-28	VT_HSV2_CD4
Ncor1	3.53E-32	-0.509745868	0.57	0.527	5.09E-28	VT_HSV2_CD4
Bhlhe40	7.23E-32	1.591402268	0.731	0.271	1.04E-27	VT_HSV2_CD4
Gramd1a	2.28E-31	0.587188274	0.592	0.194	3.29E-27	VT_HSV2_CD4
Cnbp	4.79E-31	-0.514648857	0.938	0.899	6.90E-27	VT_HSV2_CD4
Rasal3	4.89E-31	0.58365233	0.628	0.214	7.05E-27	VT_HSV2_CD4
Frmd8	6.57E-31	0.633808321	0.592	0.172	9.47E-27	VT_HSV2_CD4
Sema4a	8.28E-30	0.542013347	0.357	0.05	1.19E-25	VT_HSV2_CD4
AA467197	9.76E-30	0.75381059	0.313	0.022	1.41E-25	VT_HSV2_CD4
Lilr4b	2.96E-29	0.619202319	0.31	0.044	4.26E-25	VT_HSV2_CD4
Dusp2	7.31E-29	1.353681018	0.742	0.41	1.05E-24	VT_HSV2_CD4
Cxcr6	1.78E-28	1.088873715	0.614	0.18	2.57E-24	VT_HSV2_CD4
Klrc1	1.83E-27	0.670734675	0.259	0.018	2.64E-23	VT_HSV2_CD4
Arhgef1	4.89E-27	0.530052123	0.803	0.418	7.05E-23	VT_HSV2_CD4
B4galnt1	8.06E-27	0.893024075	0.783	0.345	1.16E-22	VT_HSV2_CD4
Serpinb9	3.51E-26	1.130295976	0.442	0.091	5.05E-22	VT_HSV2_CD4
Ppp3cc	5.68E-26	0.525641295	0.457	0.111	8.19E-22	VT_HSV2_CD4
Tspan13	3.79E-24	-0.545168697	0.462	0.455	5.46E-20	VT_HSV2_CD4
Rassf5	4.51E-24	0.539355138	0.576	0.186	6.49E-20	VT_HSV2_CD4
Emp1	9.12E-24	0.543667078	0.289	0.042	1.31E-19	VT_HSV2_CD4
Gapdh	1.14E-23	0.945023625	0.984	0.915	1.64E-19	VT_HSV2_CD4
Amd1	1.29E-23	-0.521225757	0.265	0.299	1.85E-19	VT_HSV2_CD4
Ikzf3	5.94E-23	-0.546742264	0.247	0.283	8.56E-19	VT_HSV2_CD4
Fam102a	1.16E-22	0.528416793	0.517	0.182	1.68E-18	VT_HSV2_CD4
Slfn1	2.16E-22	0.580622267	0.597	0.261	3.11E-18	VT_HSV2_CD4
Klhl6	4.26E-22	0.523539831	0.444	0.16	6.14E-18	VT_HSV2_CD4
Ube2v1	5.13E-22	0.617558269	0.494	0.121	7.39E-18	VT_HSV2_CD4

gene	p_val	avg_log2FC	pct.1	pct.2	p_val_adj	cluster
Il12rb2	6.45E-22	0.6110811	0.351	0.053	9.28E-18	VT_HSV2_CD4
Tnfrsf4	7.35E-22	-0.518599732	0.737	0.525	1.06E-17	VT_HSV2_CD4
mt-Nd2	1.85E-21	-0.576488779	0.906	0.855	2.67E-17	VT_HSV2_CD4
Smc4	3.14E-21	-0.564109771	0.403	0.412	4.52E-17	VT_HSV2_CD4
Ier5	5.15E-21	0.534897112	0.722	0.36	7.42E-17	VT_HSV2_CD4
Nkg7	6.46E-21	1.12013734	0.663	0.242	9.30E-17	VT_HSV2_CD4
Pdcd1	1.08E-20	1.088737057	0.525	0.16	1.55E-16	VT_HSV2_CD4
Lrp10	6.56E-20	0.634252281	0.684	0.261	9.45E-16	VT_HSV2_CD4
Litaf	7.89E-20	1.005116304	0.563	0.18	1.14E-15	VT_HSV2_CD4
Tap2	4.95E-19	0.628016999	0.726	0.319	7.14E-15	VT_HSV2_CD4
Efhd2	5.01E-19	0.838105993	0.625	0.198	7.21E-15	VT_HSV2_CD4
Anxa1	2.49E-18	0.539356734	0.304	0.053	3.59E-14	VT_HSV2_CD4
Rgs2	1.12E-17	-0.65876554	0.296	0.343	1.62E-13	VT_HSV2_CD4
Itgb1	1.51E-17	1.001855691	0.644	0.259	2.17E-13	VT_HSV2_CD4
Gpi1	1.79E-17	0.692377106	0.917	0.693	2.58E-13	VT_HSV2_CD4
Tap1	2.53E-17	0.583265898	0.721	0.345	3.64E-13	VT_HSV2_CD4
Itgal	9.23E-17	0.65675474	0.595	0.196	1.33E-12	VT_HSV2_CD4
Bcl2a1d	1.05E-16	1.004154198	0.674	0.234	1.51E-12	VT_HSV2_CD4
Zc3h12a	1.28E-16	0.664824246	0.548	0.202	1.84E-12	VT_HSV2_CD4
Zap70	1.70E-16	0.87749868	0.782	0.356	2.45E-12	VT_HSV2_CD4
Psap	1.77E-16	0.511857572	0.715	0.345	2.55E-12	VT_HSV2_CD4
Wipf1	7.05E-16	0.59360776	0.627	0.244	1.02E-11	VT_HSV2_CD4
Ppp1r15a	8.23E-16	-0.632580879	0.724	0.707	1.19E-11	VT_HSV2_CD4
Arhgap31	9.11E-16	-0.527122285	0.349	0.404	1.31E-11	VT_HSV2_CD4
Selplg	1.08E-15	0.718346983	0.913	0.703	1.56E-11	VT_HSV2_CD4
Ehd1	2.47E-15	0.739642605	0.523	0.156	3.55E-11	VT_HSV2_CD4
Lgals3	3.70E-15	1.134601918	0.539	0.196	5.33E-11	VT_HSV2_CD4
Grina	2.70E-14	0.518671885	0.575	0.228	3.89E-10	VT_HSV2_CD4
Gdi2	2.85E-14	0.829329153	0.844	0.509	4.11E-10	VT_HSV2_CD4
Nptn	3.78E-14	0.622434799	0.571	0.208	5.44E-10	VT_HSV2_CD4
Nfatc1	4.19E-14	0.521554128	0.499	0.174	6.03E-10	VT_HSV2_CD4
Itgb2	5.02E-14	0.735109043	0.757	0.345	7.23E-10	VT_HSV2_CD4
Surf4	8.44E-14	0.525820738	0.571	0.198	1.22E-09	VT_HSV2_CD4
Rps6ka1	1.01E-13	0.548138951	0.493	0.154	1.46E-09	VT_HSV2_CD4
Mapkapk3	1.59E-13	0.693319869	0.532	0.186	2.30E-09	VT_HSV2_CD4
Coro1a	3.55E-13	0.534923735	0.985	0.927	5.11E-09	VT_HSV2_CD4
Serpinb6b	7.00E-13	0.846881607	0.466	0.145	1.01E-08	VT_HSV2_CD4
Sh2d2a	7.75E-13	0.892504592	0.811	0.485	1.12E-08	VT_HSV2_CD4

gene	p_val	avg_log2FC	pct.1	pct.2	p_val_adj	cluster
Gna15	1.87E-12	0.5491263	0.533	0.204	2.69E-08	VT_HSV2_CD4
Furin	2.70E-12	0.542607505	0.354	0.099	3.89E-08	VT_HSV2_CD4
Def6	4.94E-12	0.56042362	0.641	0.275	7.11E-08	VT_HSV2_CD4
Pstpip1	6.56E-12	0.598346496	0.678	0.339	9.45E-08	VT_HSV2_CD4
Rgcc	9.80E-12	-0.575226549	0.443	0.392	1.41E-07	VT_HSV2_CD4
Cd4	1.46E-11	0.598074072	0.759	0.388	2.11E-07	VT_HSV2_CD4
Nfkbiz	2.25E-11	0.841998955	0.578	0.24	3.24E-07	VT_HSV2_CD4
Dusp5	2.98E-11	0.625443962	0.781	0.531	4.29E-07	VT_HSV2_CD4
Ostf1	4.34E-11	0.693515499	0.82	0.515	6.26E-07	VT_HSV2_CD4
Sell	6.04E-11	-0.536893073	0.144	0.317	8.70E-07	VT_HSV2_CD4
Cd52	9.12E-11	0.743966494	0.982	0.947	1.31E-06	VT_HSV2_CD4
Ly6c2	1.15E-10	0.908155378	0.275	0.077	1.66E-06	VT_HSV2_CD4
Icam1	1.95E-10	0.62178678	0.485	0.2	2.81E-06	VT_HSV2_CD4
Ctsa	5.79E-10	0.551585355	0.673	0.313	8.35E-06	VT_HSV2_CD4
Id2	7.04E-10	0.77448669	0.638	0.313	1.01E-05	VT_HSV2_CD4
Cd6	7.41E-10	0.628963041	0.67	0.372	1.07E-05	VT_HSV2_CD4
Capza1	9.53E-10	0.570679332	0.79	0.406	1.37E-05	VT_HSV2_CD4
Ifng	2.57E-09	0.651952298	0.303	0.091	3.71E-05	VT_HSV2_CD4
Tmbim6	2.70E-09	0.501137982	0.913	0.64	3.89E-05	VT_HSV2_CD4
Adgre5	3.04E-09	0.553856208	0.618	0.301	4.38E-05	VT_HSV2_CD4
Ctsd	1.05E-08	0.855329684	0.748	0.39	0.00015139	VT_HSV2_CD4
Dnajc15	2.49E-08	0.684390315	0.706	0.337	0.000359	VT_HSV2_CD4
Cd47	4.30E-08	0.655064943	0.906	0.636	0.0006192	VT_HSV2_CD4
Serinc3	4.66E-08	0.500067495	0.777	0.426	0.00067187	VT_HSV2_CD4
Eno1	1.06E-07	0.90747482	0.895	0.667	0.00152474	VT_HSV2_CD4
Ms4a4b	3.35E-07	0.555503264	0.914	0.709	0.00483097	VT_HSV2_CD4
Map2k3	4.53E-07	0.543642804	0.575	0.226	0.00653132	VT_HSV2_CD4
Lag3	6.15E-07	0.571852449	0.333	0.115	0.00886242	VT_HSV2_CD4
Epsti1	7.01E-07	0.667103975	0.779	0.446	0.0100968	VT_HSV2_CD4
Lpxn	1.24E-06	0.51593239	0.566	0.251	0.01782052	VT_HSV2_CD4
Zfp36	1.62E-06	-0.731405262	0.579	0.596	0.02332516	VT_HSV2_CD4
Arrb2	1.63E-06	0.567526918	0.685	0.382	0.02347621	VT_HSV2_CD4
Tigit	2.24E-06	0.652782536	0.73	0.347	0.03226126	VT_HSV2_CD4
Dusp10	1.20E-05	-0.51032774	0.465	0.438	0.17279491	VT_HSV2_CD4
Lsp1	2.03E-05	0.583952071	0.887	0.695	0.29221378	VT_HSV2_CD4
Ctla2a	5.28E-05	0.61571682	0.541	0.333	0.76086083	VT_HSV2_CD4
Gng2	0.00012383	0.505649491	0.652	0.295	1	VT_HSV2_CD4
Hif1a	0.00013184	0.567067929	0.789	0.509	1	VT_HSV2_CD4

gene	p_val	avg_log2FC	pct.1	pct.2	p_val_adj	cluster
Zyx	0.00013553	0.621346068	0.674	0.347	1	VT_HSV2_CD4
Bcl2a1b	0.00020976	0.764218997	0.749	0.416	1	VT_HSV2_CD4
Gm26917	0.00023456	0.745709536	0.568	0.358	1	VT_HSV2_CD4
Actr3	0.00083867	0.574777264	0.901	0.669	1	VT_HSV2_CD4
Lime1	0.00163331	0.617325245	0.69	0.364	1	VT_HSV2_CD4
AW112010	0.0026668	0.753671551	0.894	0.677	1	VT_HSV2_CD4
mt-Atp8	3.89E-173	-1.128805356	0.958	0.997	5.61E-169	VT_HSV2_Treg
Ikzf2.1	8.69E-140	1.99035419	0.606	0.148	1.25E-135	VT_HSV2_Treg
Eef2.1	3.05E-135	-1.134153712	0.883	0.983	4.39E-131	VT_HSV2_Treg
Foxp3	6.31E-124	1.087230515	0.36	0.002	9.09E-120	VT_HSV2_Treg
mt-Atp6.1	4.96E-93	0.977142517	0.973	0.993	7.15E-89	VT_HSV2_Treg
Il2ra.1	2.31E-90	1.556337376	0.595	0.261	3.33E-86	VT_HSV2_Treg
Pabpc1.1	7.56E-80	-0.914456008	0.833	0.973	1.09E-75	VT_HSV2_Treg
Tnfrsf9.1	7.61E-80	1.837160885	0.61	0.36	1.10E-75	VT_HSV2_Treg
Arl5a.1	6.90E-78	1.075300255	0.428	0.138	9.94E-74	VT_HSV2_Treg
Lrrc32	1.11E-77	0.798869524	0.25	0.003	1.60E-73	VT_HSV2_Treg
Tnfrsf18.1	2.09E-73	1.23027176	0.769	0.735	3.01E-69	VT_HSV2_Treg
Ctla4.1	2.40E-72	1.410117326	0.807	0.762	3.46E-68	VT_HSV2_Treg
Capg.1	1.96E-70	1.386065744	0.64	0.475	2.82E-66	VT_HSV2_Treg
Cd2	5.47E-70	0.881965503	0.883	0.916	7.88E-66	VT_HSV2_Treg
Izumo1r.1	9.62E-66	1.669875725	0.667	0.267	1.39E-61	VT_HSV2_Treg
Gnai2.1	9.14E-63	0.734074552	0.792	0.813	1.32E-58	VT_HSV2_Treg
Gnb1.1	9.82E-59	0.87285654	0.595	0.412	1.41E-54	VT_HSV2_Treg
Itgav	7.21E-57	1.040762778	0.402	0.15	1.04E-52	VT_HSV2_Treg
Pglyrp1	5.32E-56	0.986184945	0.591	0.533	7.66E-52	VT_HSV2_Treg
Tnfrsf4.1	3.62E-55	1.343962971	0.811	0.715	5.22E-51	VT_HSV2_Treg
Gimap7.1	1.97E-54	1.091034148	0.61	0.46	2.84E-50	VT_HSV2_Treg
Gzmb.1	2.85E-53	2.03718767	0.473	0.395	4.10E-49	VT_HSV2_Treg
Cyb5a	6.46E-52	0.78138549	0.621	0.585	9.31E-48	VT_HSV2_Treg
Grb2.1	7.78E-52	0.830164581	0.564	0.393	1.12E-47	VT_HSV2_Treg
Ass1.1	2.50E-44	0.902521742	0.481	0.395	3.59E-40	VT_HSV2_Treg
Ecm1	5.07E-44	1.463627896	0.413	0.137	7.30E-40	VT_HSV2_Treg
Cxcr6.1	4.18E-43	-1.799281484	0.102	0.6	6.02E-39	VT_HSV2_Treg
Aes.1	4.70E-42	0.624684394	0.716	0.713	6.76E-38	VT_HSV2_Treg
Cd40lg	8.01E-41	-1.18475875	0.064	0.534	1.15E-36	VT_HSV2_Treg
Ctsw.1	2.85E-40	-1.634686809	0.136	0.63	4.11E-36	VT_HSV2_Treg
Gm5424.1	7.76E-40	0.841900904	0.428	0.279	1.12E-35	VT_HSV2_Treg
Sdf4	1.05E-39	0.86063998	0.811	0.833	1.52E-35	VT_HSV2_Treg

gene	p_val	avg_log2FC	pct.1	pct.2	p_val_adj	cluster
Ly6e	1.12E-39	0.62420537	0.955	0.98	1.62E-35	VT_HSV2_Treg
Areg	1.31E-39	2.279508534	0.254	0.06	1.88E-35	VT_HSV2_Treg
Fasl	6.69E-39	-1.012135824	0.027	0.445	9.64E-35	VT_HSV2_Treg
Socs2	1.42E-38	1.077342838	0.299	0.108	2.05E-34	VT_HSV2_Treg
Glrx	1.61E-36	0.794327559	0.549	0.608	2.32E-32	VT_HSV2_Treg
Psen2	2.32E-36	0.762242039	0.443	0.315	3.33E-32	VT_HSV2_Treg
Rps27rt.1	4.51E-36	0.8398021	0.667	0.562	6.50E-32	VT_HSV2_Treg
Zfp36l2.1	1.86E-34	-1.140303899	0.515	0.843	2.69E-30	VT_HSV2_Treg
Mdh1	2.04E-34	0.627419107	0.606	0.605	2.94E-30	VT_HSV2_Treg
Btg1	3.44E-34	-0.726735438	0.803	0.961	4.96E-30	VT_HSV2_Treg
Bcl2a1d.1	4.58E-33	-1.502071209	0.182	0.657	6.60E-29	VT_HSV2_Treg
H2afz.1	6.04E-33	0.844031927	0.883	0.888	8.70E-29	VT_HSV2_Treg
Neb	4.09E-32	0.776124349	0.258	0.061	5.89E-28	VT_HSV2_Treg
Cmtm7	2.60E-31	0.641253417	0.58	0.556	3.74E-27	VT_HSV2_Treg
Vps37b	4.44E-31	-0.891395623	0.568	0.853	6.39E-27	VT_HSV2_Treg
Gramd3.1	9.51E-31	-0.79115106	0.242	0.682	1.37E-26	VT_HSV2_Treg
Cd27	1.18E-30	0.752260939	0.61	0.526	1.69E-26	VT_HSV2_Treg
Ccs	2.40E-30	0.676899617	0.447	0.278	3.46E-26	VT_HSV2_Treg
Samsn1	4.89E-30	0.82669169	0.655	0.64	7.04E-26	VT_HSV2_Treg
Lck.1	1.14E-29	-0.781179523	0.708	0.929	1.65E-25	VT_HSV2_Treg
Apol7e	1.97E-29	-0.613418648	0.011	0.32	2.84E-25	VT_HSV2_Treg
Sema4a.1	5.52E-29	-0.683895278	0.015	0.346	7.96E-25	VT_HSV2_Treg
Arid5a.1	6.64E-29	-0.848272271	0.341	0.739	9.57E-25	VT_HSV2_Treg
Ppp2ca.1	9.26E-29	0.516551883	0.508	0.448	1.33E-24	VT_HSV2_Treg
Samhd1	1.27E-28	0.808078247	0.773	0.721	1.82E-24	VT_HSV2_Treg
Rps26-ps1.1	1.33E-28	0.610307427	0.458	0.413	1.92E-24	VT_HSV2_Treg
B4galnt1.1	4.75E-28	-1.015791144	0.337	0.765	6.84E-24	VT_HSV2_Treg
Bhlhe40.1	1.47E-26	-1.540239297	0.295	0.71	2.12E-22	VT_HSV2_Treg
Ifitm2.1	4.18E-26	-2.189629428	0.163	0.564	6.02E-22	VT_HSV2_Treg
Ifitm3.1	6.98E-26	-1.997846096	0.208	0.591	1.01E-21	VT_HSV2_Treg
Chmp4b	1.11E-25	0.501742222	0.75	0.767	1.59E-21	VT_HSV2_Treg
Gstp1	7.75E-25	0.514979916	0.765	0.833	1.12E-20	VT_HSV2_Treg
Ptma.1	1.81E-24	0.58051866	0.996	0.987	2.61E-20	VT_HSV2_Treg
Plp2	6.13E-24	0.574157744	0.485	0.463	8.83E-20	VT_HSV2_Treg
Tgfbr2	2.16E-23	-0.629735418	0.174	0.532	3.11E-19	VT_HSV2_Treg
Hspa8.1	2.84E-23	-0.50480235	0.947	0.99	4.09E-19	VT_HSV2_Treg
Got1	8.02E-23	0.672818036	0.5	0.462	1.15E-18	VT_HSV2_Treg
Lax1.1	8.06E-23	-0.774724308	0.117	0.483	1.16E-18	VT_HSV2_Treg

gene	p_val	avg_log2FC	pct.1	pct.2	p_val_adj	cluster
Arhgef1.1	1.37E-22	-0.68166041	0.405	0.787	1.98E-18	VT_HSV2_Treg
Anp32a	1.48E-22	0.56206862	0.792	0.795	2.13E-18	VT_HSV2_Treg
Itgb1.1	1.69E-22	-1.409351159	0.246	0.628	2.44E-18	VT_HSV2_Treg
Gtf2i	2.22E-22	-0.607064796	0.087	0.42	3.20E-18	VT_HSV2_Treg
Ifitm1.1	3.81E-22	-2.08456012	0.042	0.35	5.49E-18	VT_HSV2_Treg
Faim	4.40E-22	0.504373096	0.288	0.193	6.34E-18	VT_HSV2_Treg
Rnf19a.1	5.56E-22	-0.674645643	0.11	0.447	8.00E-18	VT_HSV2_Treg
Taf10.1	1.11E-21	0.530034132	0.473	0.405	1.59E-17	VT_HSV2_Treg
Rasal3.1	1.28E-21	-0.621699826	0.212	0.61	1.85E-17	VT_HSV2_Treg
Evl	1.46E-21	-0.584763706	0.129	0.472	2.11E-17	VT_HSV2_Treg
Gpx4	1.52E-21	0.569779096	0.727	0.785	2.19E-17	VT_HSV2_Treg
Cst7	3.06E-21	0.503291221	0.337	0.323	4.41E-17	VT_HSV2_Treg
Gramd1a.1	4.12E-21	-0.645037919	0.193	0.575	5.93E-17	VT_HSV2_Treg
Stk17b	6.19E-21	-0.669837825	0.667	0.916	8.92E-17	VT_HSV2_Treg
Slfn2.1	1.11E-20	-0.852546019	0.617	0.9	1.61E-16	VT_HSV2_Treg
Tcf7	1.33E-20	-0.817151202	0.083	0.313	1.92E-16	VT_HSV2_Treg
Matk	4.78E-20	0.598590548	0.269	0.11	6.89E-16	VT_HSV2_Treg
Ier5.1	5.05E-20	-0.736486438	0.341	0.708	7.27E-16	VT_HSV2_Treg
Gem	5.21E-20	0.912403021	0.265	0.141	7.51E-16	VT_HSV2_Treg
Gpr132	5.69E-20	-0.723713343	0.371	0.72	8.20E-16	VT_HSV2_Treg
Ifi27l2a	7.46E-20	0.705185789	0.943	0.947	1.07E-15	VT_HSV2_Treg
Hmha1	8.84E-20	-0.559516847	0.5	0.837	1.27E-15	VT_HSV2_Treg
Mgst2	1.56E-19	0.639042186	0.28	0.088	2.25E-15	VT_HSV2_Treg
H2-Q7	1.81E-19	0.547103896	0.826	0.868	2.61E-15	VT_HSV2_Treg
Dusp2.1	2.58E-19	-1.316487932	0.458	0.726	3.72E-15	VT_HSV2_Treg
Tspan13.1	2.64E-19	0.699755599	0.549	0.457	3.80E-15	VT_HSV2_Treg
Ube2h	2.91E-19	0.518106746	0.322	0.217	4.18E-15	VT_HSV2_Treg
S100a10	4.87E-19	0.51524102	0.83	0.871	7.01E-15	VT_HSV2_Treg
Frmd8.1	6.40E-19	-0.625614521	0.193	0.573	9.22E-15	VT_HSV2_Treg
Pcbp2	6.75E-19	-0.510513568	0.818	0.962	9.72E-15	VT_HSV2_Treg
Ehd3	1.36E-18	-0.503993996	0.027	0.265	1.96E-14	VT_HSV2_Treg
Ubald2	1.43E-18	0.613917488	0.78	0.792	2.06E-14	VT_HSV2_Treg
Srsf2	4.78E-18	-0.624087954	0.417	0.775	6.88E-14	VT_HSV2_Treg
Tnfsf11	8.95E-18	-1.018916776	0.045	0.311	1.29E-13	VT_HSV2_Treg
Laptm5.1	1.52E-17	-0.661504184	0.841	0.96	2.19E-13	VT_HSV2_Treg
Btg2	2.06E-17	-0.560180213	0.523	0.831	2.97E-13	VT_HSV2_Treg
Lilr4b.1	2.44E-17	-0.599183415	0.045	0.298	3.52E-13	VT_HSV2_Treg
Ppp3cc.1	6.61E-17	-0.57743261	0.117	0.442	9.52E-13	VT_HSV2_Treg

gene	p_val	avg_log2FC	pct.1	pct.2	p_val_adj	cluster
Chd7	6.78E-17	-0.509177332	0.136	0.474	9.76E-13	VT_HSV2_Treg
Iigp1	7.25E-17	0.610272339	0.258	0.071	1.04E-12	VT_HSV2_Treg
Rassf5.1	7.70E-17	-0.537352013	0.193	0.559	1.11E-12	VT_HSV2_Treg
Anxa1.1	8.53E-17	-0.621202027	0.038	0.294	1.23E-12	VT_HSV2_Treg
Pigx	1.44E-16	0.50183244	0.473	0.465	2.07E-12	VT_HSV2_Treg
Set	1.48E-16	0.506707526	0.564	0.592	2.13E-12	VT_HSV2_Treg
Malat1.1	2.81E-16	0.824323696	0.894	0.988	4.04E-12	VT_HSV2_Treg
Ppp1r15a.1	2.89E-16	0.748554968	0.712	0.723	4.16E-12	VT_HSV2_Treg
Prkcq	2.07E-15	-0.583467836	0.246	0.583	2.97E-11	VT_HSV2_Treg
Cd4.1	2.43E-15	-0.718541516	0.375	0.744	3.50E-11	VT_HSV2_Treg
Itgal.1	3.36E-15	-0.721207106	0.208	0.577	4.85E-11	VT_HSV2_Treg
AA467197.1	3.74E-15	-0.639263129	0.042	0.3	5.39E-11	VT_HSV2_Treg
Gdi2.1	5.08E-15	-0.866553128	0.534	0.829	7.31E-11	VT_HSV2_Treg
Itk	5.32E-15	-0.587483738	0.523	0.807	7.66E-11	VT_HSV2_Treg
Ostf1.1	5.47E-15	-0.815495778	0.508	0.807	7.88E-11	VT_HSV2_Treg
Sell.1	7.00E-15	0.673536138	0.394	0.148	1.01E-10	VT_HSV2_Treg
Ncl	9.42E-15	0.579675627	0.716	0.771	1.36E-10	VT_HSV2_Treg
Ikzf3.1	1.41E-14	0.548199413	0.367	0.245	2.04E-10	VT_HSV2_Treg
Hcst	1.83E-14	-0.602627407	0.723	0.906	2.64E-10	VT_HSV2_Treg
Tob1	2.21E-14	-0.526968081	0.163	0.415	3.18E-10	VT_HSV2_Treg
Efhd2.1	2.46E-14	-0.766677408	0.246	0.605	3.54E-10	VT_HSV2_Treg
Psap.1	3.13E-14	-0.551277748	0.348	0.699	4.51E-10	VT_HSV2_Treg
Tspan32	4.32E-14	0.556276748	0.36	0.23	6.22E-10	VT_HSV2_Treg
Nkg7.1	4.63E-14	-1.031711601	0.273	0.644	6.67E-10	VT_HSV2_Treg
Fam102a.1	7.20E-14	-0.577344374	0.197	0.502	1.04E-09	VT_HSV2_Treg
Slfn1.1	9.87E-14	-0.625109997	0.273	0.582	1.42E-09	VT_HSV2_Treg
Rhoh	2.61E-13	0.532322165	0.564	0.534	3.76E-09	VT_HSV2_Treg
Arl5c	2.75E-13	0.525145772	0.314	0.198	3.96E-09	VT_HSV2_Treg
Plac8.1	6.46E-13	-1.537265478	0.182	0.458	9.31E-09	VT_HSV2_Treg
Ifng.1	8.42E-13	-1.123734932	0.057	0.296	1.21E-08	VT_HSV2_Treg
Dgat1	1.63E-12	0.595223087	0.447	0.394	2.34E-08	VT_HSV2_Treg
Emp1.1	1.66E-12	-0.525549034	0.057	0.278	2.38E-08	VT_HSV2_Treg
Gm8186	2.14E-12	-0.565022527	0.42	0.759	3.09E-08	VT_HSV2_Treg
Cenpa	3.29E-12	0.551694612	0.379	0.28	4.74E-08	VT_HSV2_Treg
Zap70.1	6.09E-12	-0.7530854	0.405	0.761	8.77E-08	VT_HSV2_Treg
Serpinb9.1	1.09E-11	-0.913961293	0.14	0.425	1.57E-07	VT_HSV2_Treg
Odc1	1.45E-11	0.535953348	0.549	0.588	2.08E-07	VT_HSV2_Treg
Dusp5.1	1.57E-11	-0.745182242	0.523	0.77	2.26E-07	VT_HSV2_Treg

gene	p_val	avg_log2FC	pct.1	pct.2	p_val_adj	cluster
Adgre5.1	1.62E-11	-0.707753537	0.292	0.605	2.34E-07	VT_HSV2_Treg
Ube2v1.1	1.72E-11	-0.563903874	0.163	0.476	2.48E-07	VT_HSV2_Treg
Il12rb2.1	1.77E-11	-0.550171739	0.08	0.337	2.55E-07	VT_HSV2_Treg
Rgs2.1	1.99E-11	0.714710282	0.36	0.297	2.87E-07	VT_HSV2_Treg
Rbck1	2.90E-11	-0.559057852	0.242	0.545	4.17E-07	VT_HSV2_Treg
Cpm	3.03E-11	0.508816235	0.348	0.197	4.36E-07	VT_HSV2_Treg
Arhgap31.1	3.68E-11	0.569441717	0.473	0.348	5.30E-07	VT_HSV2_Treg
Itgb2.1	3.96E-11	-0.682892654	0.39	0.737	5.71E-07	VT_HSV2_Treg
Wipf1.1	4.53E-11	-0.609292282	0.284	0.609	6.52E-07	VT_HSV2_Treg
Litaf.1	5.88E-11	-0.880848851	0.231	0.544	8.47E-07	VT_HSV2_Treg
Txnip	1.02E-10	-0.518549426	0.322	0.562	1.47E-06	VT_HSV2_Treg
Pdcd1.1	1.09E-10	-1.002035271	0.208	0.508	1.57E-06	VT_HSV2_Treg
Nptn.1	1.13E-10	-0.581548313	0.235	0.555	1.63E-06	VT_HSV2_Treg
Smc4.1	1.56E-10	0.568466482	0.432	0.402	2.24E-06	VT_HSV2_Treg
Ubash3a	2.37E-10	-0.502291592	0.186	0.493	3.42E-06	VT_HSV2_Treg
Cd28	2.76E-10	-0.580889568	0.515	0.807	3.97E-06	VT_HSV2_Treg
Mapkapk3.1	2.93E-10	-0.738053305	0.235	0.515	4.22E-06	VT_HSV2_Treg
Rgcc.1	4.76E-10	-0.531477037	0.227	0.449	6.86E-06	VT_HSV2_Treg
Arl4c	5.68E-10	-0.521837046	0.254	0.512	8.18E-06	VT_HSV2_Treg
Dazap1	5.89E-10	-0.519092324	0.197	0.498	8.48E-06	VT_HSV2_Treg
Sh2d2a.1	1.03E-09	-0.832737509	0.519	0.796	1.49E-05	VT_HSV2_Treg
Ly6c2.1	1.45E-09	-1.219211373	0.064	0.267	2.09E-05	VT_HSV2_Treg
Bcl2a1b.1	1.82E-09	-0.918915436	0.458	0.733	2.62E-05	VT_HSV2_Treg
Arrb2.1	3.28E-09	-0.654249805	0.39	0.672	4.73E-05	VT_HSV2_Treg
Igtp	3.78E-09	0.575864087	0.572	0.545	5.45E-05	VT_HSV2_Treg
Zfp36l1	2.78E-08	0.51679287	0.58	0.67	0.00039975	VT_HSV2_Treg
Thy1	3.62E-08	-0.796285126	0.633	0.86	0.0005209	VT_HSV2_Treg
Zfp36.1	4.40E-08	0.965489298	0.64	0.577	0.00063439	VT_HSV2_Treg
Furin.1	7.41E-08	-0.53758819	0.117	0.343	0.00106689	VT_HSV2_Treg
Nfatc1.1	1.15E-07	-0.512328339	0.216	0.483	0.00165848	VT_HSV2_Treg
Zc3h12a.1	2.68E-07	-0.519548761	0.269	0.53	0.00386231	VT_HSV2_Treg
Spn	1.17E-06	-0.501737764	0.223	0.497	0.01687099	VT_HSV2_Treg
Gpi1.1	3.64E-06	-0.525927222	0.727	0.906	0.05245726	VT_HSV2_Treg
Rrad	4.67E-06	0.504724108	0.432	0.416	0.06722095	VT_HSV2_Treg
Ms4a4b.1	5.57E-06	-0.517652334	0.705	0.905	0.08018807	VT_HSV2_Treg
Zyx.1	9.53E-06	-0.645786776	0.402	0.658	0.13732698	VT_HSV2_Treg
Eno1.1	1.38E-05	-0.791094907	0.686	0.884	0.19812379	VT_HSV2_Treg
Gapdh.1	1.49E-05	-0.701000227	0.886	0.982	0.21400224	VT_HSV2_Treg

gene	p_val	avg_log2FC	pct.1	pct.2	p_val_adj	cluster
Ctsd.1	2.85E-05	-0.704917341	0.477	0.729	0.41011678	VT_HSV2_Treg
Id2.1	0.00017544	-0.573507616	0.383	0.621	1	VT_HSV2_Treg
Serpinb6b.1	0.00229506	-0.523142235	0.227	0.448	1	VT_HSV2_Treg
Lgals3.1	0.00258452	-0.581209072	0.295	0.52	1	VT_HSV2_Treg
Nfkbiz.1	0.00368777	-0.543758378	0.348	0.559	1	VT_HSV2_Treg
Fos	0.00900294	0.696877049	0.424	0.417	1	VT_HSV2_Treg
Eef2.2	1.79E-128	-1.139130827	0.929	0.981	2.58E-124	VT_uninfected_CD4
mt-Atp6.2	6.91E-57	0.850229449	0.996	0.992	9.96E-53	VT_uninfected_CD4
Rps29	2.24E-55	0.913904182	1	0.996	3.22E-51	VT_uninfected_CD4
mt-Nd2.1	1.64E-50	1.030102274	0.959	0.9	2.36E-46	VT_uninfected_CD4
Gnai2.2	1.92E-48	0.627355621	0.817	0.812	2.76E-44	VT_uninfected_CD4
Aes.2	8.38E-48	0.676559359	0.73	0.712	1.21E-43	VT_uninfected_CD4
Hspa8.2	9.48E-45	-0.649960317	0.975	0.989	1.37E-40	VT_uninfected_CD4
Rps28	5.49E-43	0.792029128	1	0.993	7.91E-39	VT_uninfected_CD4
mt-Cytb	1.59E-41	0.775378841	0.996	0.985	2.29E-37	VT_uninfected_CD4
Ube2s.1	2.02E-41	0.893481994	0.635	0.549	2.90E-37	VT_uninfected_CD4
mt-Atp8.1	2.86E-40	0.61557616	1	0.995	4.13E-36	VT_uninfected_CD4
Gnb1.2	3.25E-40	0.714893983	0.436	0.419	4.68E-36	VT_uninfected_CD4
Rps27rt.2	4.81E-40	1.027531344	0.66	0.563	6.92E-36	VT_uninfected_CD4
Rps24	3.45E-38	0.801953731	1	0.995	4.97E-34	VT_uninfected_CD4
Ifitm3.2	6.21E-38	-3.40529238	0.025	0.597	8.95E-34	VT_uninfected_CD4
mt-Nd4l	3.22E-37	0.75774034	0.996	0.974	4.63E-33	VT_uninfected_CD4
Ly6e.1	3.17E-36	-0.713609537	0.863	0.984	4.57E-32	VT_uninfected_CD4
Ifitm2.2	6.31E-32	-3.373908401	0.025	0.568	9.09E-28	VT_uninfected_CD4
Laptm5.2	2.05E-31	-0.888057482	0.855	0.959	2.95E-27	VT_uninfected_CD4
Ppp2ca.2	2.15E-31	0.62267629	0.469	0.45	3.09E-27	VT_uninfected_CD4
Gpx1.1	2.48E-31	0.901134073	0.672	0.688	3.58E-27	VT_uninfected_CD4
Rps3a1	4.04E-31	0.610243107	1	0.994	5.83E-27	VT_uninfected_CD4
Ly6a	1.86E-30	-1.666724227	0.44	0.925	2.68E-26	VT_uninfected_CD4
Amd1.1	2.30E-30	0.869164178	0.394	0.262	3.31E-26	VT_uninfected_CD4
Rps5	7.59E-30	0.567362684	1	0.994	1.09E-25	VT_uninfected_CD4
Pitpna	1.02E-29	0.534035518	0.361	0.369	1.47E-25	VT_uninfected_CD4
Eif1	3.78E-29	0.566598473	1	0.989	5.44E-25	VT_uninfected_CD4
Rpl35a	4.48E-28	0.627011318	1	0.994	6.46E-24	VT_uninfected_CD4
Rpl30	8.27E-28	0.571130684	1	0.994	1.19E-23	VT_uninfected_CD4
Cnbp.1	1.12E-27	0.677668168	0.929	0.935	1.62E-23	VT_uninfected_CD4
Srgn	1.22E-27	-0.74711504	0.967	0.978	1.75E-23	VT_uninfected_CD4
mt-Nd3	1.90E-27	0.656290354	0.759	0.792	2.73E-23	VT_uninfected_CD4

gene	p_val	avg_log2FC	pct.1	pct.2	p_val_adj	cluster
Malat1.2	3.71E-27	0.990628491	1	0.983	5.35E-23	VT_uninfected_CD4
Rps27	1.46E-26	0.738238881	1	0.996	2.10E-22	VT_uninfected_CD4
Rps19	5.80E-26	0.69170167	1	0.996	8.36E-22	VT_uninfected_CD4
Ifitm1.2	8.89E-26	-3.404239212	0	0.35	1.28E-21	VT_uninfected_CD4
Plac8.2	9.56E-26	-2.479319128	0.025	0.464	1.38E-21	VT_uninfected_CD4
Uba52	1.41E-25	0.579665128	1	0.982	2.03E-21	VT_uninfected_CD4
Rpl8	1.16E-24	0.585565068	1	0.994	1.67E-20	VT_uninfected_CD4
Rexo2	1.96E-24	0.560702518	0.386	0.382	2.82E-20	VT_uninfected_CD4
Ncor1.1	2.22E-24	0.545137269	0.485	0.57	3.19E-20	VT_uninfected_CD4
Rps4x	5.27E-24	0.575593755	1	0.994	7.58E-20	VT_uninfected_CD4
Rgcc.2	5.97E-24	1.233254317	0.573	0.433	8.61E-20	VT_uninfected_CD4
Tigit.1	7.36E-24	-2.009515821	0.1	0.722	1.06E-19	VT_uninfected_CD4
Serinc3.1	1.31E-23	-1.345734239	0.183	0.771	1.88E-19	VT_uninfected_CD4
Rpl21	7.57E-22	0.535895854	1	0.997	1.09E-17	VT_uninfected_CD4
Gapdh.2	4.15E-21	-1.187908062	0.946	0.979	5.98E-17	VT_uninfected_CD4
Rps27a	8.97E-21	0.546178215	1	0.994	1.29E-16	VT_uninfected_CD4
Gbp2	1.30E-20	-0.990117092	0.083	0.466	1.87E-16	VT_uninfected_CD4
Ifi27l2a.1	1.44E-20	-0.93969549	0.78	0.954	2.07E-16	VT_uninfected_CD4
Mxd1	2.40E-20	-1.015022314	0.129	0.592	3.46E-16	VT_uninfected_CD4
mt-Nd1	4.03E-20	0.566077961	0.938	0.928	5.81E-16	VT_uninfected_CD4
Bcl3	7.83E-20	-0.848197107	0.058	0.482	1.13E-15	VT_uninfected_CD4
Eif5	1.24E-19	0.695814681	0.577	0.605	1.78E-15	VT_uninfected_CD4
Rsrp1	1.94E-19	0.633930482	0.506	0.653	2.79E-15	VT_uninfected_CD4
Gzmb.2	4.97E-19	-2.577362487	0.025	0.414	7.16E-15	VT_uninfected_CD4
Rps20	2.21E-18	0.590939142	1	0.996	3.18E-14	VT_uninfected_CD4
Tap1.1	4.89E-18	-0.969291372	0.207	0.709	7.04E-14	VT_uninfected_CD4
Jak3	7.70E-18	-0.674210473	0.041	0.44	1.11E-13	VT_uninfected_CD4
Selplg.1	9.62E-18	-1.102754173	0.598	0.908	1.39E-13	VT_uninfected_CD4
Gramd3.2	1.07E-17	-0.60563812	0.245	0.68	1.54E-13	VT_uninfected_CD4
Ccnd2	1.51E-17	0.511960514	0.39	0.455	2.18E-13	VT_uninfected_CD4
Prdx6	3.64E-17	0.566140853	0.755	0.826	5.24E-13	VT_uninfected_CD4
AA467197.2	4.02E-17	-0.830537988	0	0.301	5.79E-13	VT_uninfected_CD4
Tap2.1	1.08E-16	-0.878981449	0.187	0.713	1.56E-12	VT_uninfected_CD4
Irf1	1.66E-16	-0.75232347	0.307	0.706	2.40E-12	VT_uninfected_CD4
Klhl6.1	1.97E-16	-0.593228277	0.1	0.434	2.83E-12	VT_uninfected_CD4
Zcchc11	1.99E-16	0.56745551	0.29	0.273	2.87E-12	VT_uninfected_CD4
mt-Nd4	2.92E-16	0.579498114	0.809	0.846	4.21E-12	VT_uninfected_CD4
Ctsa.1	3.36E-16	-1.043618673	0.145	0.664	4.85E-12	VT_uninfected_CD4

gene	p_val	avg_log2FC	pct.1	pct.2	p_val_adj	cluster
Znrf1	3.76E-16	0.509323494	0.336	0.388	5.41E-12	VT_uninfected_CD4
Rpl36a	7.39E-16	0.51383929	0.963	0.976	1.06E-11	VT_uninfected_CD4
Lgals3.2	1.55E-15	-2.001777413	0.087	0.528	2.23E-11	VT_uninfected_CD4
Serpinb9.2	1.98E-15	-1.322603795	0.037	0.428	2.85E-11	VT_uninfected_CD4
Sema4d	2.18E-15	-0.631189571	0.124	0.565	3.14E-11	VT_uninfected_CD4
Cox8a	2.48E-15	-0.661359751	0.838	0.96	3.57E-11	VT_uninfected_CD4
Actg1	4.02E-15	-0.989324843	0.988	0.995	5.79E-11	VT_uninfected_CD4
Tnfrsf4.2	4.35E-15	-1.815897342	0.212	0.74	6.26E-11	VT_uninfected_CD4
Gna15.1	4.79E-15	-0.90635603	0.083	0.523	6.89E-11	VT_uninfected_CD4
Coro1a.1	4.86E-15	-0.76513146	0.938	0.981	7.00E-11	VT_uninfected_CD4
Dnajb1	5.69E-15	0.652349805	0.519	0.61	8.19E-11	VT_uninfected_CD4
Trafd1	1.75E-14	-0.516132361	0.062	0.381	2.52E-10	VT_uninfected_CD4
Pglyrp1.1	1.90E-14	-1.057323774	0.095	0.554	2.73E-10	VT_uninfected_CD4
Gbp7	1.91E-14	-0.50083178	0.079	0.404	2.75E-10	VT_uninfected_CD4
Dnaja1	2.93E-14	0.680563965	0.801	0.864	4.22E-10	VT_uninfected_CD4
Rps7	3.82E-14	0.50872839	1	0.989	5.51E-10	VT_uninfected_CD4
Ftl1	4.00E-14	0.516761861	0.988	0.976	5.76E-10	VT_uninfected_CD4
Lag3.1	5.48E-14	-1.10705528	0.017	0.327	7.89E-10	VT_uninfected_CD4
Ehd1.1	6.31E-14	-1.043138755	0.054	0.511	9.08E-10	VT_uninfected_CD4
Samhd1.1	8.89E-14	-0.639457692	0.373	0.738	1.28E-09	VT_uninfected_CD4
AY036118	9.17E-14	0.637848202	0.938	0.925	1.32E-09	VT_uninfected_CD4
Lax1.2	9.61E-14	-0.604561141	0.104	0.482	1.38E-09	VT_uninfected_CD4
Rpl12	9.76E-14	0.535271999	0.979	0.972	1.41E-09	VT_uninfected_CD4
Icam1.1	3.92E-13	-1.066165703	0.091	0.477	5.64E-09	VT_uninfected_CD4
Dusp10.1	5.45E-13	1.017651208	0.577	0.458	7.85E-09	VT_uninfected_CD4
P2ry10	6.13E-13	0.560455072	0.34	0.37	8.83E-09	VT_uninfected_CD4
Ctla4.2	6.48E-13	-1.013525061	0.274	0.785	9.33E-09	VT_uninfected_CD4
Sdcbp2	7.19E-13	-0.606604507	0.054	0.363	1.04E-08	VT_uninfected_CD4
Lman2	8.27E-13	-0.545983158	0.129	0.554	1.19E-08	VT_uninfected_CD4
Serpinb6b.2	9.36E-13	-1.224915959	0.054	0.455	1.35E-08	VT_uninfected_CD4
Ms4a6b	1.02E-12	-0.789754118	0.614	0.908	1.47E-08	VT_uninfected_CD4
Emp1.2	1.22E-12	-0.521231445	0.025	0.278	1.76E-08	VT_uninfected_CD4
Csrnp1	1.44E-12	-0.686261521	0.183	0.559	2.07E-08	VT_uninfected_CD4
Frmd8.2	1.71E-12	-0.595034479	0.149	0.573	2.47E-08	VT_uninfected_CD4
Ldha	2.13E-12	-0.981640276	0.784	0.95	3.07E-08	VT_uninfected_CD4
Ifi47	4.15E-12	-0.534601369	0.328	0.688	5.98E-08	VT_uninfected_CD4
Gpi1.2	5.21E-12	-0.839930452	0.656	0.908	7.50E-08	VT_uninfected_CD4
Clk1	6.81E-12	0.544781094	0.481	0.499	9.81E-08	VT_uninfected_CD4

gene	p_val	avg_log2FC	pct.1	pct.2	p_val_adj	cluster
AU020206	8.41E-12	-0.505793595	0.091	0.438	1.21E-07	VT_uninfected_CD4
Nfkbia	8.49E-12	-0.912403082	0.705	0.925	1.22E-07	VT_uninfected_CD4
Nfkbiz.2	9.33E-12	-1.176975216	0.12	0.567	1.34E-07	VT_uninfected_CD4
Hif1a.1	9.45E-12	-1.140750951	0.315	0.784	1.36E-07	VT_uninfected_CD4
Arid5a.2	1.17E-11	-0.578107805	0.378	0.736	1.69E-07	VT_uninfected_CD4
Ube2v1.2	1.23E-11	-0.630094423	0.075	0.479	1.77E-07	VT_uninfected_CD4
Cebpb	1.26E-11	-0.575869627	0.17	0.49	1.81E-07	VT_uninfected_CD4
Rac2	1.36E-11	-0.656701143	0.942	0.972	1.96E-07	VT_uninfected_CD4
Lilr4b.2	1.51E-11	-0.594100012	0.041	0.298	2.17E-07	VT_uninfected_CD4
Il12rb2.2	1.55E-11	-0.632355096	0.025	0.339	2.23E-07	VT_uninfected_CD4
S100a6	2.14E-11	-1.955345181	0.361	0.786	3.09E-07	VT_uninfected_CD4
Apobec3	2.37E-11	-0.813478465	0.183	0.643	3.41E-07	VT_uninfected_CD4
Pim1	3.71E-11	-0.889373886	0.506	0.827	5.35E-07	VT_uninfected_CD4
Slc38a2	3.94E-11	0.574893294	0.531	0.575	5.68E-07	VT_uninfected_CD4
Slfn2.2	4.74E-11	-0.714142612	0.614	0.899	6.82E-07	VT_uninfected_CD4
Snhg12	4.85E-11	0.539716077	0.324	0.307	6.99E-07	VT_uninfected_CD4
Bcl2l11	5.74E-11	-0.564316939	0.095	0.363	8.27E-07	VT_uninfected_CD4
Lrp10.1	7.56E-11	-0.827258188	0.183	0.668	1.09E-06	VT_uninfected_CD4
Cd52.1	7.75E-11	-1.000710091	0.954	0.98	1.12E-06	VT_uninfected_CD4
Isg20	8.08E-11	-0.62989359	0.158	0.566	1.16E-06	VT_uninfected_CD4
Batf	1.20E-10	-0.954758507	0.212	0.666	1.73E-06	VT_uninfected_CD4
Zc3h12a.2	1.30E-10	-0.786120849	0.129	0.535	1.88E-06	VT_uninfected_CD4
Chp1	1.48E-10	-0.50913849	0.116	0.491	2.13E-06	VT_uninfected_CD4
Lef1	1.76E-10	0.547320334	0.452	0.531	2.53E-06	VT_uninfected_CD4
Prkch	2.18E-10	-0.55357146	0.299	0.704	3.14E-06	VT_uninfected_CD4
Tnfrsf9.2	2.18E-10	-1.129974739	0.041	0.385	3.14E-06	VT_uninfected_CD4
Pdcd1.2	2.27E-10	-1.114189258	0.108	0.511	3.27E-06	VT_uninfected_CD4
Cd2.1	2.38E-10	-0.646706781	0.689	0.924	3.43E-06	VT_uninfected_CD4
Rilpl2	2.76E-10	-1.171031541	0.158	0.642	3.97E-06	VT_uninfected_CD4
Pkm	5.18E-10	-1.20812105	0.602	0.918	7.46E-06	VT_uninfected_CD4
Ccr2	6.67E-10	-0.704605983	0.079	0.387	9.61E-06	VT_uninfected_CD4
Igtp.1	6.69E-10	-0.515536416	0.27	0.558	9.64E-06	VT_uninfected_CD4
Ddit4	8.39E-10	-1.00192649	0.104	0.473	1.21E-05	VT_uninfected_CD4
Ttc39b	1.26E-09	-0.557621809	0.124	0.489	1.82E-05	VT_uninfected_CD4
Runx2	1.47E-09	-0.505969089	0.058	0.368	2.12E-05	VT_uninfected_CD4
AW112010.1	1.84E-09	-1.293159026	0.531	0.89	2.65E-05	VT_uninfected_CD4
Dusp2.2	2.55E-09	-1.311894558	0.357	0.729	3.67E-05	VT_uninfected_CD4
Rabac1	2.68E-09	0.520655197	0.668	0.714	3.86E-05	VT_uninfected_CD4

gene	p_val	avg_log2FC	pct.1	pct.2	p_val_adj	cluster
Elovl1	2.93E-09	-0.515397039	0.066	0.4	4.22E-05	VT_uninfected_CD4
Lck.2	3.05E-09	-0.533497275	0.784	0.925	4.40E-05	VT_uninfected_CD4
Traf1	3.76E-09	-0.839425079	0.237	0.714	5.41E-05	VT_uninfected_CD4
Grina.1	4.87E-09	-0.542108386	0.166	0.561	7.02E-05	VT_uninfected_CD4
Gimap5	5.39E-09	-0.710281818	0.295	0.719	7.76E-05	VT_uninfected_CD4
Litaf.2	6.84E-09	-1.080224193	0.124	0.548	9.85E-05	VT_uninfected_CD4
Pdcd1lg2	6.89E-09	-0.517225507	0.041	0.32	9.92E-05	VT_uninfected_CD4
Tnfrsf18.2	7.97E-09	-1.037951807	0.303	0.755	0.00011474	VT_uninfected_CD4
Cd47.1	7.98E-09	-0.976633618	0.552	0.897	0.00011501	VT_uninfected_CD4
Surf4.1	2.52E-08	-0.555320841	0.145	0.556	0.00036358	VT_uninfected_CD4
Hilpda	2.84E-08	-1.351028706	0.141	0.549	0.00040936	VT_uninfected_CD4
S100a10.1	3.42E-08	-1.152408547	0.643	0.879	0.00049226	VT_uninfected_CD4
Mapkapk3.2	3.62E-08	-0.596372105	0.133	0.518	0.00052109	VT_uninfected_CD4
Casp3	4.14E-08	-0.561679687	0.058	0.383	0.00059628	VT_uninfected_CD4
Klf6	4.91E-08	0.673667104	0.639	0.616	0.00070768	VT_uninfected_CD4
Ifngr1	5.48E-08	-0.524187032	0.614	0.873	0.0007893	VT_uninfected_CD4
Ctla2b	6.34E-08	-0.73940662	0.075	0.374	0.00091324	VT_uninfected_CD4
Ogfr	6.83E-08	-0.529922907	0.145	0.496	0.00098424	VT_uninfected_CD4
Wipf1.2	9.30E-08	-0.532047819	0.199	0.611	0.00133954	VT_uninfected_CD4
Fmnl1	9.44E-08	-0.520016622	0.224	0.62	0.00135981	VT_uninfected_CD4
Rps6ka1.1	9.72E-08	-0.633598853	0.1	0.479	0.00139972	VT_uninfected_CD4
Sdf4.1	1.30E-07	-0.967562869	0.444	0.848	0.00187664	VT_uninfected_CD4
Lasp1	1.45E-07	-0.537219201	0.108	0.473	0.00208655	VT_uninfected_CD4
Ptpn7	1.46E-07	-0.543274539	0.112	0.476	0.00210058	VT_uninfected_CD4
Il2ra.2	1.64E-07	-0.65144034	0.037	0.286	0.00235625	VT_uninfected_CD4
Tmbim6.1	2.28E-07	-0.705188968	0.589	0.903	0.00329076	VT_uninfected_CD4
Stx11	2.62E-07	-0.522987219	0.033	0.297	0.00377979	VT_uninfected_CD4
Rab8a	3.21E-07	-0.63129576	0.274	0.714	0.00461698	VT_uninfected_CD4
Def6.1	5.10E-07	-0.594822539	0.207	0.627	0.00734276	VT_uninfected_CD4
Nkg7.2	5.77E-07	-1.14618961	0.207	0.645	0.00830463	VT_uninfected_CD4
Bhlhe40.2	5.80E-07	-1.556794241	0.245	0.711	0.00835438	VT_uninfected_CD4
Fermt3	5.85E-07	-0.576829859	0.191	0.61	0.00841994	VT_uninfected_CD4
Nucb1	6.07E-07	-0.50385972	0.095	0.431	0.00874333	VT_uninfected_CD4
Sla	1.12E-06	-0.794051387	0.224	0.651	0.01609997	VT_uninfected_CD4
Gm19585	1.18E-06	-0.616300793	0.141	0.518	0.01697168	VT_uninfected_CD4
Rbm3	1.37E-06	-0.569161511	0.946	0.961	0.01980431	VT_uninfected_CD4
Pkp3	1.60E-06	-1.029216361	0.212	0.621	0.02305468	VT_uninfected_CD4
Tubb2a	1.77E-06	0.850352959	0.253	0.152	0.02545367	VT_uninfected_CD4

gene	p_val	avg_log2FC	pct.1	pct.2	p_val_adj	cluster
Zgpat	1.90E-06	-0.551489643	0.191	0.596	0.02730897	VT_uninfected_CD4
Il2rb	2.13E-06	-1.291103382	0.241	0.745	0.03065039	VT_uninfected_CD4
Efhd2.2	2.25E-06	-0.85824682	0.145	0.607	0.03243696	VT_uninfected_CD4
Cd6.1	2.54E-06	-0.780886254	0.29	0.66	0.03656219	VT_uninfected_CD4
Fam110a	2.74E-06	-0.536029287	0.087	0.393	0.03940002	VT_uninfected_CD4
Sqstm1	3.64E-06	-0.641373028	0.618	0.89	0.05249946	VT_uninfected_CD4
Map2k3.1	4.84E-06	-0.806628701	0.129	0.563	0.06969015	VT_uninfected_CD4
Rgs2.2	5.50E-06	0.515633242	0.324	0.299	0.07927753	VT_uninfected_CD4
Hopx	5.60E-06	-0.709589583	0.191	0.586	0.0807272	VT_uninfected_CD4
Tapbp	5.93E-06	-0.542270434	0.307	0.702	0.08538052	VT_uninfected_CD4
Id2.2	6.18E-06	-0.964507986	0.237	0.626	0.08899891	VT_uninfected_CD4
P4hb	7.35E-06	-0.52538755	0.216	0.601	0.10593992	VT_uninfected_CD4
Ptms	7.49E-06	-0.694858343	0.149	0.541	0.10795614	VT_uninfected_CD4
Clic1	7.76E-06	-0.730502452	0.697	0.923	0.11174511	VT_uninfected_CD4
Rnh1	9.66E-06	-0.685446051	0.145	0.568	0.13920739	VT_uninfected_CD4
Actn1	1.07E-05	0.551221151	0.336	0.246	0.15350569	VT_uninfected_CD4
Pstpip1.1	1.08E-05	-0.667977335	0.27	0.665	0.15592632	VT_uninfected_CD4
Arpc1b	1.14E-05	-0.674374245	0.768	0.935	0.1638443	VT_uninfected_CD4
Ctla2a.1	1.24E-05	-1.231503838	0.261	0.534	0.17854232	VT_uninfected_CD4
Acot7	1.45E-05	-0.597947258	0.124	0.498	0.20814736	VT_uninfected_CD4
Mrps16	1.80E-05	-0.534093025	0.245	0.671	0.25912565	VT_uninfected_CD4
Epsti1.1	1.99E-05	-0.874771947	0.328	0.768	0.28710805	VT_uninfected_CD4
Furin.2	2.03E-05	-0.506080985	0.079	0.343	0.29211682	VT_uninfected_CD4
Glmp	2.58E-05	-0.54875217	0.203	0.612	0.37177611	VT_uninfected_CD4
Dnajc15.1	3.05E-05	-0.968062345	0.241	0.693	0.43983404	VT_uninfected_CD4
Pycard	3.49E-05	-0.59226006	0.249	0.663	0.50338533	VT_uninfected_CD4
Glipr2	3.60E-05	-0.565307958	0.149	0.491	0.51792531	VT_uninfected_CD4
Aldoa	3.79E-05	-0.905032819	0.784	0.916	0.54570141	VT_uninfected_CD4
Lpxn.1	3.99E-05	-0.571190964	0.178	0.555	0.57472325	VT_uninfected_CD4
Rhog	4.21E-05	-0.678204404	0.481	0.855	0.60683408	VT_uninfected_CD4
Dctpp1	4.33E-05	-0.51636013	0.066	0.366	0.62379197	VT_uninfected_CD4
Vim	4.51E-05	-1.131501532	0.598	0.8	0.65023117	VT_uninfected_CD4
Gng2.1	4.54E-05	-0.632848301	0.199	0.64	0.65409462	VT_uninfected_CD4
Cd69	6.16E-05	-0.631375642	0.39	0.677	0.88710798	VT_uninfected_CD4
Zap70.2	6.70E-05	-0.95948415	0.303	0.764	0.9648883	VT_uninfected_CD4
Itgb2.2	7.65E-05	-0.738943943	0.295	0.74	1	VT_uninfected_CD4
Itgal.2	7.80E-05	-0.542430887	0.183	0.577	1	VT_uninfected_CD4
Capza1.1	0.00012985	-0.69464654	0.332	0.775	1	VT_uninfected_CD4

gene	p_val	avg_log2FC	pct.1	pct.2	p_val_adj	cluster
Tmem167	0.00016667	-0.524794226	0.237	0.643	1	VT_uninfected_CD4
Eif4h	0.00017764	-0.568826204	0.22	0.621	1	VT_uninfected_CD4
Rab1b	0.00018116	-0.706106797	0.22	0.677	1	VT_uninfected_CD4
Nptn.2	0.00018634	-0.620213306	0.178	0.556	1	VT_uninfected_CD4
Ctsd.2	0.00018728	-0.971824253	0.295	0.736	1	VT_uninfected_CD4
Lsp1.1	0.00019661	-0.722671535	0.647	0.88	1	VT_uninfected_CD4
S100a11	0.00023756	-0.812161883	0.556	0.817	1	VT_uninfected_CD4
Sh2d1a	0.00025153	-0.559755758	0.245	0.596	1	VT_uninfected_CD4
Gadd45b	0.00026292	-0.553196447	0.303	0.67	1	VT_uninfected_CD4
Cap1	0.00027516	-0.518828537	0.295	0.704	1	VT_uninfected_CD4
Ccr8	0.00044987	-0.550472784	0.062	0.269	1	VT_uninfected_CD4
B4galnt1.2	0.00051638	-0.712179469	0.353	0.763	1	VT_uninfected_CD4
Crlf2	0.00053517	-0.619389736	0.216	0.592	1	VT_uninfected_CD4
Sh2d2a.2	0.00073008	-0.896315387	0.448	0.797	1	VT_uninfected_CD4
Cish	0.00091107	-0.577242014	0.228	0.577	1	VT_uninfected_CD4
Ppp1ca	0.00091256	-0.583896271	0.73	0.892	1	VT_uninfected_CD4
Prelid1	0.00096912	-1.016321407	0.461	0.845	1	VT_uninfected_CD4
Atp5d	0.00136762	-0.521775667	0.726	0.935	1	VT_uninfected_CD4
Mif4gd	0.00144296	-0.636285707	0.228	0.601	1	VT_uninfected_CD4
Psma5	0.00153332	-0.522220642	0.253	0.647	1	VT_uninfected_CD4
Lgals1	0.00180301	-1.455139178	0.56	0.821	1	VT_uninfected_CD4
Psmb8	0.0018958	-0.502152564	0.73	0.943	1	VT_uninfected_CD4
Nfkbid	0.00205317	-0.537640626	0.253	0.542	1	VT_uninfected_CD4
Psme2	0.00212269	-0.617233539	0.656	0.913	1	VT_uninfected_CD4
Anxa2	0.00225467	-1.209683064	0.158	0.568	1	VT_uninfected_CD4
Tgfb1	0.0024797	-0.701286429	0.307	0.706	1	VT_uninfected_CD4
Glrx.1	0.00253694	-0.934470347	0.228	0.621	1	VT_uninfected_CD4
Icos	0.003284	-0.640194509	0.552	0.826	1	VT_uninfected_CD4
S100a4	0.0036761	-0.750698974	0.286	0.651	1	VT_uninfected_CD4
Sh3bgrl3	0.00391475	-0.549437414	0.9	0.957	1	VT_uninfected_CD4
Ccr7	0.00395735	0.618493924	0.419	0.251	1	VT_uninfected_CD4
Ubl5	0.00434814	-0.508744468	0.693	0.9	1	VT_uninfected_CD4
Ctsw.2	0.00455873	-0.702152489	0.282	0.622	1	VT_uninfected_CD4
Pgam1	0.00462007	-0.684753085	0.237	0.618	1	VT_uninfected_CD4
Eno1.2	0.00515016	-0.977823787	0.647	0.885	1	VT_uninfected_CD4
Ap2s1	0.00613215	-0.629223586	0.237	0.654	1	VT_uninfected_CD4
Ptprcap	0.00706745	-0.760350415	0.519	0.871	1	VT_uninfected_CD4
Wdr1	0.00894109	-0.657798947	0.32	0.723	1	VT_uninfected_CD4

VITA

Brianna Traxinger was born in 1990 in Anchorage, Alaska, where she attended Bettye Davis East Anchorage High School. She graduated from the Colorado College in 2013 with a Bachelor of Arts in biology and a minor in Spanish. She studied T- and B-cell mediated autoimmunity in the labs of Jordan Jacobelli, Rachel Friedman, and Cara Mack at National Jewish Health and the University of Colorado Anschutz before joining the University of Washington Pathobiology PhD program in 2016. There, under the mentorship of Jennifer Lund and Martin Prlic at Fred Hutch, she studied vaginal regulatory T cells in health and infection.